Evaluating the Impact of FOWT Displacement on Energy Yield for Wind Farm Optimization

Vanshika Gupta

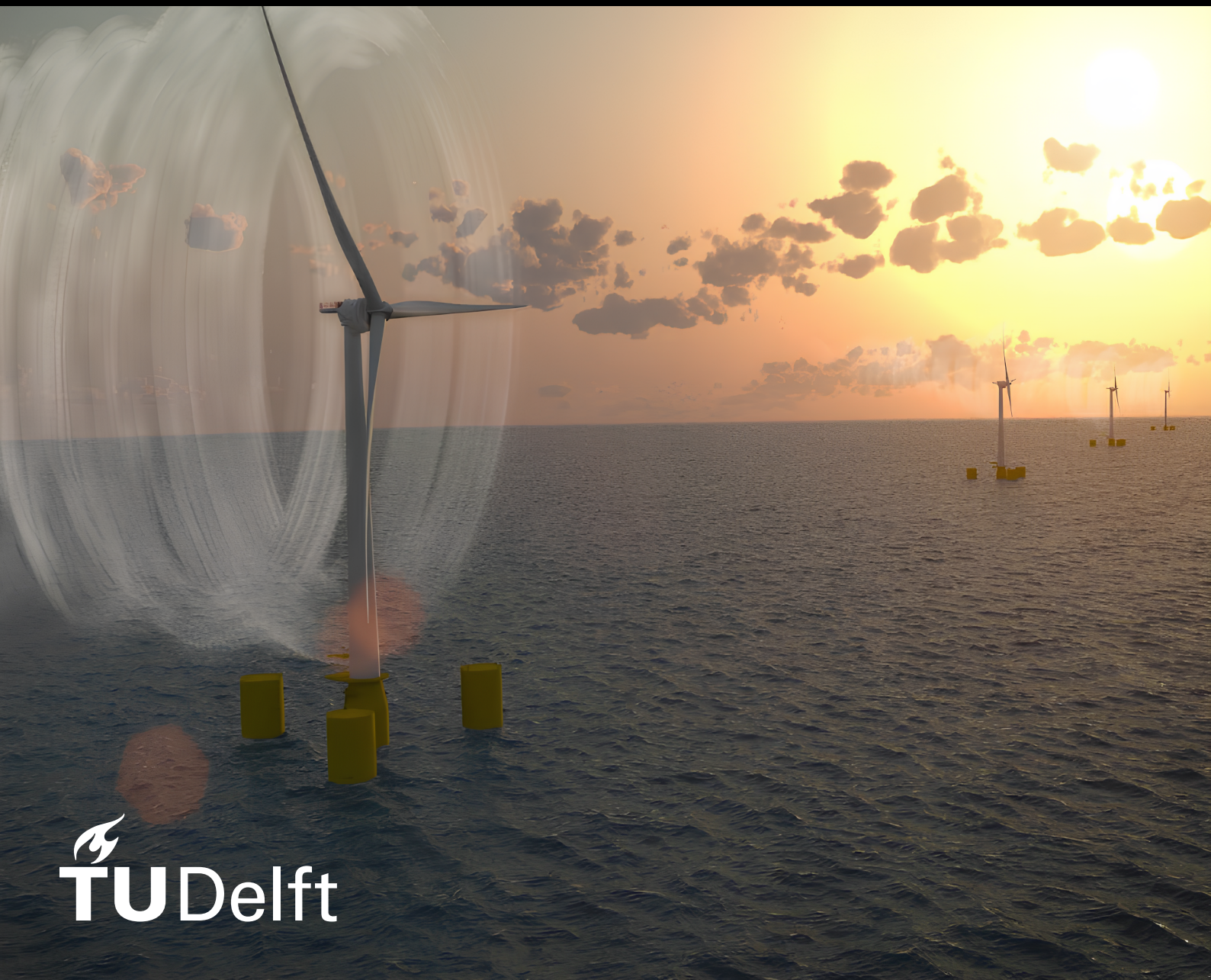

TU Delft

Evaluating the Impact of FOWT Displacement on Energy Yield for Wind Farm Optimization

by

Vanshika Gupta

Student Name	Student Number
Vanshika Gupta	5720583

Supervisors: Dr. Axelle Viré and Ir. Matteo Baudino Bessone
Project Duration: February, 2024 - October,2024
Faculty: Faculty of Aerospace Engineering, Delft

Cover image adapted from Journal Général de l'Europe.
An electronic version of this thesis is available at Delft University Repository.

TU Delft

Contents

Summary

The field of floating offshore wind energy is rapidly advancing, offering a promising solution to harness stronger and more consistent wind resources in deep-water regions, where conventional bottom-fixed turbines are not viable. Floating Offshore Wind Turbines (FOWTs), mounted on floating substructures, enable the deployment of wind turbines in deep offshore locations without the need for extensive foundations. This approach can significantly lower project costs, primarily by reducing substructure procurement expenses for comparable water depths. As a result, the installed capacity of FOWTs is projected to reach approximately 18.9 GW by 2030.

However, the design of cost-efficient FOWTs presents significant challenges due to the complex interactions between aerodynamic and hydrodynamic loads, as well as the coupling of various subsystems. One of the key hurdles is reducing the Levelized Cost of Energy (LCoE) to ensure the economic viability of Floating Offshore Wind Farms (FOWFs). Additionally, the flexibility of the floating substructure, which moves in six degrees of freedom (DOF), introduces complexities in the wake profile, such as enhanced wake meandering, which may affect the wake losses and the overall farm energy production.

Despite the potential impact of floater movements on energy yield, the specific effects on optimal wind farm layout design remain under-explored. Furthermore, the impact of these displacements on the LCoE needs to be examined to determine whether incorporating floater displacements into optimization frameworks leads to more accurate results or merely adds unnecessary complexity and computational cost.

This thesis evaluates the role of static floater displacements, specifically tilt and surge, in the optimization of FOWFs. Two distinct scenarios have been compared to assess how these displacements affect energy yield, the LCoE, and the optimal wind farm layout. The first scenario (Case A) disregards the static equilibrium displacements of the floating turbines, while the second scenario (Case B) incorporates these displacements into the analysis. To conduct the analysis, this thesis develops a wake modeling strategy focusing on wind-induced floater displacements, wherein the tilt and surge displacements of the floater are computed for each turbine using the PyWake framework, based on the effective wind speed experienced by its rotor. This wake modeling approach is then integrated into an OpenMDAO-based optimization framework to minimize the LCoE of the wind farm, which is used for the comparison between the two cases, to achieve the objectives of this study.

A case study of a 42-turbine sample wind farm in the North Sea, arranged in a rectangular gridded layout, was analyzed using the optimization framework. The results showed minimal differences in AEP, LCoE, and layout design between the scenarios that account for floater displacements (Case B) and those that neglect them (Case A). However, the computational time required for the optimization process increased by approximately fourfold for Case B. Case B resulted in a 0.25% reduction in AEP and a 0.162 €/MWh increase in LCoE, primarily due to changes in wake behavior caused by tilt and surge displacements. The optimal layout also shifted in orientation and spacing, with Case B yielding slightly lower power in the final configuration. Despite these effects, the overall impact on the LCoE was modest, suggesting that while incorporating floater displacements could potentially improve the accuracy of results for FOWFs, it might not justify the added computational costs for larger wind farms.

Acknowledgements

Completing this thesis has been an incredible journey, and I am truly fortunate to have received unwavering support from so many remarkable individuals along the way.

First and foremost, I would like to express my deepest gratitude to my supervisor, Dr. Ir. Axelle Viré, for offering me the opportunity to work on this thesis, which has kept me inspired and driven over the past nine months. Your expert guidance, unwavering support, and insightful feedback have been pivotal in shaping this research. You have steered me in the right direction throughout this journey which has not only helped me stay on course but also deepened my understanding and interest in floating wind energy. I feel truly privileged to have had the opportunity to work under your supervision.

Then, I would like to extend my heartfelt thanks to my PhD supervisor, Ir. Matteo Baudino Bessone, whose unwavering expertise, patience, and commitment have been the backbone of my thesis. Your thoughtful advice and continuous support have not only shaped my academic growth but also inspired me personally. The way you approach problem-solving, with such professionalism, has been a true inspiration to me. I am especially thankful for your detailed feedbacks, which have shaped this dissertation into what it is today. I deeply appreciate the opportunity to have worked with you and am sincerely grateful for your guidance throughout this journey.

To the members of my thesis committee, Dr. Ir. Dominic von Terzi and Dr. Ir. Gianfranco la Rocca, I am deeply appreciative of your interest in my thesis topic. Thank you for taking out the time to be a part of my thesis assessment committee and attending my defence. Your questions and feedback would be invaluable in this final phase of my thesis.

A special thanks to my colleagues and friends, whose camaraderie, support, and thoughtful discussions have made this two year masters' journey more enjoyable and enriching. I am particularly grateful to Vibhor, Aparna, Aswin and Jaggu for your positivity, constant encouragement and moral support during moments of difficulty. Your companionship made this journey not only manageable but truly fun, and for that, I am deeply thankful.

Lastly, but most importantly, I would like to express my profound gratitude to my parents, for their unconditional love, support, and encouragement throughout my academic journey. Your encouragement has been the foundation of my success and without your unwavering belief in me, it would not have been possible to reach here.

To all of you, I extend my sincerest appreciation. Thank you.

List of Figures

List of Tables

Nomenclature

Abbreviations

Abbreviation	Definition
FOWT	Floating Offshore Wind Turbine
FOWF	Floating Offshore Wind Farm
AEP	Annual Energy Production
LCoE	Levelized Cost of Energy
DOF	Degree of Freedom
NREL	National Renewable Energy Laboratory
IEA	International Energy Agency
CFD	Computational Fluid Dynamics
DWM	Dynamic Wake Meandering
ALM	Actuator Line Method
BEM	Blade Element Momentum Theory
HAWC2	Horizontal Axis Wind turbine simulation Code 2nd generation
CGI	Circular Gauss Integration
RQ	Research Question
MDAO	Multidisciplinary Design Analysis and Optimization
XDSM	Extended Design Structure Matrix
WINDOW	Windfarm Integrated Design and Optimization Workflow
COBYLA	Constrained Optimization BY Linear Approximation
DV	Design Variable
WD	Wind Direction
WS	Wind Speed
WT	Wind Turbine
WS_{eff}	Effective Wind Speed
TI	Turbulence Intensity
O&M	Operation and Maintenance
C_{CapEx}	Life-cycle, discounted Capital Expenditure
C_{OpEx}	Life-cycle, discounted Operational Expenditure

Symbols

Symbol	Definition	Unit
U_∞	Freestream Wind Speed	[m/s]
P	Power	[MW]
f	Power	[-]
t	Total time period of one year	[hr]
D	Rotor Diameter	[m]
C_T	Thrust Coefficient	[-]
l	Horizontal projection of mooring cable profile	[m]
h	Vertical projection of mooring cable profile	[m]
H	Horizontal component of cable tension	[N]
V	Vertical component of cable tension	[N]
L_0	Length of the mooring line	[m]
w	Weight of the cable per unit length in water	[kg/m]
EA	Extensional stiffness of the unstretched cable	[m]
T	Thrust	[N]
A	Surface Area of the Rotor Disc	$[m^2]$
U	Wind Speed	[m/s]
$C_{prd,y}$	Yearly Production Cost of the Semi-submersible Assembly	[€]
C_{ins}	Installation Cost	[€]
$C_{O\&M}$	Operation and Maintenance Cost	[€]
R_{out}	Outer column radius of the semi-submersible	[m]
Fr	Freeboard of the Semi-submersible	[m]
D_{mr}	Diameter of the Mooring Line	[m]
L_{mr}	Length of the Mooring Line	[m]
R_{mr}	Distance between the Anchor and the Fairlead	[m]
$H_{mr,rel}$	Relative height of the fairlead over draft	[m]
Dr	Draft	[m]
R_{offs}	Radial position of the semi-submersible outer columns	[m]
Sp	Layout Spacing	[m]
r	Discount Rate	[-]
d	Turbine Footprint	[m]
Mr_{str}	Mooring Characteristic Strength	[N]
T_{Fr}	Tension at Fairlead	[N]
θ	Tilt Angle	[°]
α	Layout Rotation	[°]
ρ	Density at Hub-Height	$[kg/m^3]$

1

Introduction and Literature Study

1.1. Wind Energy: Driving the Future of Renewable Energy

A worldwide transition towards renewable energy sources is essential to mitigate the severe impact of climate change. Among the various renewable energy sources, wind energy stands out as the most rapidly advancing, and cost-effective alternative, with minimal environmental footprint [1] to generate clean electrical energy. Notably, wind power ranks as the third largest renewable energy source globally, following hydropower and solar power. This technology is at the forefront of the transition to sustainable energy, supporting the objective of achieving net-zero emissions by 2050 and limiting the global temperature rise to 1.5°C [2].

In contrast to solar power plants, which are limited to generating electricity during daylight hours, wind farms have the capability to provide a more consistent and stable energy output, producing electricity continuously. Onshore wind energy has rapidly advanced, emerging as one of the fastest-growing renewable energy sources. It has achieved cost competitiveness in numerous regions with traditional fossil fuels, showcasing its economic viability and potential for broad adoption [3].

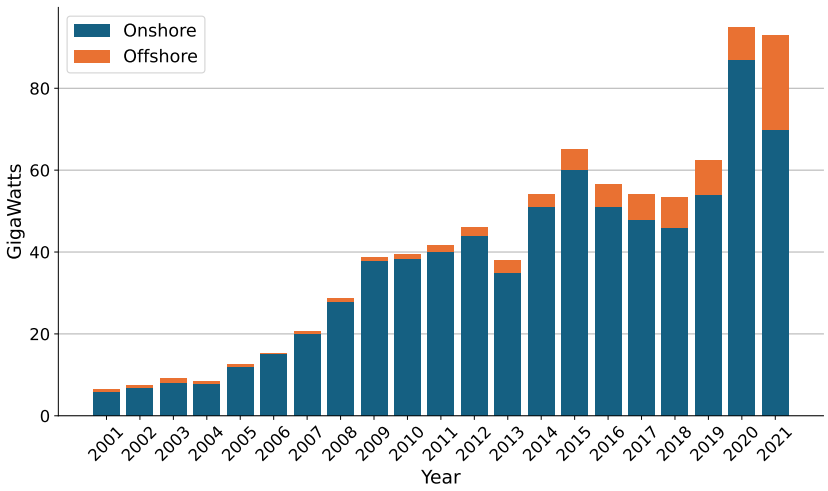

Figure 1.1: Annual Installed Capacities of Onshore and Offshore Wind Turbines between 2001 and 2021, adapted from [3]

Over recent decades, the offshore wind energy sector has also expanded significantly, with a

total offshore wind power capacity of 35.3 GW installed by 2020, predominantly in the North Atlantic Ocean and the North Sea [4]. Offshore wind farms benefit from higher and more consistent wind speeds than onshore sites, leading to more reliable and substantial energy production. Additionally, their offshore locations allow for larger turbines, minimizing noise and visual impact on human populations and ecosystems. The proximity of many offshore wind farms to major coastal urban centers also minimizes energy transmission losses and infrastructure expenses [5]. Figure 1.1 shows the annual installed capacity of wind energy, onshore and offshore in the past two decades.

Economically viable deployment of offshore wind turbines with bottom-mounted foundations has been restricted to shallow waters, up to about 50m deep, primarily in the Northern Sea and the Baltic Sea [6]. These areas benefit from abundant wind resources in relatively shallow depths. Nevertheless, vast wind resources are also present in deeper offshore areas, such as the Mediterranean Sea and distant offshore regions north of Scotland and Ireland. The industry is moving towards floating offshore wind turbines (FOWTs) to harness the vast wind potential in deeper waters. Mounting wind turbines on floating substructures allows for a more cost-effective deployment farther offshore without the need to construct large bottom-mounted foundations required for these water depths [7]. The installed capacity of FOWTs has been estimated to increase from 121 MW in 2023 to 18.9 GW in 2030 [8]. Concepts for onshore and offshore installation at different water depths have been displayed in Figure 1.2.

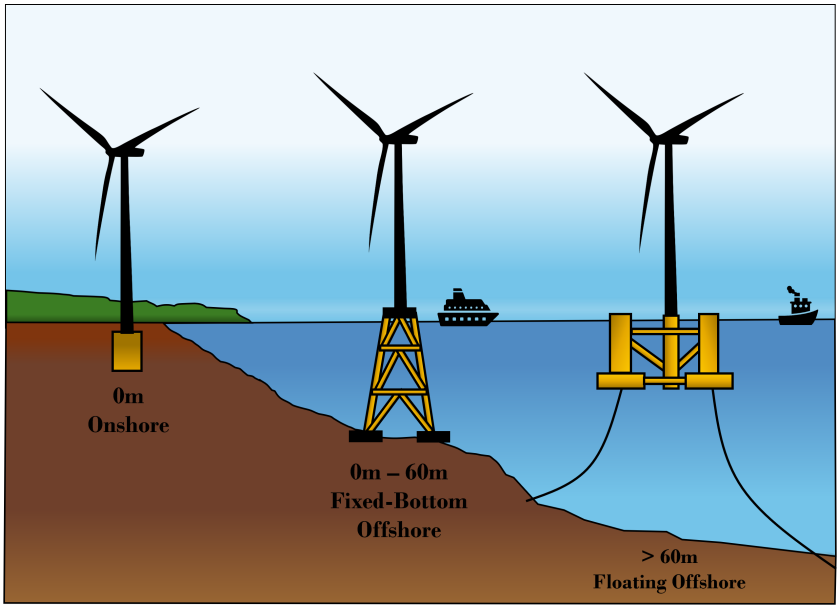

Figure 1.2: Wind Turbines with Different Bottom-mounting Concepts

The design of FOWTs is inherently complex, despite their many advantages. The combined influence of wind, waves, and currents allows the floating platform to move with six degrees of freedom. Moreover, these turbines are subject to a variety of loads, such as aerodynamic loads, hydrodynamic loads, and loads due to the mooring lines used to attach the floating substructure to the sea bed, which adds further to the complexity. The following sections will provide a detailed explanation of the underlying theory of FOWTs and the challenges they encounter.

1.2. Fundamentals of Floating Offshore Wind Turbines

Floating offshore wind turbines are supported by floating substructures constructed from concrete, steel, or a hybrid of both, providing the necessary buoyancy and stability to remain afloat. The floaters are securely anchored to the seabed using mooring lines, ensuring the turbines are held in place while floating on the water surface.

An example of an installed FOWT has been displayed in Figure 1.13, mounted on a semi-submersible floating substructure. The mooring lines, depicted in white, securely anchor the floater to the seabed. The underwater power cables, shown in red, transport the generated electricity to an offshore substation, where the voltage is stepped up. From there, the electricity is transmitted to an onshore substation located on the coast, and finally, power lines distribute this electricity to homes and other end-users.

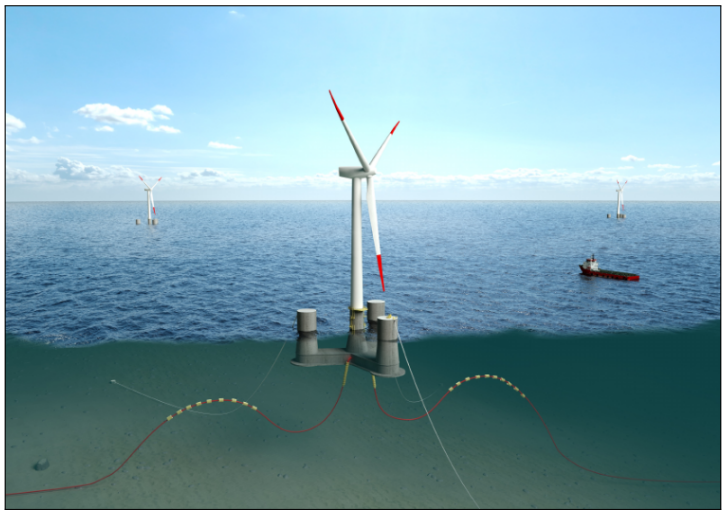

Figure 1.3: DTU 10MW FOWT Mounted on a OO-Star Wind Floater Semi 10MW Floating Substructure [9]

For optimal energy production, floating wind turbines must maintain maximum stability with minimal movement, ensuring ideal inflow conditions. To ensure this, the floater should be able to counteract the thrust and inertial forces, as illustrated in Figure 1.4, from the wind turbine and dampen them to reduce the movement of the whole structure [10].

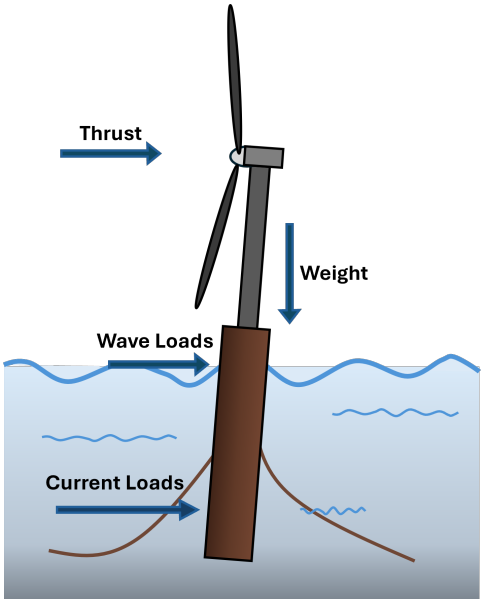

Figure 1.4: Loads on a FOWT (Illustration Adapted from [11])

To achieve this, various types of floating substructures are being designed and developed. There are four general types of floating platforms, each with unique characteristics, as illustrated in Figure 1.5. These categorizations are made based on the approach utilized by a particular floater type to achieve stability.

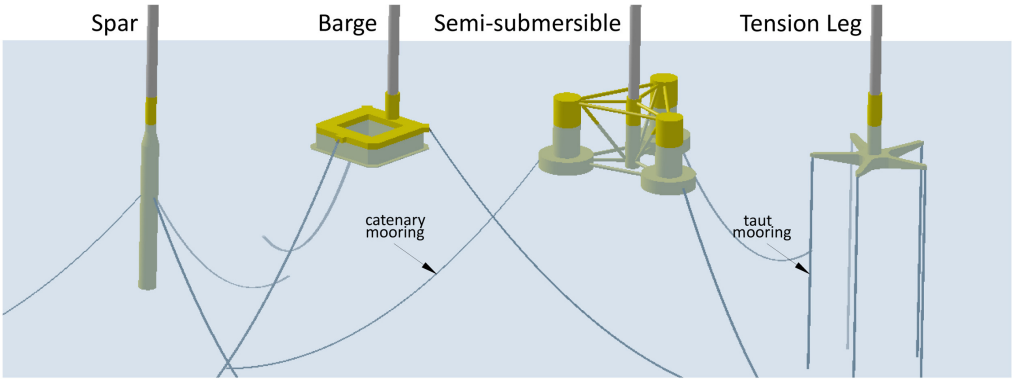

Figure 1.5: Floating Platform Concepts for FOWTs [10]

- **Spar Platform**: Spar platforms use gravity to stabilize the floating turbine. They consist of a vertical cylinder directly connected to the wind turbine tower. The cylinder features a ballast at its base, where most of the weight of the substructure is concentrated, ensuring the turbine remains vertical [10]. The geometry of the cylinder provides buoyancy, while the ballast offers stability. For larger-diameter turbines, longer cylinders are needed to support the weight, which can complicate transportation and installation.
- **Tension-Leg Platform (TLP)**: TLPs consist of a submerged body connected to three to six mooring lines, and a central column connected to the turbine tower. For instance, the Provence Grand Large project by SBM Offshore features the world's first TLP floaters, consisting of three mooring lines [12] connected to the central body. They use mooring stabilization to support the FOWT. This design aims to minimize platform dimensions, thereby reducing manufacturing costs.

- **Barge Platform**: Barge platforms are shallow, wide floating structures. Their large surface area maintains extensive contact with the water, providing stability through waterplane stabilization. Barge platforms are cost-effective for shallow water wind projects but have significant wave-induced motions.
- **Semi-Submersible Platform (Semi-Sub)**: The Semi-submersible floaters feature three to five cylindrical columns interconnected by beams or braces, with the wind turbine tower positioned at the center of the substructure or on the top of one of the columns. They employ both gravity and waterplane stabilization to support the turbine. This design aims to minimize the interaction of the substructure with surface waves, which is especially advantageous in the splash zone where inertial and viscous forces from wave and current loads are more pronounced near the sea surface and diminish with increasing water depth [13].

1.3. Wakes of FOWTs

The reduction in wind speed and the increased turbulence created downstream of a wind turbine, as a consequence of energy extraction from the wind, is termed "wake." This wake propagates and gradually reverts to free-stream conditions further downstream. When the wake intersects the swept area of a downstream turbine, the latter is deemed to be shadowed by the upstream turbine [14]. Wind turbine wakes are generally divided into two regions: the near wake and the far wake, as shown in Figure 1.6. The near wake extends about 2 to 5 rotor diameters downstream and is characterized by sharp velocity gradients and increased turbulence due to tip and root vortices [15]. In this region, a significant velocity deficit creates a shear layer that separates the higher-velocity outer flow from the slower-moving wake core. As the flow moves downstream, this shear layer dissipates, and the wake expands, marking the start of the far wake region. In the far wake, the turbulence intensity increases, mixing the freestream flow with the lower velocity flow in the wake, gradually restoring freestream conditions.

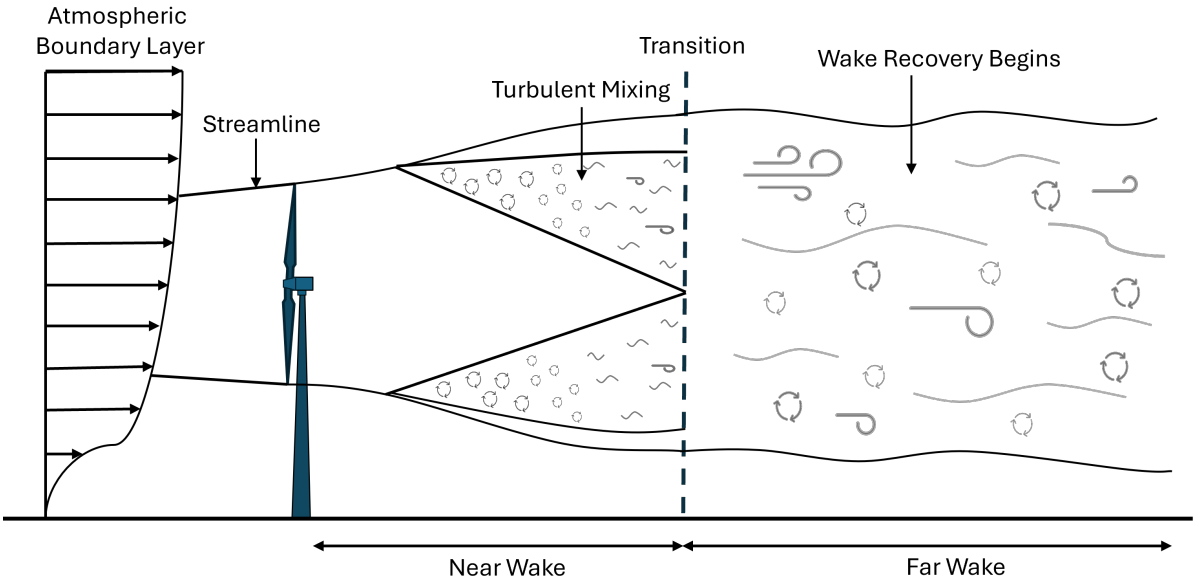

Figure 1.6: Velocity Profile in the near wake and the far wake of a Wind Turbine.

The presence of the wake elevates turbulence levels, resulting in increased dynamic mechanical

loading on the downstream turbines, ultimately raising the Levelized Cost of Energy (LCoE) [16]. Effectively mitigating these wake effects through strategic site selection and optimal arrangement of wind farms has the potential to improve the overall energy output of the wind farm [17]. However, with the growth of the onshore and offshore wind turbine industries, preferred sites for wind farm installation are becoming increasingly saturated, necessitating the proximity of wind farms to one another [18]. This proximity results in inter-farm wake interactions, where the wake produced by an upwind farm adversely affects the power generation capacity of a downwind farm. Studies have shown that wind farm wakes dissipate at a slower rate than individual turbine wakes and can extend their influence up to about 50 km downstream [19]. As wind turbine installations expand into deeper waters, the saturation of onshore sites is alleviated; however, new challenges emerge due to the wake dynamics of Floating Offshore Wind Turbines (FOWTs). These dynamics are further complicated by the interactions of wind, waves, and currents with the substructure, which induce static displacement of the floating turbines from their equilibrium position, in turn, influencing their wake profiles.

Floating offshore wind turbines encounter more intricate aerodynamic behaviors than traditional fixed-bottom turbines, owing to the movement of the floating substructure [20]. The wake dynamics of FOWTs exhibit unsteadiness, which is primarily thought to arise due to these floater motions, which encompass six degrees of freedom (DOF), as illustrated in Figure 1.7.

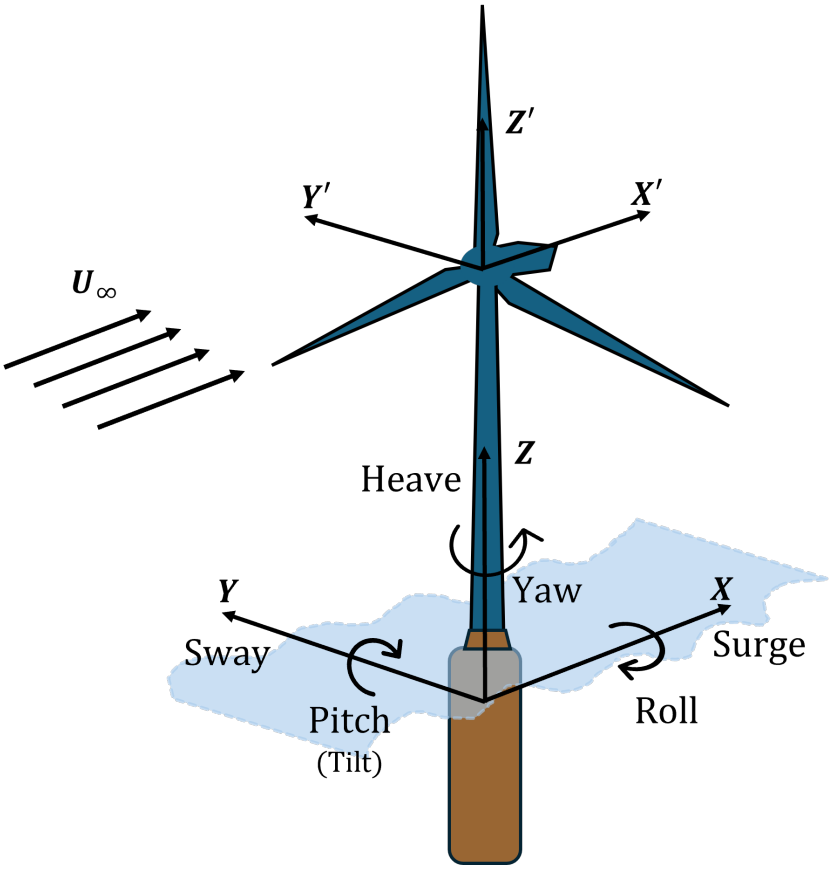

Figure 1.7: Degrees of Freedom for a Floating Offshore Wind Turbine.

These movements are categorized into translational DOFs: heave, sway, and surge; and rotational DOFs: yaw, pitch, and roll. Among the six degrees of freedom of the floater, the turbine experiences significantly greater displacement in the surge and pitch directions compared to

the other degrees of freedom, highlighting their dominant role in the dynamic response of the floating platform [21]. This has also been displayed in Figure 1.8.

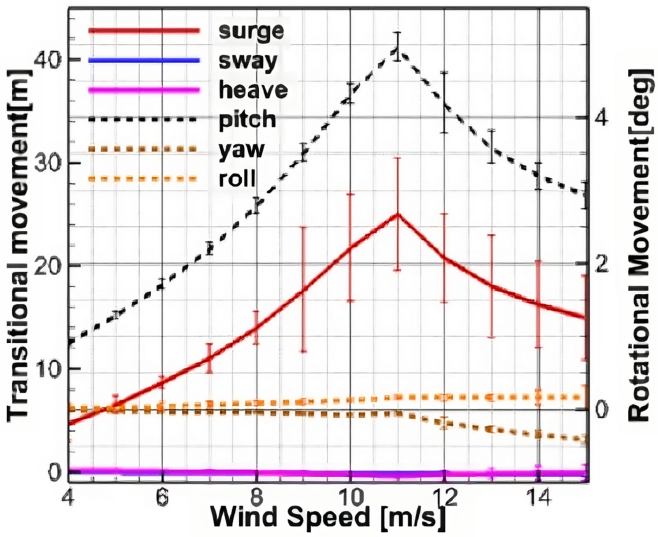

Figure 1.8: Average Platform Displacements with respect to Wind speed [22]

To optimize the energy yield from a wind farm, it is crucial to grasp the implications of wake effects on the power output of wind turbines. According to Shakoor et al. [23] in their study on wake modeling, the wake generated by an upstream turbine can significantly reduce the power output of downstream turbines that fall within the shadow of the upstream turbine's wake. This phenomenon occurs because the wake effect reduces the wind speed available to downstream turbines, decreasing their power generation efficiency. Accurately modeling wake effects is crucial for optimizing wind farm operations. By analyzing turbine wake interactions, developers can design layouts that minimize wake overlap and reduce power losses, improving overall efficiency through strategic turbine positioning.

Wind tunnel experiments using Particle Image Velocimetry (PIV) and Hot-Wire Anemometry (HWA) have shown that the frequency, amplitude, and type of platform motions (pitch and roll) significantly impact the wake symmetry and power output of wind turbines. Fu. et. al. found that these oscillations notably altered the wake symmetry, with roll motions causing the least momentum loss [24]. Similarly, Taruffi et. al. used a 1:148 scaled model of the DTU 10MW wind turbine mounted on a hexapod to simulate 6 DOF motions, revealing that above a threshold frequency of about 4 Hz, the thrust amplitude deviates from quasi-static estimations, indicating clear unsteady effects for single DOF motions at rated wind speeds [25].

Alongside wind tunnel experiments, numerical simulations have also been a common analysis method for understanding the dynamics of floating offshore wind turbines. A study by Danmei Hu et al. analyzed FOWTs under pitch and yaw motions and found that aerodynamic performance is more volatile during pitching compared to yawing [26]. The pitch motion as interpreted by them has been illustrated in Figure 1.9. The tail vortex distribution, which changes over time for both motions, compresses most at the extremes of yaw and pitch movements. The wake becomes increasingly unpredictable and unstable with higher amplitude and frequency of pitch movements, due to stronger interaction between platform motion and incoming wind. Additionally, faster wake recovery was observed with increased movement intensity.

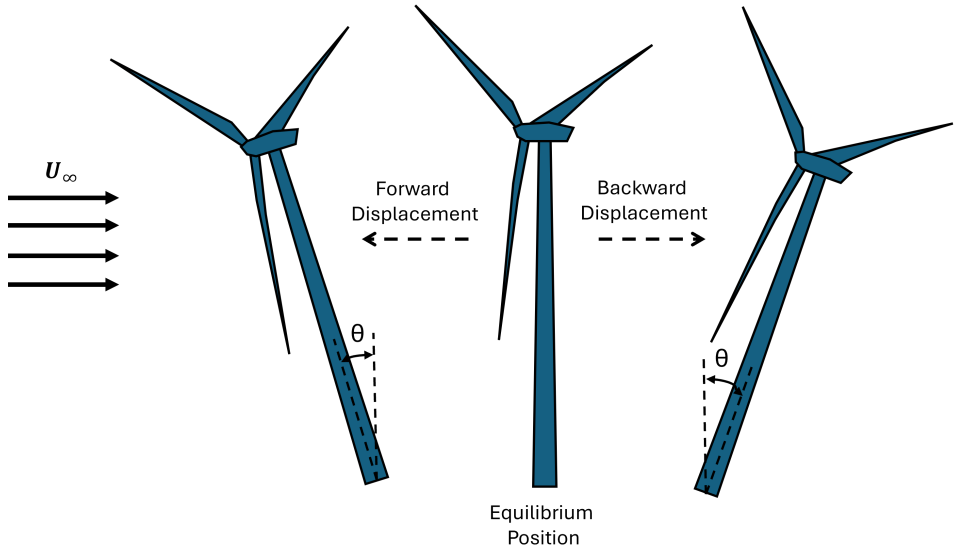

Figure 1.9: Schematic of pitch displacement from the equilibrium position.

The altered wake dynamics impact the performance of downstream turbines, as they encounter reduced wind speeds within the wake of upstream turbines. This reduction affects the power output of each turbine and the overall Annual Energy Production (AEP) of the wind farm. Accurate AEP computation is crucial for estimating the energy production of a wind farm, which in turn is vital for calculating the Levelized Cost of Energy (LCoE), a key metric for assessing the economic feasibility of a wind farm. Therefore, developing advanced design and wake modeling techniques is essential to ensure the efficient and reliable operation of FOWTs, considering the impact of platform motion on turbine performance.

1.4. Wake Modeling

A large number of wind turbine wake models have been developed in the past years to model the wake deficit and to achieve a better understanding of the wake dynamics of wind turbines. There are two major classifications of these wake models: computational or implicit wake models and analytical or empirical or explicit wake models [23].

1.4.1. Computational Models: Medium and High Fidelity Wake Models

Computational models predict wake effects by solving fluid dynamics equations to map the velocity field within the wake region [27, 28, 29, 30]. High-fidelity models are crucial for capturing complex wake interactions in wind farms, as they solve the full set of Navier-Stokes equations to provide a detailed representation of airflow dynamics around and between turbines. These models excel in accurately simulating wake behavior and assessing its influence on wind farm power output. Therefore, despite their significant computational resource and time requirements, high-fidelity models are frequently employed to validate and verify lower-fidelity models. On the other hand, medium-fidelity models strive to strike a balance between computational efficiency and accuracy by employing reduced-order modeling techniques that simplify the Navier-Stokes equations, while still capturing key phenomena such as vortex shedding and wind shear.

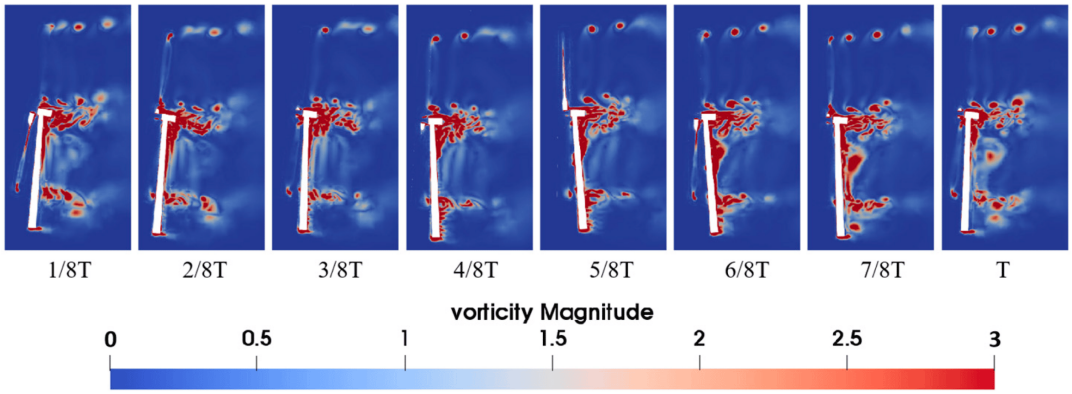

Figure 1.10: Instantaneous Unsteady vorticity contours visualized for a full-scale CFD model of NREL 5MW wind turbine undergoing coupled pitch and surge motion at period T/2 [31]

The most accurate wake prediction methods for floating offshore wind farms are high-fidelity models, such as CFD-based models. Dynamic oscillations of the wind turbine at prescribed motions individual or coupled, as shown in Figure 1.10, can be completely visualized through CFD-based models. A fully coupled aero-hydrodynamic numerical model, FOWT-UALM-SJTU has been developed by [32] using an unsteady actuator line model for aerodynamic simulations coupled with a hydrodynamic simulation model on the CFD tool, OpenFOAM. The coupled simulations were conducted on the NREL-5MW FOWT model, mounted on a semi-submersible platform. This model was capable of computing the unsteady aerodynamic forces, the 6 DOF platform motions, as well as the tension due to the mooring system.

Wise et. al. [33] used the mid-fidelity model, FAST.Farm and simulated a case with two floating offshore wind turbines to investigate the effect of wake meandering in a FOWF. For this analysis, three different types of floating platforms were used: semi-submersible, spar bouy, and TLP. Figure 1.11 shows the wake of a FOWT mounted on a spar buoy platform with and without a 10° pitch misalignment. The wake of the backward-pitched turbine is deflected upwards. The FAST.Farm model is an extension to the NREL OpenFAST model which couples a dynamic wake meandering (DWM) model with an aeroelatic tool [34].

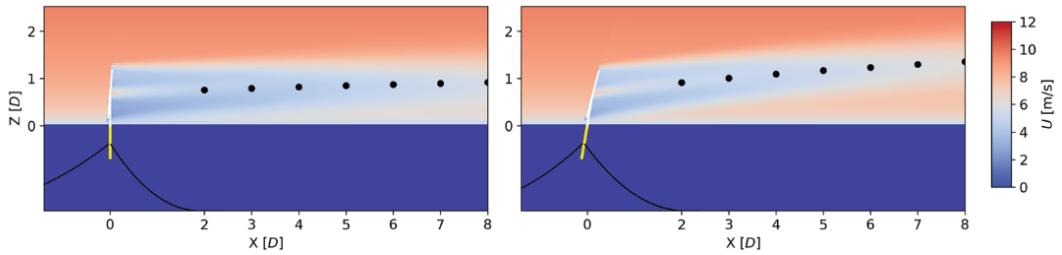

Figure 1.11: Visualization of the wind speed deficit in the wake with and without a 10° pitch [33]

Arabgolarcheh et al. (2022) [35] developed a mid-fidelity CFD-ALM model by integrating Computational Fluid Dynamics (CFD) with the actuator line method (ALM). This model investigates the impact of floating platform motions on wake evolution and the aerodynamic performance of FOWTs. Tested on the NREL 5MW wind turbine, it examines the effects of pitch and surge motions. Unlike the BEM model, the ALM model accurately simulates skewed flow during platform pitching and captures blade-vortex interactions, vortex pairing, and turbulent ring states.

Despite being very accurate in their prediction of the wake due to their high computational efficiency, such high-fidelity and mid-fidelity models are very expensive and take a huge amount of computational time, making them unfeasible for performing multiple simulation tasks such as layout optimization. Therefore, efforts have been made in recent years to develop lower-fidelity models for floating offshore applications.

1.4.2. Analytical Models: Low Fidelity Wake Models

Analytical wake prediction models employ mathematical formulations based on principles of mass conservation to describe wake velocities, or they utilize empirical relationships to account for wake decay, aiming to enhance predictions of power output from wind farms [36, 37, 38, 39]. These models are referred to as low-fidelity models due to their relatively simplified approach, which prioritizes lower computational demands and shorter processing times. By focusing on estimating the energy output without delving into the precise details of the airflow dynamics, these models offer a more efficient, albeit less detailed, method for predicting the performance of wind farms. This streamlined approach allows for quick assessments of energy production potential, making it a valuable tool for preliminary analysis, operational planning and optimization studies in wind energy projects.

In 1983, N.O Jensen developed a low-fidelity wake model, the Jensen model or the Park model [36], which was later modified in 1986 by Katic et. al. [37]. It is one of the oldest kinematic models, which is a far-wake model. This model assumes a linearly expanding turbulent wake behind the turbine and ignores the contribution of vortex shedding as it is significant only in the near wake region. It was based on the conservation of momentum downstream of the wind turbine with a velocity deficit that is only dependent on the distance behind the rotor. The top-hat shape of the NOJ model has been visualized in Figure 1.12.

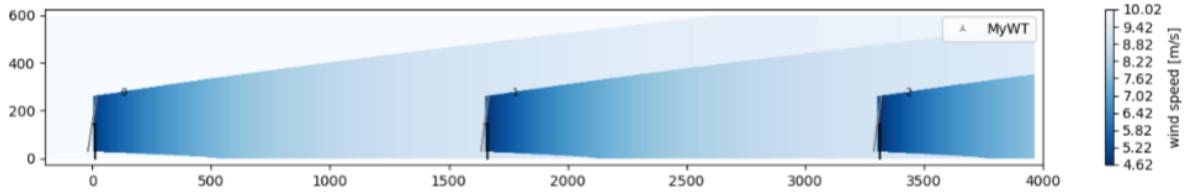

Figure 1.12: Top-hat shaped wake profile of the N.O. Jensen wake model for tilted turbines in PyWake [40]

While low-fidelity wake models that explicitly simulate the performance of Floating Offshore Wind Turbines (FOWTs), accounting for wake losses due to floater displacements, are not yet available, several studies have attempted to adapt existing wake models for this purpose. One such example is a comprehensive low-fidelity wake model developed in MATLAB to optimize the layout of floating offshore wind farms across four Mediterranean island sites, with the objective of minimizing the Levelized Cost of Energy (LCoE) [41]. This model assumed the turbines to be stationary and employed the Jensen kinematic model to calculate wake losses, alongside an area overlap method to evaluate shadowing effects from upstream turbines on downstream turbines. It also used a sum-of-squares approach to assess cumulative wake interactions from all upstream turbines. The accuracy of the model's results was validated by comparing them with those from PyWake, a wake loss simulation tool developed by the Technical University of Denmark (DTU) [42], as the effects of the substructure displacement were considered negligible for this analysis.

Wang et. al. [43] developed a low-fidelity 3D analytical wake prediction method, which is based on the Gaussian wake loss model by Bastankhah et. al. [44]. It includes a modification

to the incoming wind flow velocity of the Gaussian model by taking into account the velocity induced due to platform motions and environmental factors. This model takes into account the effect of wind shear, tower shadow, tilt angle, surge motion as well as turbulence, thus making it suitable for application to FOWTs. The expression for the new incoming wind velocity and the derived wake velocity expression derived in this research were validated using the measurements from the experiment on the NREL 5MW conducted in the AABL wind tunnel at ISU [45]. The predicted wind flow distribution at a distance of 2.5D and 5D have been demonstrated in Figure 1.13. They concluded that the incoming wind disturbances considered in this research significantly influence the wake, and are thus indispensable while modeling wake prediction.

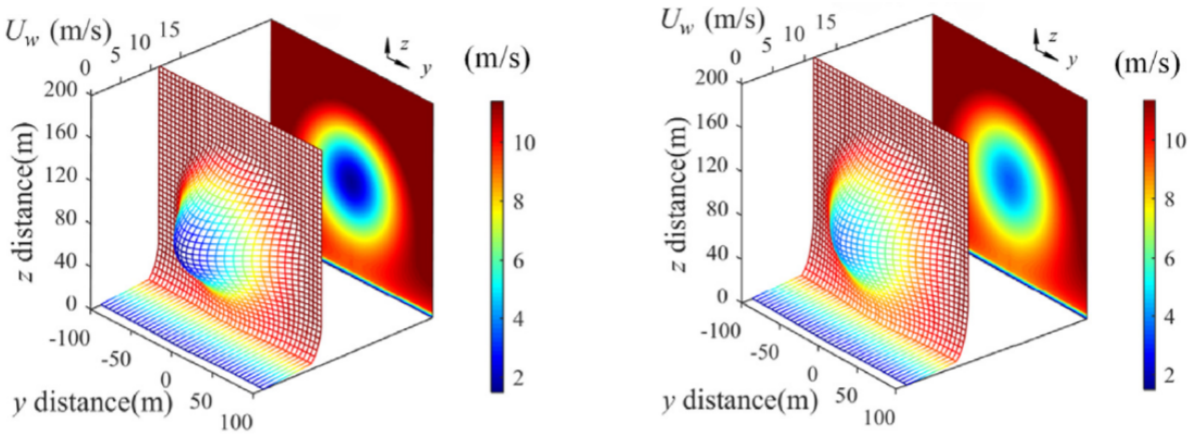

(a) x = 2.5D **(b)** x = 5D

Figure 1.13: Predicted velocity distribution in the YZ plane at an x location of a) 2.5D and b) 5D from the turbine [43]

Leikvoll investigated the losses due to static tilt and its impact on the power performance of FOWTs in their study [40]. Two different wind farm layouts were simulated: a three-turbine farm and a 10 × 10 farm, by modifying PyWake to incorporate the static tilt of the FOWTs based on wind speed using the Bastankhah Gaussian and Jensen wake models. An extension was added to PyWake, enabling it to calculate the tilt according to the incoming wind speed using an external floating platform motion data. The study analyzed power losses, the effect on AEP, and tilt loss with variable turbine spacing for the different wake models and wind farm layouts. The findings highlighted that the appropriate selection of the wake model and an optimal wind farm layout is crucial in minimizing wake losses due to tilt in floating offshore wind farms (FOWFs).

Riva et al. investigated a method to incorporate all degrees of freedom (DOF) motions of the floating platform into the static wind farm simulator, PyWake, in their study [46]. Using HAWC2 simulations of a floating offshore wind turbine model of the IEA 15MW turbine with the WindCrete spar-buoy floater, an artificial neural network-based surrogate model was trained. This model outputs the static floater displacements (averaged in the final periods of the simulation) based on inputs of wind speed, wind direction, current speed, and current direction, with a uniform distribution. These static DOFs were then input into PyWake to compute the power production and AEP of the wind farm. The Gaussian wake deficit model in PyWake was used in combination with the CGI Rotor average model and the Jimenez wake deflection model. The flow map of the side and front view of the flow field have been displayed in Figure 1.14, where the upward and downward deflection of the wake can be observed according

to the rotor tilt angle. The study concluded that the AEP of the wind farm increases by about 0.07% to 0.08% compared to a fixed-bottom farm, depending on the combination of wind and current speed and direction. The effect of wave loads was considered negligible in this study.

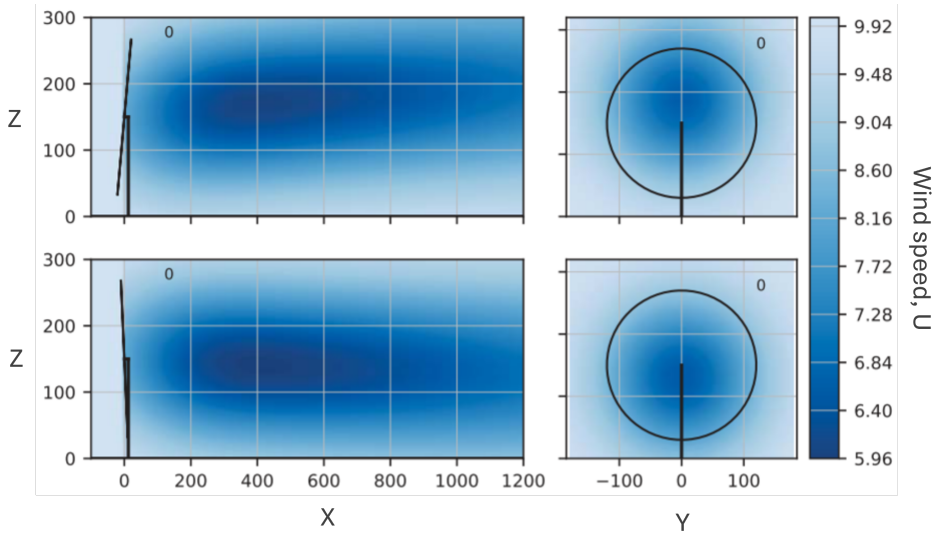

Figure 1.14: Wind speed in the flow field of a wind turbine at a pitch of 10° (top) and −5° (bottom). The wind speed displayed in the front view is computed at 4D behind the turbine [46]

The existing literature indicates that while experimental setups and high-fidelity simulation tools offer the most accurate wake modeling capabilities for FOWFs, their application in design processes, particularly in iterative procedures like multidisciplinary optimization, is often too computationally expensive. Therefore, transitioning to low-fidelity wake modeling tools which are computationally efficient becomes essential for preliminary design and optimization tasks.

Several low-fidelity wake modeling tools, such as PyWake and FLORIS, along with their respective adaptations to incorporate floater movements, have been developed as practical alternatives for simulating wake effects in floating offshore wind farms. Despite their potential, there is a lack of comprehensive evaluation regarding the effectiveness of incorporating floater displacements for optimizing wind farm layouts using these models. Specifically, the extent to which including the equilibrium displacements of the floater impacts the AEP and thus the LCoE of a floating offshore wind farm remains underexplored. Additionally, there has been limited research on determining which specific degree of freedom, such as surge, pitch, heave, etc., exerts the greatest influence on the resulting optimized wind farm layout. Addressing these gaps is crucial for enhancing the accuracy of optimization studies and ensuring more effective wind farm designs tailored to floating offshore environments.

1.5. Research Formulation

1.5.1. Problem Statement

Floating Offshore Wind Turbines (FOWTs) are mounted on dynamic substructures that undergo movements due to various loads encountered due to the waves, and ocean currents, as discussed in the preceding sections. These forces cause the floater to move in six Degrees of Freedom (DOFs), introducing complexities that affect the wake profiles generated downstream of the turbines. Unlike fixed-bottom wind turbines, where wake deflection is typically achieved through active control strategies, the natural displacement of the floating substructures can inherently deflect wake profiles. This displacement can impact the energy production of the

wind farm, either positively or negatively, as downstream turbines may experience varying wind speeds depending on their exposure to the wake of upstream turbines. Consequently, this can influence power generation across the entire wind farm, ultimately affecting the Levelized Cost of Energy (LCoE).

Despite the potential importance of these effects, research on the extent to which static floating turbine displacements impact energy production and the optimal layout configuration of a floating offshore wind farm remains limited. Specifically, it is uncertain whether accounting for these displacements for AEP analysis meaningfully influences optimization parameters and results in a minimized LCoE for the optimal layout.

This leads to the primary problem statement of this thesis:

Is it important to account for the effects of the floating wind turbines' displaced equilibrium positions on the AEP when optimizing the wind farm layout for minimizing the LCoE?

Furthermore, to quantify the impact of floater displacements, there is a need for low-fidelity wake models that can effectively simulate the wake of floating wind turbines. While high- and medium-fidelity models have been employed in prior studies for energy production assessments, they are not computationally efficient for use in multidisciplinary optimization. Thus, a low-fidelity wake model is needed that incorporates the static displacements of floating turbine substructures for AEP computation that can be integrated into an MDAO framework.

1.5.2. Research Questions

To explore the problem statement, specific research questions have been developed to guide each phase of the thesis. These questions have been structured to address the primary objectives of the study and are outlined as follows:

RQ1: What strategy can be employed to adapt PyWake for modeling static equilibrium displacements of the floating wind turbine, specifically in the tilt and surge DOFs?

PyWake is a Python-based tool designed for steady-state wind farm simulations. It includes various engineering wake models that can be employed to study wake characteristics and estimate the AEP. Currently, PyWake assumes floater displacements to be negligible, making it suitable only for fixed-bottom wind farms. However, owing to its adaptable and modular architecture, it is possible to extend its applicability to floating offshore wind farms. Leveraging this, a strategy for modeling static tilt and surge floater displacements using PyWake has been explored in this thesis.

RQ2: What are the observable variances in the computed AEP for FOWFs when accounting for or neglecting floating turbine displacements, and what are the primary causes of these deviations?

The power output of a floating offshore wind farm can be influenced by wake deflection resulting from floater movements, in contrast to a fixed-bottom wind farm. This is because power is proportional to the cube of the x-component of wind speed (U). For a turbine without

structural tilt or floater displacements, this x-component is simply U. However, for a turbine undergoing tilt displacement, this component is given by Equation 1.1, potentially affecting the power, depending on the magnitude of the tilt angle (denoted by θ). This causes the wake to deflect vertically, consequently leading to variations in the AEP of the wind farm. The extent of these variations, along with the underlying causes, have been investigated in this study.

$$U_x = U \cos\theta \tag{1.1}$$

RQ3: What are the differences in the optimal wind farm configuration obtained when accounting for static tilt and surge vs not accounting for it?

Incorporating floater displacements, such as tilt and surge, may lead to variations in the optimal wind farm layout. To assess the magnitude of these differences, this study performs an optimization of the wind farm layout in two scenarios: one that includes floater displacements and one that does not. The resulting optimization parameters and design variables have been analyzed and compared to determine the extent of the impact these displacements have on the optimal wind farm configuration.

RQ4: How does the incorporation of static floater displacements in the optimization framework impact the LCoE of the wind farm?

The Levelized Cost of Energy (LCoE) is directly influenced by the Annual Energy Production (AEP) of the wind farm. Consequently, any impact of floater movements on the AEP will also affect the LCoE. Additionally, accounting for wake losses induced due to floater displacements may alter other parameters within the optimization framework, such as substructure design and cable topology, which changes according to the placement of turbines in the optimal layout. This, in turn, could further influence the minimized LCoE achieved for the optimal configuration. This study will quantify the effect of accounting for these displacements on the LCoE to understand their broader implications on cost efficiency.

1.5.3. Approach

To address these research questions, an approach that incorporates tilt and surge displacements of the FOWTs' substructure has been integrated into the wake modeling library, PyWake. The accuracy and efficiency of this implementation have been verified against two existing approaches from the literature. This enhanced wake modeling approach has then been integrated into the AEP computation module of an OpenMDAO-based framework for the multidisciplinary optimization of FOWFs aiming the minimization of the LCoE. Two scenarios have been investigated: one that accounts for the displaced equilibrium positions of the floater and the other that neglects them. The results from these two cases have been compared extensively to understand the impacts of these considerations on energy production and the optimal layout design of the wind farm which leads to the minimum LCoE.

1.6. Report Structure

This section provides an overview of the upcoming thesis structure, outlining the key content and summarizes the focus of each chapter:

- **Chapter 2**:
  A brief introduction to the PyWake framework and an outline of the approach used

to integrate static floater displacements, into the AEP computation process have been provided in this chapter.

- **Chapter 3**:
  In this chapter, the results from the PyWake implementation have been verified by comparing them with two established models from the literature to ensure the accuracy and reliability of the approach.
- **Chapter 4**:
  This chapter outlines the methodology for incorporating the floater displacements into the optimization framework and describes the multi-disciplinary optimization process used to minimize the LCoE of the wind farm.
- **Chapter 5**:
  This chapter presents the results from the optimization study and provides a comparative analysis between the two cases: neglecting and accounting for floater displacements.
- **Chapter 6**:
  This final chapter provides a synopsis of the key findings from this thesis and presents recommendations for future work and development based on the insights gained from the study.

2

Incorporation of Static Floater Motions in PyWake

2.1. Introduction to PyWake

PyWake is a Python-based wake modeling library developed at the Technical University of Denmark (DTU) for simulating wind farm flows and evaluating the performance of wind turbines in a farm setting [42]. It encompasses several established models for wake deficit, wake deflection, superposition, and rotor averaging, allowing for flexible analysis of wind farm behavior under different conditions. This section provides a brief description of PyWake's architecture.

The central component in PyWake is the `WindFarmModel`. It receives the initial reference wind conditions and turbulence intensity from the `Site` object, while the `WindTurbines` object supplies the wind turbine geometry along with the power and thrust coefficient curves. The workflow of the `WindFarmModel` object has been demonstrated in Figure 2.1. As output, it returns the object, `SimulationResults`, which contains a dataset of the computed effective wind speed (WS_{eff}), power data, and thrust coefficient of every turbine in the wind farm.

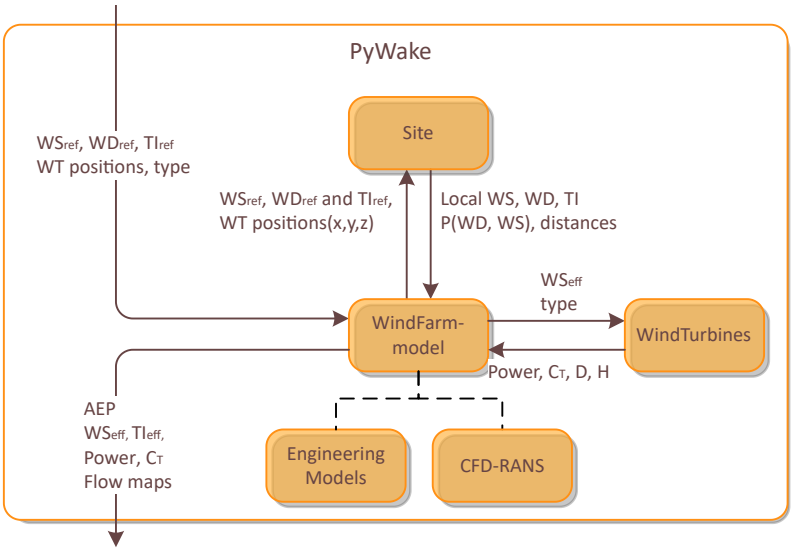

Figure 2.1: PyWake Architecture Flow Chart [42]

Two primary engineering wind farm models are central to PyWake: `PropagateDownwind` and `All2AllIterative`. The `PropagateDownwind` model calculates the wake effects propagating downstream without considering blockage effects, making it faster but less comprehensive. It iterates over turbines in downstream order, updating the effective wind speed and calculating the wake deficits sequentially. In contrast, the `All2AllIterative` model includes blockage effects by iterating through turbines multiple times until the effective wind speeds converge, which is computationally intensive but more accurate.

These wind farm models can be combined with various other engineering models in PyWake to simulate complex wind farm behaviors. Figure 2.2 demonstrates the engineering models incorporated within the PyWake library. This includes wake deficit models that calculate the reduction in wind speed due to turbine wakes, superposition models that define how deficits from multiple turbines add up, blockage deficit models that account for upstream wind speed reductions, and turbulence models that describe the added turbulence downstream of turbines. Additionally, rotor average models can be used to calculate the average wind speed over the rotor area, and deflection models can account for wake deflection due to factors like yaw or pitch misalignment and sheared inflow.

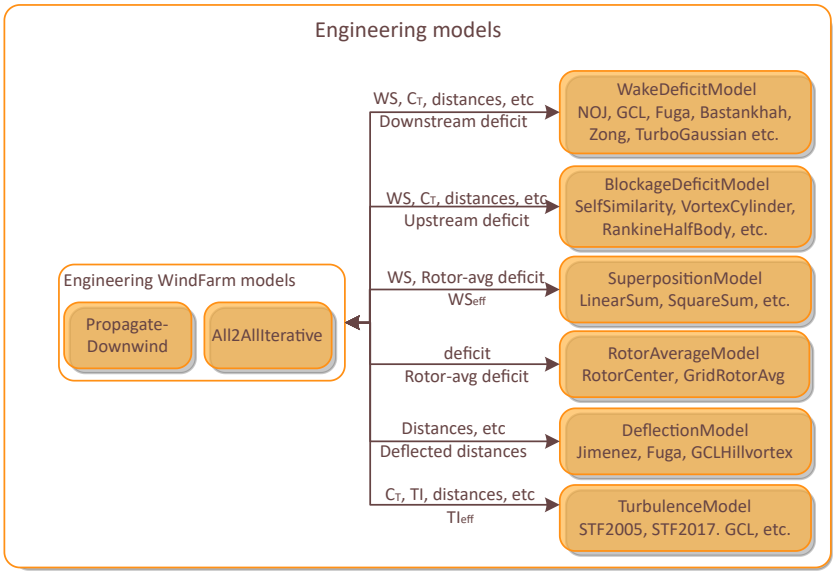

Figure 2.2: Engineering Wake Models Available within PyWake [42]

2.2. Static Floater Displacements of FOWTs

This thesis specifically considers two degrees of freedom of the floater: tilt and surge. The variations in tilt and surge are assumed to be dependent solely on wind speed and direction. Factors such as current speed and direction, as well as waves, are considered negligible for this analysis.

2.2.1. Tilt

Tilt refers to the rotation of the floating platform around its transverse axis (Y-axis), as shown in Figure 2.3a. In this context, backward pitching or heeling of the turbine is considered positive, while forward pitching is considered negative. When the turbine heels backward at a tilt angle of $+\theta°$, as shown in the figure, the wake is deflected vertically upwards. Conversely, forward heeling of the turbine leads to a vertically downward wake deflection.

This thesis investigates the effect of static tilt of the wind turbine, defined as the forward or backward pitching of the turbine and its substructure as a whole caused by average loads. To simplify integration with the PyWake framework, only the rotor's tilt is considered to represent this static tilt, while the turbine tower and the substrcure are assumed to remain in their non-displaced equilibrum positions. It has been further assumed that the tower does not interfere with the wake profile of the turbine. This simplification has been visually represented in Figure 2.3b.

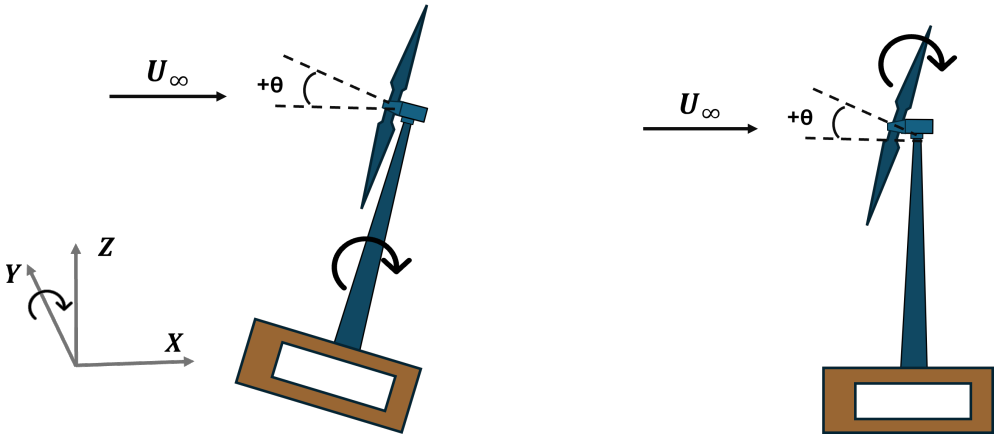

(a) Actual Static Tilt of a FOWT **(b)** Rotor Tilt of a FOWT

Figure 2.3: Illustrations of floating offshore wind turbines depicting a) Actual static tilt of the turbine and the substructure, b) Rotor tilt considered for integration with PyWake.

2.2.2. Surge

Surge refers to the horizontal displacement of a wind turbine along the X-axis in both the upwind and downwind directions. The downwind displacement of the turbine caused by a positive thrust force has been displayed in Figure 2.4. This motion impacts the wind speed in the wake region behind the turbine, as the turbine's backward displacement shifts the wake downstream.

In the figure, WT1 and WT2 represent the initial, undisplaced positions of the turbines, while WT1' and WT2' denote their displaced equilibrium positions under the influence of a constant thrust force. For a fixed-bottom wind farm, WT1, operating in freestream wind conditions (U_∞), produces a wake (shown in blue), which subsequently interacts with the downstream turbine WT2, reducing the wind speed experienced by WT2 to U_2 due to the wake of WT1.

However, in the case of a floating wind farm, the turbines will displace along the X-axis either upwind or downwind. In this scenario, the surge displacement of the downstream turbine WT2, denoted as b, is smaller than the surge displacement of the upstream turbine WT1, denoted as a. As a result, the distance between the displaced equilibrium positions of the turbines, X_2, is reduced compared to the original distance X_1, between their initial equilibrium positions.

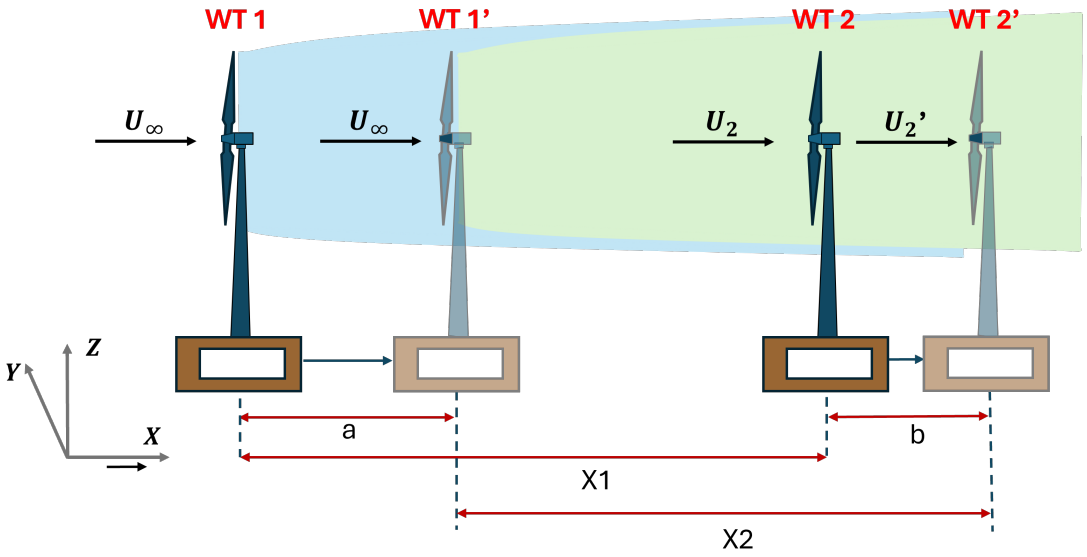

Figure 2.4: Illustration of the impact of surge motion on the wind speed and the distance between turbines. Blue colour demonstrates the original layout and green demonstrates turbines after surge.

2.3. PyWake for FOWTs

The methodology adopted to develop a wake model with static tilt and surge displacements of the floater using PyWake has been illustrated in the form of a flowchart in Figure 2.5.

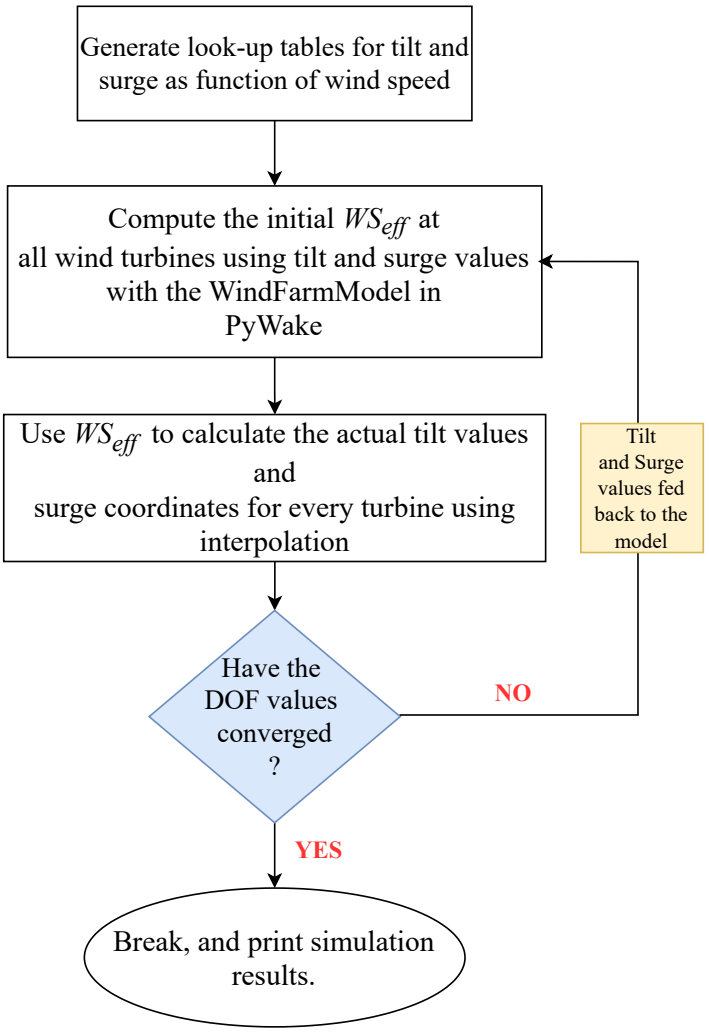

Figure 2.5: A Flowchart of the Methodology to Compute the AEP of a FOWF using PyWake

The methodology begins with the generation of tilt and surge look-up tables as a function of wind speed. The tilt and surge values are interpolated from these look up tables with the effective wind speed (WS_{eff}) at the hub height for each wind turbine of the wind farm to determine its tilt and surge displacement with respect to the initial position. The tilt and surge values depend on both the wind turbine and the selected substructure design. Then the look-up tables are passed to the `WindFarmModel` block within the PyWake framework. Here, the wake modeling is executed using the Jimenez wake deflection model, a wake deficit model, and a rotor-average model.

The next step involves the initial estimation of the effective wind speed, denoted as WS_{eff}, based on the tilt and surge values corresponding to freestream wind conditions from the look-up tables. This initial WS_{eff} is then used to compute updated tilt and surge values through interpolation on the look-up tables. Following this, a convergence check is performed to determine if the values for the floater's motion have stabilized. If the DOF values converge, indicating that the computed tilt and surge align with the initial estimates used for calculating WS_{eff}, the loop terminates, and the final tilt and surge values for the turbines in the wind farm are yeilded as an output of the module.

If convergence is not achieved, the updated tilt and surge values are fed back into the process

as new initial estimates for effective wind speed. This iterative procedure continues until convergence, ensuring the computed floater motion values are consistent with the simulated local wind conditions. Once convergence is attained, the `WindFarmModel` is invoked again, with the updated surge displacements and tilt values input for all wind directions and wind speeds. This process generates the power output for each turbine corresponding to each wind direction and speed. The resultant power is then utilized to calculate the Annual Energy Production (AEP) for the wind farm by summation of the power for all wind turbines at all wind speeds and directions multiplied by the probability of occurence, as described in Equation 2.1. In this equation, i, j, and k represent the turbine number, wind direction, and wind speed, respectively. The variable P represents the power output generated by each turbine under the specified conditions. f indicates the probability of occurrence for a particular wind speed and wind direction bins, and T indicates the total time period of one year, quantified as 24×365.

$$AEP = \sum_{i} \sum_{j} \sum_{k} \frac{P_{i,j,k} \times f_{i,j,k}}{T_{year}} \tag{2.1}$$

This methodology forms the foundation for the subsequent research presented in this thesis. In Chapter 3, the model has been applied to two distinct case studies, which also serves to verify its correct implementation. Once the correct implementation of the model is verified, it is integrated into a multidisciplinary optimization framework, the details of which are elaborated upon in the subsequent chapters of this thesis.

3

Model Verification: Comparative Analysis with Literature

3.1. Verification: Case 1

The integration of static tilt motion in PyWake for the AEP computation of floating offshore wind farms (FOWFs) has been verified against the approach presented by Leikvoll et al. [40], which employs a similar method for incorporating tilt motion as used in this thesis. In their study, only the static tilt displacement of the FOWT was modeled using a look-up table with turbine tilt angles corresponding to various wind speeds. The Jimenez wake deflection model within PyWake was applied to account for the impact of tilt on the turbine's wake behavior. Since their model does not consider surge, the verification was limited to the tilt displacement. The objective of this comparison is to ensure that the implementation of static tilt motion in PyWake, as applied in this thesis, aligns with the established methodology outlined in the literature.

3.1.1. Wind Farm Setup

Multiple three turbine wind farm setups have been used in the benchmark paper [40], but for the verification, a three turbine array, the side view of which has been shown in Figure 3.1, was chosen. The wind turbine used here is a 15MW wind turbine with a rotor diameter of 236m and a hub height of 144m. The turbines have a spacing of 7 times the diameter between them. The turbine and wind farm parameters, adapted from the paper, have been tabulated in Table 3.1.

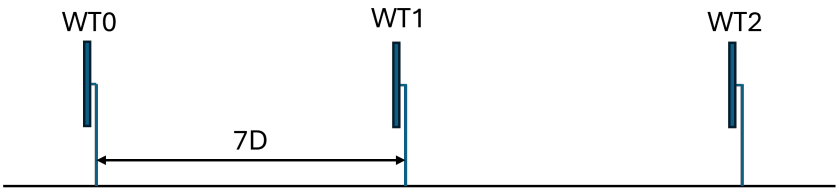

Figure 3.1: Three Turbine Wind Farm Setup

Parameter	Unit	Value
Wind Turbine	-	NREL 5 MW
Rotor Diameter	m	236
Hub Height	m	144
Rated Power	MW	15
Rated Wind Speed	m/s	11
Tip Speed	m/s	104
Specific Power	W/m^2	343
No. of Wind Turbines	-	3
Layout Spacing	m	$7D$
Turbulence Intensity	-	6%

Table 3.1: Verification Case-1 Wind farm setup: Wind Turbine and Site Parameters

3.1.2. Results: Fixed vs Floating Farm

In this section, the power results for both fixed-bottom and floating offshore wind farms, obtained through the modified PyWake model, have been compared with the findings reported in the literature by [40]. The results, corresponding to a wind speed of 11 m/s and a wind direction of 270°, have been summarized in Table 3.2 for comparison.

Wind Turbine	Power (MW) of Fixed Farm		Power (MW) of Floating Farm (Tilt)		% Gain or Loss	
	Simulation	Reference	Simulation	Reference	Simulation	Reference
WT0	14.71	14.709	14.416	14.414	-1.99%	-2.01%
WT1	7.84	7.84	8.37	8.2	6.81%	4.69%
WT2	6.52	6.52	7.07	7.27	8.55%	11.56%

Table 3.2: Comparison of Power between the Fixed and Floating wind farms

The table shows that no variation in power output has been observed for the fixed-bottom farm configuration in the simulation compared to the reference. This is because PyWake was applied to the same wind farm setup as the paper without any modifications or enhancements for this case. The next column displays the power generated by the turbines in the floating farm setup, where tilt displacement is allowed for the turbine, specifically tilt. Slight discrepancies compared to the reference paper have been observed in this case. These differences can be attributed to subtle variations in the method used to compute the floater motions for the simulation. Additionally, the look-up table generated for this study may differ slightly from the one used in the reference paper. As actual data was unavailable, a plot digitizer was employed to extract tilt values from the paper as a function of wind speed. The look-up table used has been displayed in Figure 3.2.

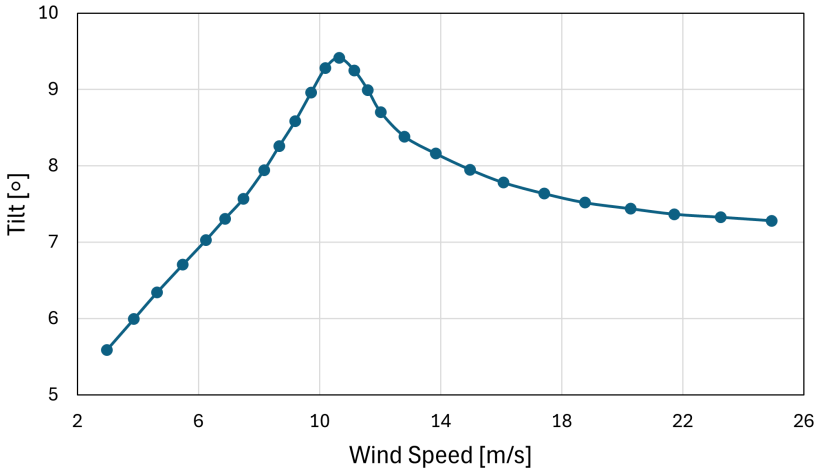

Figure 3.2: Tilt as a function of wind speed computed for Verification

The power output of the first wind turbine (WT0), which is directly exposed to the freestream wind, is the highest, whereas the power output decreases progressively for the subsequent turbines. As in the benchmark study, the power generated by the upstream wind turbine when accounting for tilt is lower than in the case when the thrust-induced tilt displacement is neglected. This variation is due to the relation between the tilt and the freestream wind speed and the effect this has on the power output. WT0, which faces the full freestream wind, tilts by approximately 9°, resulting in reduced power generation compared to the non-tilted scenario. However, this tilt causes the wake generated by WT0 to deflect upward, meaning that the downstream turbine, WT1 is only partially being subjected to the wake. Consequently, the effective wind speed experienced by the downstream wind turbine is higher than in the case when the tilt displacement is neglected, and the wind turbine generates more power than in the fixed configuration.

The power output of the three wind turbines as a function of freestream wind speed in both accounting for and neglecting tilt configurations have been presented in Figure 3.3. WT0, the first turbine, reaches its rated power of 15 MW at a lower wind speed than the downstream turbines, WT1 and WT2, which attain maximum power at higher wind speeds. Notably, the floating WT0 reaches its maximum power output at a slightly higher wind speed compared to the fixed WT0, which achieves 15 MW at the rated wind speed. In contrast, for WT1 and WT2, the floating configuration produces slightly higher power output than the fixed setup before reaching their rated power.

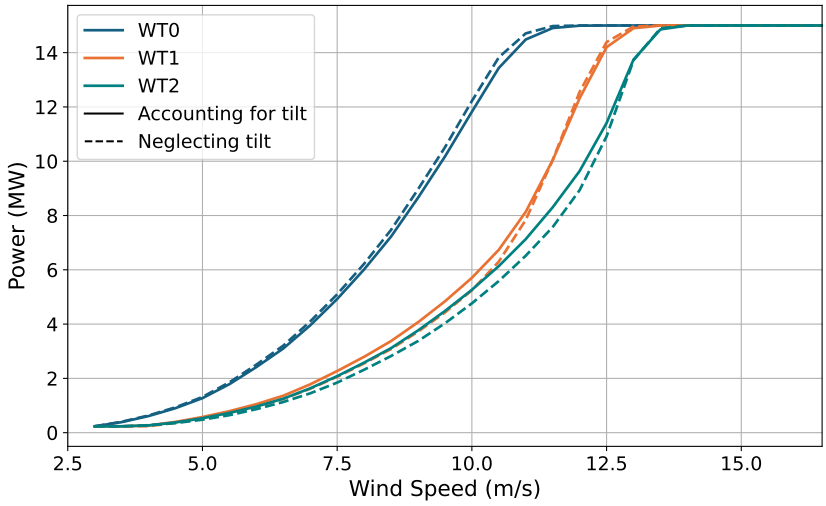

Figure 3.3: Plot of power output vs wind speed for the Fixed vs Floating farm

To compare with the reference paper results, the differences in power generation between the two configurations, as computed in the simulations, have been plotted alongside the reference results in Figure 3.4. The percentage differences are largely consistent, with only minor discrepancies observed.

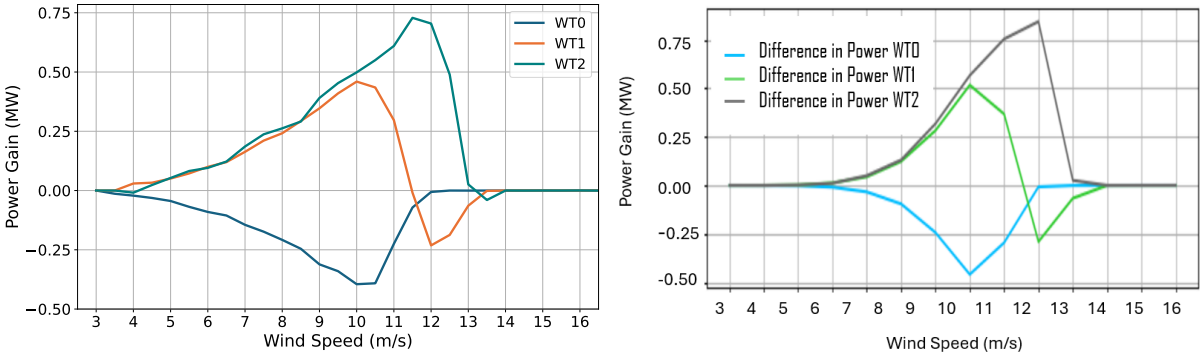

(a) Power Gain: Simulation

(b) Power Gain: Reference [40]

Figure 3.4: Comparison of power gain for each turbine from the a) Simulation with the b) Reference

It should be noted that, for this verification case, a constant wind speed across the entire rotor disc has been assumed, based on the wind speed at the hub height of the turbine or the center of the rotor. As a result, even a small deflection of the wake from the centerline can lead to a greater increase in power output compared to a scenario where more points across the rotor-swept area will be used to compute the rotor-averaged wind speed, which would provide a more realistic representation of the turbine's performance.

3.1.3. Flow Maps

Flow maps were generated to illustrate the wake dynamics behind the wind turbines and the static displacements of the FOWTs for both configurations. The side (XZ) and top (XY) views of the wind farm have been presented in Figure 3.5, and Figure 3.6, respectively. In these maps, the turbine tower is represented by a black line, while the rotor is depicted as a gray line. The blue contours downstream indicate varying wind speeds within the wake, with darker

shades signifying lower wind speeds, primarily concentrated in the core of the wake. As the wind moves further downstream, the speed gradually recovers towards freestream conditions, represented by the lighter shades. However, before full recovery occurs, the wind encounters another downstream turbine, which is affected by this wind speed deficit.

In the fixed-bottom case, this reduced wind speed does not alter the rotor configuration, leaving the wake undeflected. In contrast, when floater displacements are taken into account, as shown in Figure 3.5b and Figure 3.6b, the rotor pitches backward, leading to wake deflection. WT0 exhibits a greater tilt compared to WT1 and WT2, with WT1 experiencing more tilt than WT2, due to the varying local wind speeds, which influence the thrust on each turbine.

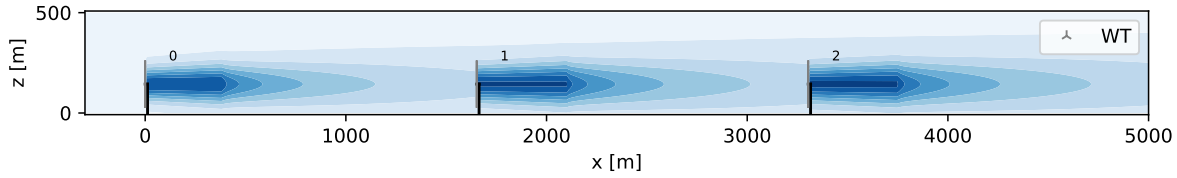

(a) Fixed Wind Farm

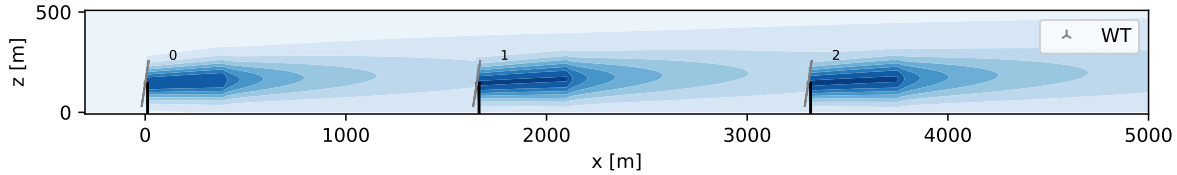

(b) Floating Wind Farm

Figure 3.5: Side view (XZ) Flow Maps for the a) Fixed and b) Floating Wind Farm Case

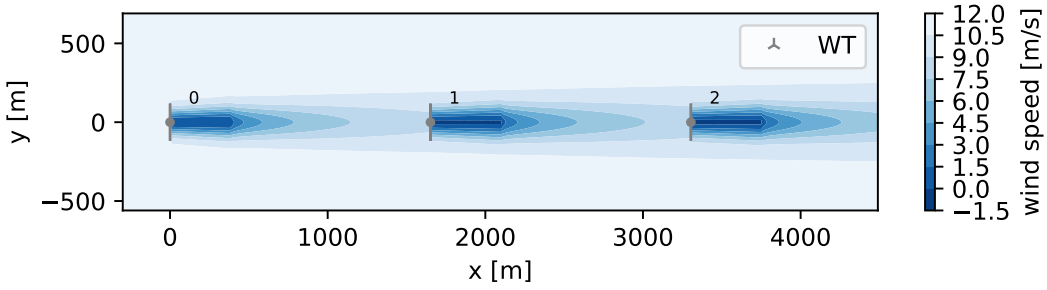

(a) Fixed Wind Farm

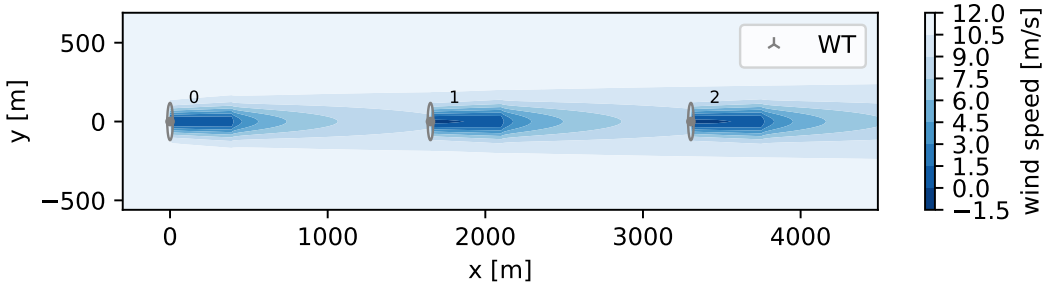

(b) Floating Wind Farm

Figure 3.6: Top View (XY) Flow Maps for the a) Fixed and b) Floating Wind Farm Case

3.2. Verification: Case 2

A second verification has been conducted to further assess the FOWF wake modeling strategy which accounts for static floater displacements by comparing its results with a more advanced model from the literature. For this case, the study by Riva et al. on the integration of floater motions into the PyWake framework has been selected [46]. In this benchmark model, the computation of floater motions has been incorporated into PyWake through a block called `'InputModifierModel'`, which takes the local wind and current speeds and directions, along with turbine positions, as inputs and provides the averaged equilibrium displacements of the turbines. The `'InputModifierModel'` block hosts a surrogate model, coupled with HAWC2, an aeroelastic solver, to compute the floater degrees of freedom (DOFs).

For the verification process, an initial simulation of a bottom-fixed wind farm has been conducted and compared with the reference results. This establishes a baseline and confirms the correct functionality of the PyWake model without incorporating any modifications for floater motions. Subsequently, the PyWake model was applied to simulate the tilt and surge motions individually, followed by a combined simulation of both motions to evaluate the impact of each degree of freedom. These floating configurations have also been compared with the reference results, to determine which configuration yields the most comparable outcomes.

It is, however, important to note that the methods, assumptions, and considerations used in the reference paper differ significantly from those adopted in this thesis. The reference model employs an external medium-fidelity model, and a surrogate model to compute equilibrium displacements of the floater in all degrees of freedom. This verification adapts only the tilt and surge look-up tables from the curves provided in the reference paper and compares the power outputs computed using the low fidelity approach of this thesis with those in the paper. Moreover, current speed, and direction, considered in the reference have been neglected for this verification process. Consequently, the results may not be directly comparable, but an estimate of the extent to which they diverge from a higher-fidelity model that incorporates additional DOFs has been provided.

3.2.1. Wind Farm Setup

The wind farm and wind turbine setup adapted from the reference paper have been described in this section. The wind farm consists of four IEA 15MW wind turbines, separated by 5 times the rotor diameter in the downstream direction (x-axis) and 4 times the rotor diameter in the lateral direction (y-axis). The turbines have a design rotor tilt of 6°. The Horns Rev 1 site [47] has been chosen for this study, providing the Weibull distribution necessary for the analysis. A uniform wind rose has been employed, meaning that the probability of occurrence of wind from each wind direction sector is the same. The parameters of the wind turbine and the wind farm have been detailed in Table 3.3 and the top-view of the wind farm layout has been displayed in Figure 3.7.

Parameter	Unit	Value
Wind Turbine	-	IEA 15 MW
Rotor Diameter	m	241.94
Rated Power	MW	15
Hub Height	m	150
Cut-in Wind Speed	m/s	3
Rated Wind Speed	m/s	10.59
Cut-out Wind Speed	m/s	25
Shaft Tilt Angle	°	6
Wind Shear Coefficient	-	0.1
No. of Wind Turbines	-	4
Spacing in the x direction	m	5D
Spacing in the y direction	m	4D

Table 3.3: Verification Case-2 Wind Farm Setup: Wind Turbine and Site Parameters

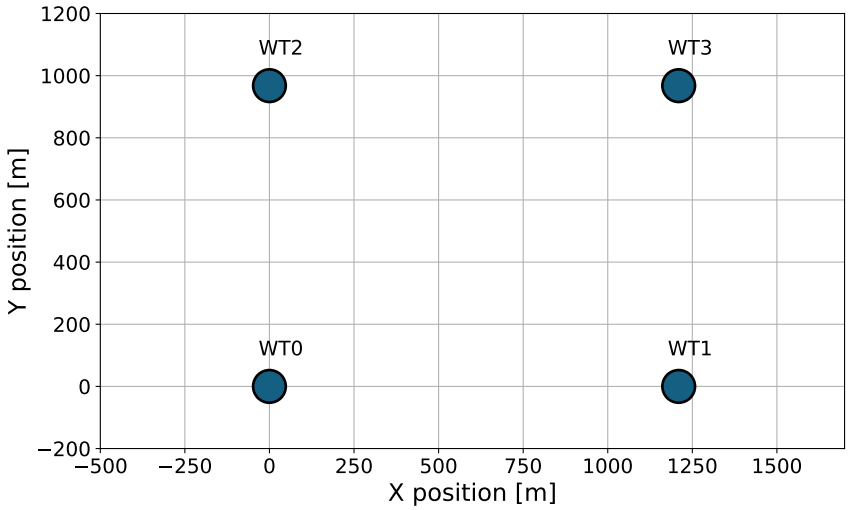

Figure 3.7: Wind Farm Layout for Case-2

To evaluate the AEP for this wind farm, small bin widths for wind speed and wind direction have been considered: 1 m/s for wind speed and 1° for wind direction. The choice of a small wind speed bin size and small wind direction bins are crucial for layout optimization studies and accurate AEP calculations [48]. The look-up tables for a current speed of 0 m/s were extracted from the reference paper, and have been displayed in Figure 3.8.

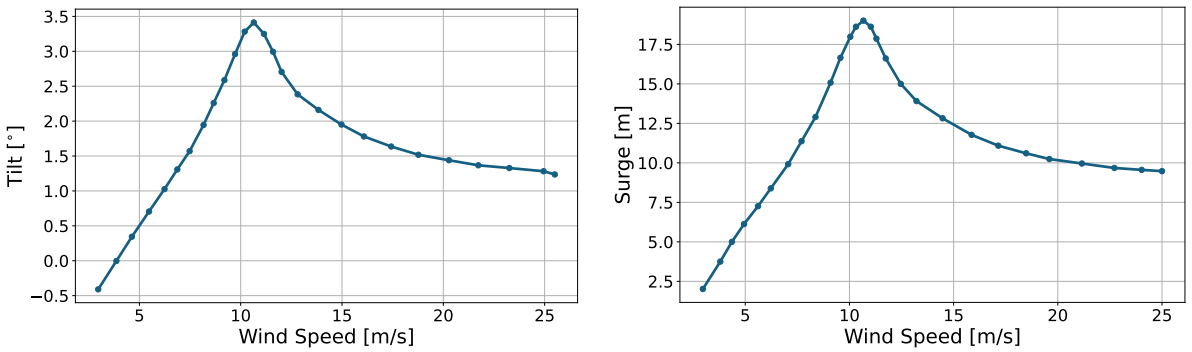

(a) Tilt vs WS

(b) Surge vs WS

Figure 3.8: Tables of Tilt and Surge as a function of Wind Speed (WS) at a current speed of 0 m/s.

3.2.2. Results: Fixed-Bottom Wind Farm

The fixed-bottom case was simulated with an initial rotor tilt of 6° for all turbines, considering all wind directions and wind speeds between cut-in and cut-out. The variation in the power production of a single turbine with different tilt angles at a wind speed of 10 m/s and a wind direction of 270° has been illustrated in Figure 3.9. The turbine produces maximum power when the wind aligns with the rotor shaft. This scenario occurs at a tilt angle of −6° due to the initial design tilt angle and the presence of wind shear. However, the power output of a single turbine decreases as the tilt angle increases. This occurs because a smaller surface area of the rotor is exposed perpendicularly to the wind, resulting in a reduced ability to harness wind power.

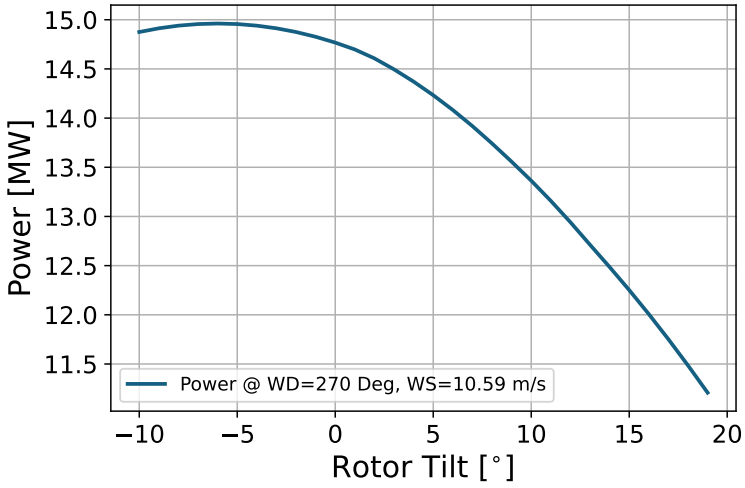

Figure 3.9: Variation of Electrical power generated by a Wind Turbine (WT0) vs Rotor Tilt Angles

The Annual Energy Production (AEP) computed for the fixed-bottom wind farm layout has been presented in Table 3.4. This value is approximately 0.14% higher than the AEP reported in the reference paper, which was 302.76 GWh. The slight discrepancy is likely due to the use of different engineering wake deficit models: the reference study employed the Zong Gaussian wake deficit model, while the present simulation utilized the Bastankhah Gaussian wake model. Other simulation settings in PyWake were kept consistent with the reference paper to the extent permitted by the available data.

No. of WTs	WD [°]	WS [m/s]	AEP [GWh]	
			Simulation	Reference
4	0 - 360	3 - 25	303.19	302.76

Table 3.4: AEP in GWh for the Fixed-bottom wind farm

The flow maps for a wind direction of 270° and a wind speed of 10 m/s have been illustrated in Figure 3.10 and Figure 3.11, providing two different views of the wind farm. Since the turbines are pre-set to a rotor tilt angle of 6°, the rotors, denoted by the gray lines in the figures, are slightly pitched towards the back even for the fixed-bottom case.

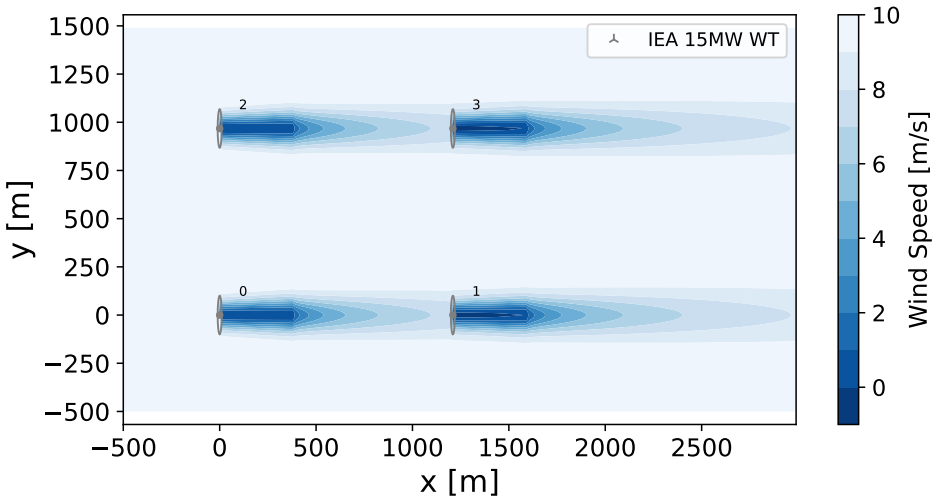

Figure 3.10: Wind Speed in the Wake of the Fixed Wind Turbines: XY View

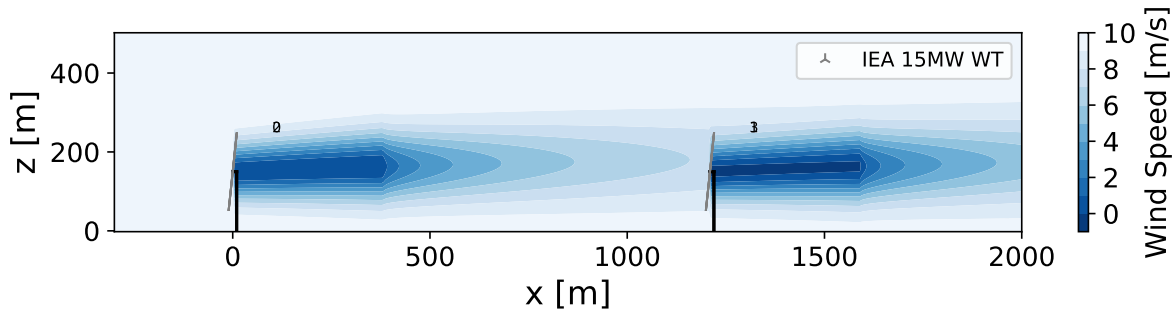

Figure 3.11: Wind Speed in the Wake of the Fixed Wind Turbines: ZX View

3.2.3. Results: Floating Offshore Wind Farm

To simulate the floating case, first, the tilt values and the new turbine coordinates due to surge at respective WS_{eff} were computed using the approach described in Section 2.3. These values were then fed to the WindFarmModel object to compute the AEP for the combined case as well as the individual degree of freedom cases as tabulated in Table 3.5.

S. No.	Case	AEP [GWh]	% Difference from the fixed-bottom case
1	Only Tilt	301.761	0.471
2	Only Surge	303.179	0.004
3	Combined tilt and surge	301.757	0.473

Table 3.5: AEP of the FOWF and comparison with the Fixed-Bottom farm

In the reference study, the floating wind farm's AEP was approximately 0.07% to 0.08% higher than that of the fixed-bottom wind farm, with variations depending on current speed and direction. However, a reduction of around 0.473% in AEP was observed for the simulation of the combined DOF floating farm case compared to the fixed-bottom configuration. The individual tilt displacement case resulted in an AEP value very similar to that of the combined floater displacement case. In contrast, the surge displacement case produced results nearly identical to the fixed-bottom case, with a slight decrease of approximately 0.004%.

The discrepancies observed in comparison with the results of the reference paper can be attributed to modeling variations and different assumptions between the two approaches. In the reference paper, a neural network-based approach was used to leverage HAWC2 simulations and calculate floater motions pertaining to five degrees of freedom, whereas only two degrees of freedom were considered in this thesis. The increase in AEP observed in the reference case may arise from the additional DOFs, that have been neglected in this study. Moreover, the impact of the current was also neglected in this thesis but considered in the reference paper, which could further contribute to the discrepancy. Additionally, the use of a different wake deficit model could also be a factor in these observed differences.

The flow maps for both the top (XY) and side (ZX) views of the flow field at a wind direction of 270° and a wind speed of 10 m/s have been displayed in Figure 3.12 and Figure 3.13, respectively. These visualizations illustrate the upstream turbines exhibiting higher tilt and the downstream turbines with lower tilt. This is however true only up until the rated wind speed, after which with an increase in the wind speed the tilt values start to decrease. Additionally, the side view highlights the vertical upward deflection of the wake, which alters the wind speed encountered by the downstream rotor. This deflection impacts the flow dynamics and subsequently affects the performance of the downstream turbines.

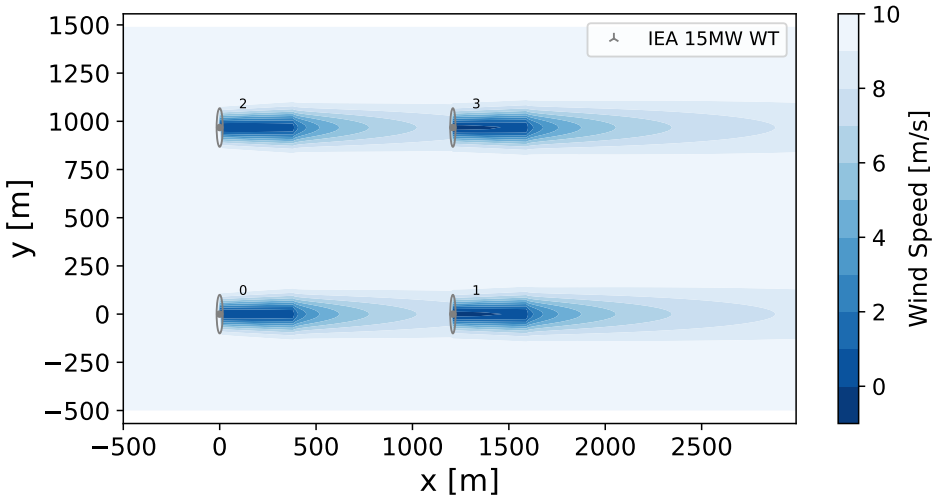

Figure 3.12: Flow Map (XY View) depicting velocity deficit downstream at WD = 270° and WS = 10 m/s

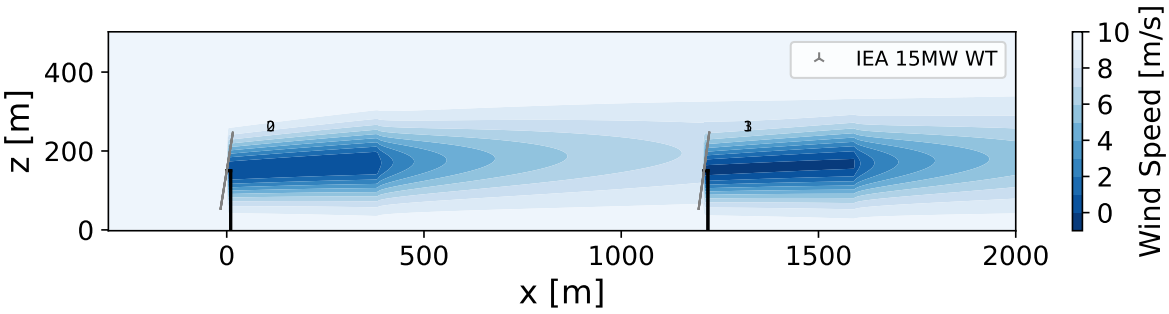

Figure 3.13: Flow Map (ZX View) depicting velocity deficit downstream at WD = 270° and WS = 10 m/s

The impact of surge displacement on AEP is minimal because the backward movement of the turbine does not significantly influence the stabilized wake, which forms the basis for AEP calculations, as dynamic motion effects are not considered in this process. The minor variation that does occur stems from the slightly reduced distance between turbines, which brings the downstream turbine closer to the upstream one, thus positioning it deeper within the wake deficit and reducing the wind speed experienced by the rotor. At wind speeds below the rated value, the downstream turbine experiences less surge compared to the upstream turbine, due to the lower wind speeds in the wake. However, when the wind speed exceeds the rated level, the effect reverses, with the upstream turbine experiencing less surge as the thrust on the downstream turbine decreases after reaching rated conditions.

The surge displacements for individual turbines are illustrated in Figure 3.14a for a wind direction of 270° and Figure 3.14b for a wind direction of 300°, both at a wind speed of 10 m/s, which is below the turbine's rated speed. The corresponding flow maps are depicted in Figure 3.15. For a wind direction of 270°, the downstream turbines, WT1 and WT3, are within the wake, while WT0 and WT2 are exposed to freestream conditions, resulting in lower surge displacements for the downstream turbines. In contrast, for a wind direction of 300°, only WT1 is within the wake of WT2, while the other turbines experience freestream conditions, leading to a lower surge displacement for WT1. If wind speeds above the rated level were considered, the turbines in the wake would experience higher surge displacements than those in freestream

conditions.

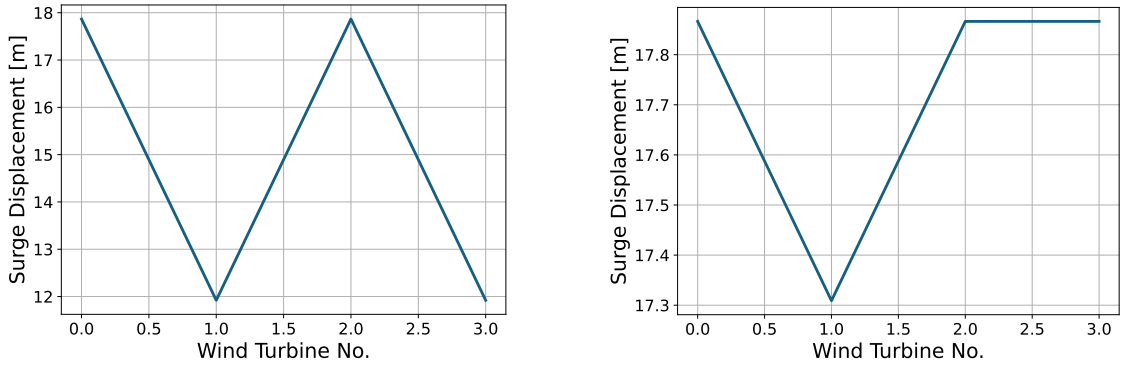

(a) Surge displacement at WD=270°

(b) Surge displacement at WD=300°

Figure 3.14: Surge displacements for each wind turbine at different Wind Directions.

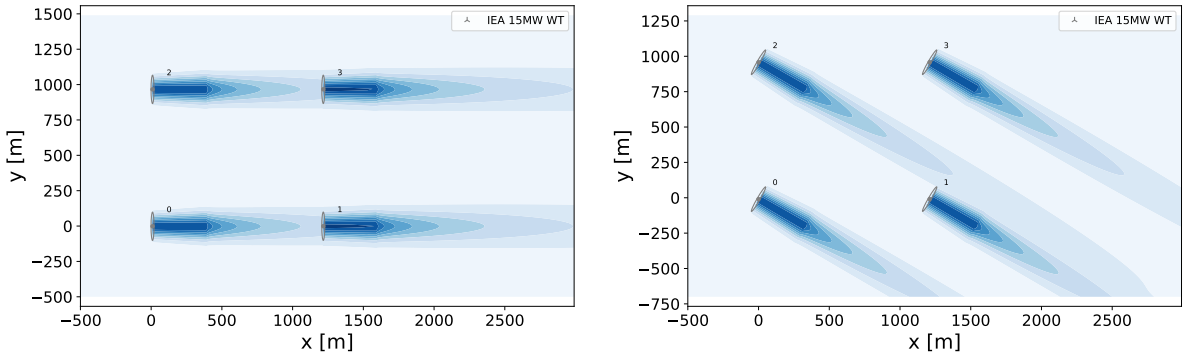

(a) Flow map at WD=270°

(b) Flow map at WD=300°

Figure 3.15: Top view Flow maps for the Only Surge case at different wind directions.

3.2.4. Analysis on the Power Production of the FOWTs

The relationship between power output and wind speed for the first-row turbines (WT0 and WT1) at a wind direction of 270° and a wind speed of 10 m/s has been depicted in Figure 3.16, for both the fixed-bottom and floating configurations. The upstream turbine (WT0) reaches its rated power at the rated wind speed of 10.59 m/s, while the downstream turbine (WT1) achieves its maximum power of 15 MW at a higher wind speed. This delay is due to the downstream turbine operating within the wake of WT0, where it experiences a reduced wind speed compared to the freestream conditions. As WT0 is fully exposed to the rated wind speed, it reaches maximum power, whereas WT1, encountering lower wind speeds, produces less power. Consequently, WT1 requires a freestream wind speed of approximately 13 m/s to reach its rated wind speed and achieve maximum power output.

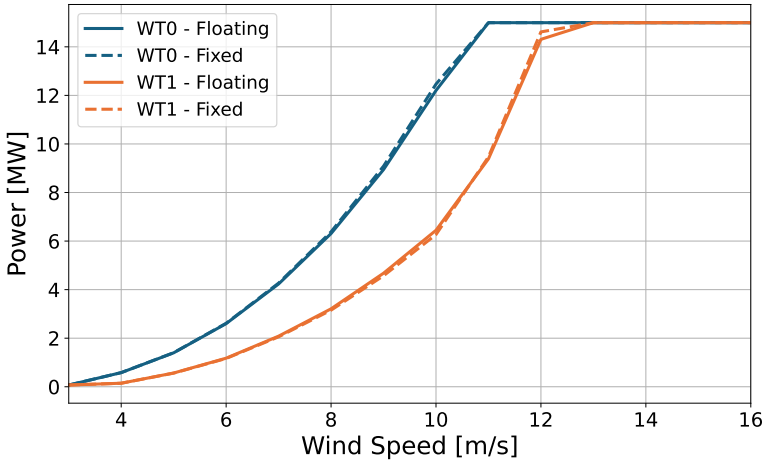

Figure 3.16: Power Output for the Fixed vs Floating Turbines

The power production for the turbines in the first and second rows are identical and overlap, as the turbines in both rows operate under the same conditions. For this reason, the power curves for the second-row turbines have not been shown here. This overlap occurs at this wind direction because there is no horizontal wake deflection, as the yaw angle has been assumed to be zero in this case.

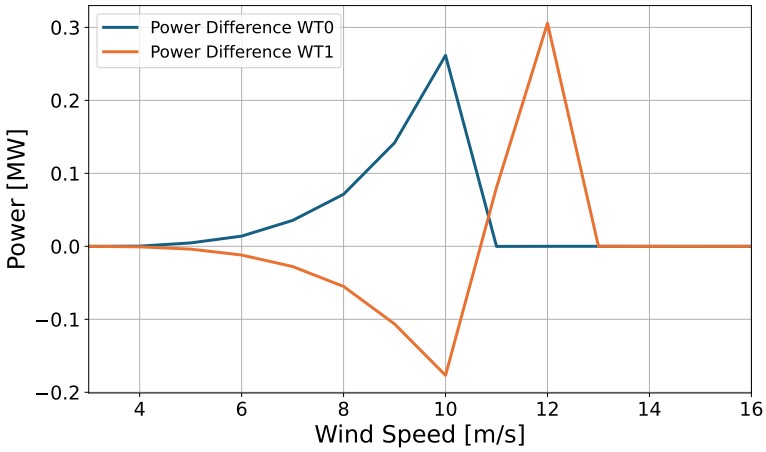

Figure 3.17: Power loss/gain for the first row turbines, between the two cases: fixed-bottom wind farm, and floating wind farm.

The differences in power generation between the fixed-bottom and floating configurations for turbines WT0 and WT1 are illustrated in Figure 3.17. The upstream turbine (WT0) in the fixed-bottom configuration produces more power than its floating counterpart up to near the rated wind speed. This is primarily due to the tilt and surge motions of the floating turbine, which reduce its power output when operating independently. Conversely, the downstream turbine (WT1) generates more power in the floating configuration up to the rated wind speed, as shown by the negative power difference. Beyond this point, the power difference becomes positive, indicating that the fixed-bottom turbine momentarily produces more power before both configurations converge at their rated power outputs.

The power generation of the wind farm is also influenced by the wind direction. This has been depicted for the fixed-bottom WT0 at four different wind directions in Figure 3.18. This

variation arises because the turbine that is upstream in one direction may become downstream in another, thereby operating within the wake of other turbines. For instance, in the wind directions 180° and 270°, WT0 is upwind and faces freestream conditions, the rated wind speed in this case, and hence achieves the rated power of 15MW at the rated wind speed of 10.59 m/s. However, in the other directions, WT0 is positioned downstream, thus achieving the rated power at higher wind speeds due to wake effects.

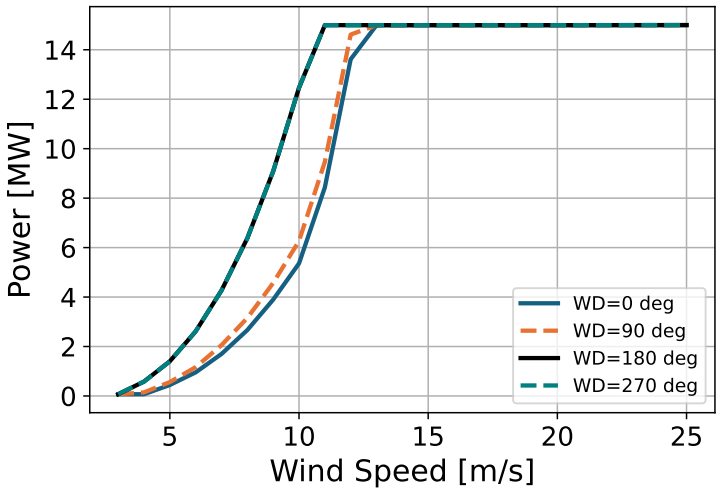

Figure 3.18: Power Curve of Fixed-bottom WT0 at wind directions ranging from 0° to 270°

4

Optimization Setup of the FOWF

This chapter introduces the OpenMDAO-based optimization framework, WINDOW, developed by S. Perez Moreno at TU Delft [49], designed for the optimization of offshore wind farms. It further details the modification of the framework for the integration of substructure and mooring line analysis for the optimization of floating offshore wind farms into the framework developed by M. Bessone [50], and finally, outlines the modifications made to adapt WINDOW for the specific objectives of this thesis.

4.1. WINDOW: OpenMDAO Framework for Wind Farm Optimization

The WINDOW framework, developed by S. Perez Moreno at TU Delft, integrates multiple disciplines, each modeled as individual analysis blocks, which are interconnected to simulate the performance of a wind farm and minimize the levelized cost of energy (LCoE). The framework consists of several wind farm modules, including electrical system analysis, support structure analysis, O&M analysis, AEP computation, cable length and type analysis, and cost modeling [51]. The MDAO tool is designed to allow modules and analysis blocks of varying fidelities and complexities to be seamlessly integrated into the workflow's inner layer.

The outer layer hosts the optimization algorithms, which drive the optimization process based on the specific use case defined by the user. For instance, the user might aim to minimize the LCoE by optimizing the wind farm layout, electrical infrastructure design, and support structure design. A set of design variables are driven by an optimization algorithm to achieve the specified objective. Figure 4.1 illustrates the basic EXtended Design Structure Matrix (XDSM) of the tool, which represents the architecture of the MDAO framework.

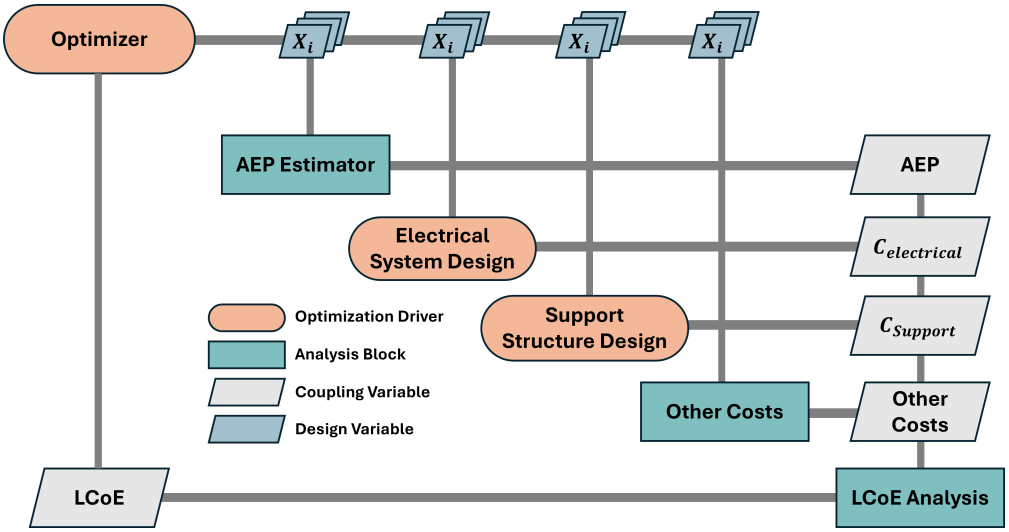

Figure 4.1: Fundamental MDAO Architecture of WINDOW, adapted from [49]

In the diagram, X_i represents a global design variable, which is driven by the optimization algorithm. The variables shown in the light gray blocks are the computed outputs from the various modules, that are passed to the objective function (LCoE analysis) block, from which the computed LCoE is fed back to the optimizer. The 'Optimizer' block acts as the top-level controller, which drives the layout design variables until the minimum of this LCoE is found. Meanwhile, the electrical infrastructure and support structure are optimized by a nested optimizer during each iteration of the main optimization process.

Building on the WINDOW framework for offshore wind farms, an optimization workflow has been developed by M. Baudino Bessone specifically for floating offshore wind farms (FOWFs) by incorporating additional modules and modifying existing ones to simulate the performance of FOWFs [50]. In this framework, the workflow has been structured as three nested problems: the super-problem, which optimizes the wind farm layout to minimize the Levelized Cost of Energy (LCoE), the sub-problem, which focuses on designing the optimal semi-submersible floater for the wind turbine to minimize the total substructure assembly cost, and the Cable topology analysis, which optimizes the cable costs according to the topology, and lengths corresponding to the wind farm layout. The substructure assembly includes the semi-submersible body, mooring lines, and anchors. Key analysis blocks include substructure analysis, installation, maintenance, and AEP analysis.

In the AEP analysis block, PyWake has been employed for the computation of AEP, which offers the option to use either the Bastankhah Gaussian wake model or the N.O. Jensen wake model. However, since these models are currently applicable only to fixed-bottom wind farms, the effect of floating turbine displacements has been considered negligible in this analysis. Nevertheless, the floating substructures of FOWTs can move in six degrees of freedom (DOFs), with tilt and surge DOFs significantly influencing the AEP and thus the LCoE of the wind farm. Omitting these movements from the layout optimization problem for FOWFs can result in an under- or over-prediction of the energy production and thus the optimal parameters that are required for LCoE minimization.

To evaluate the impact of incorporating floater motions on the optimization parameters—particularly the design variables and objective function values—the optimization framework for FOWFs has been modified in this thesis. A detailed explanation of these modifications,

along with the methodology, has been provided in the following section.

4.2. Incorporation of FOWF Wake Model in WINDOW

The XDSM of the optimization framework for FOWFs including the modifications has been illustrated in Figure 4.2. In this framework, a floater motions analysis block has been added to compute the movement of the semi-submersible substructure as a function of wind speed. This data is then passed to the AEP analysis module, `FarmAEP`, where it is used as a look-up table for computing the actual displacement and pitch of the wind turbine at the local effective wind speed. The internal working of the `FloaterDOFs` and `FarmAEP` modules has been detailed in Section 4.2.1 and Section 4.2.2, respectively.

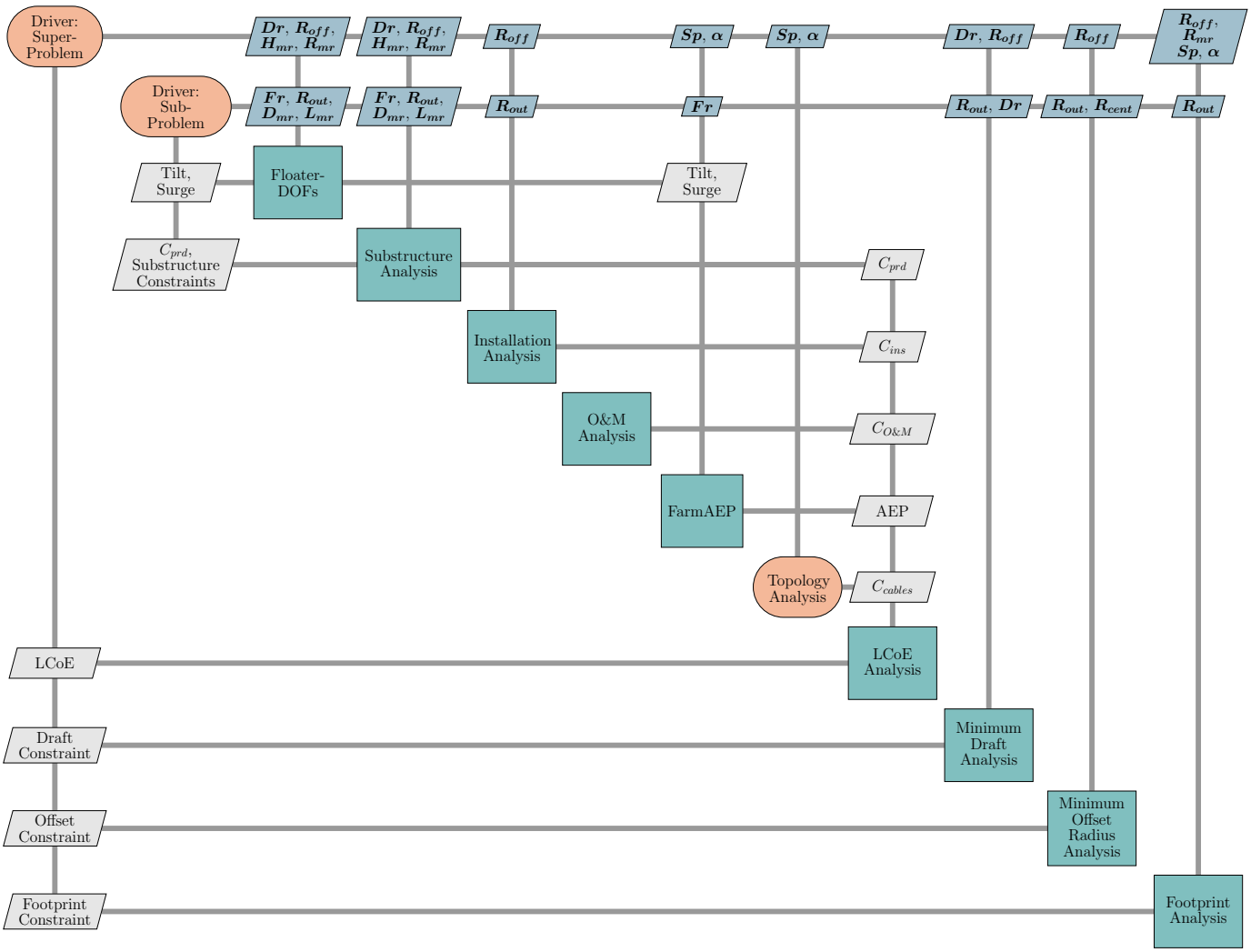

Figure 4.2: XDSM of the MDAO Framework

4.2.1. FloaterDOFs Block: Generating the Look-Up Tables

The `FloaterDOFs` block has been implemented as an OpenMDAO ExplicitComponent and is responsible for computing the displaced equilibrium positions of the floating platform (tilt, and surge) under steady loads at varying freestream wind speeds. This block has been added to the sub-problem optimization module, as the tilt, and surge values will depend on the shape of the substructure which is being optimized under the sub-problem. In each iteration,

the substructure design is provided as input to the `FloaterDOFs` block, which computes the corresponding arrays of tilt, surge, and heave values at different wind speeds. These computed arrays are then fed back to the sub-problem driver. A closer look at the `FloaterDOFs` block has been depicted in Figure 4.3.The driver continues to optimize the substructure design, adjusting it iteratively until an optimal configuration is found. Once the optimization process is complete, the final equilibrium position values are passed to the AEP analysis block for further computation.

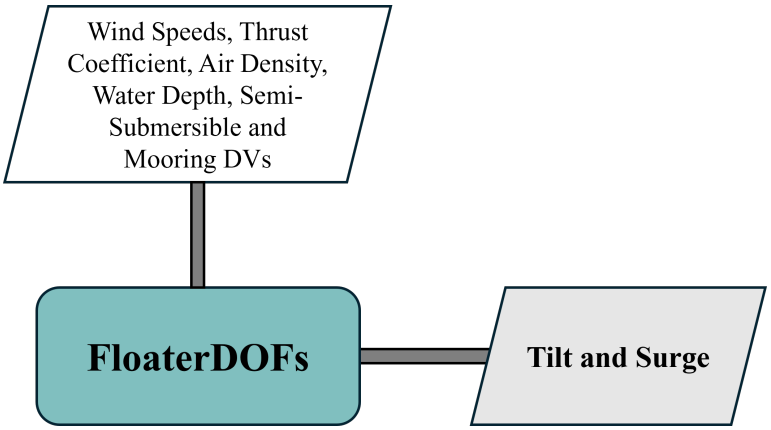

Figure 4.3: Analysis block with inputs (white parallelogram) and generated outputs (grey parallelogram) to compute the Floater Displacements as a function of Wind Speed, `FloaterDOFs` in the MDAO Framework.

A predefined function that solves the simplified system of equations for catenary lines has been used to compute the static tilt and surge motions of the floating sub-structure as a function of wind speed. This function, along with the forces exerted on the semi-submersible by the mooring lines, calculates the equilibrium displacement of the sub-structure in the heave, surge, and pitch directions by determining the increase in mooring line tension in both the vertical and horizontal directions. For this calculation, the mooring line is assumed to be slack and resting on the seabed. The catenary equations employed for this have been adapted from [52] and are shown in Equation 4.1. In these equations, l and h represent the horizontal and vertical projections of the cable profile and are mathematical functions of the horizontal and vertical components of tension, denoted as H and V, respectively. Here, L_0 is the length of the cable, w is its weight per unit length in water, and EA represents the extensional stiffness of the unstretched cable. This system of equations was then solved using Python's 'fsolve' from the Scipy library.

$$\begin{aligned} l &= L_0 - \frac{V}{w} + \frac{L_0 H}{EA} + \frac{H}{w}\sinh^{-1}\left(\frac{V}{H}\right) \\ h &= \frac{1}{w}\left[\sqrt{H^2+V^2} - H + \frac{V^2}{2EA}\right] \end{aligned} \tag{4.1}$$

Using this function, the sub-structure displacements could be computed only at the rated wind conditions. However, for the purpose of this analysis, sub-structure displacements are required across the full range of wind speeds, from cut-in to cut-out. Since the system of equations is not directly dependent on wind speed, they were solved for different thrust values, which are wind speed dependent. The thrust was calculated using Equation 4.2, where ρ represents the air density at the hub height, A is the rotor disc area, C_T is the thrust coefficient at different

wind speeds obtained from the input thrust curve, and U represents the wind speeds from cut-in to cut-out. By sequentially inputting these thrust values in `fsolve`—replacing the single thrust value at rated power—the corresponding tilt and surge displacements were obtained as a function of wind speed.

$$T = \frac{1}{2}\rho A C_T U^2 \tag{4.2}$$

4.2.2. FarmAEP Block: Wake Modeling for FOWFs

The `FarmAEP` module in the XDSM diagram shown in Figure 4.2 is an OpenMDAO wrapper for the Python-based wake model library, PyWake [42]. This module leverages the OpenMDAO ExplicitComponent framework and integrates it with PyWake to use it effectively as an analysis block in the optimization framework. For a given site and wind turbine, the `FarmAEP` module calculates the probability of wind occurring in each wind direction sector and fits a Weibull distribution to the wind speed data for each sector. Using the provided time series input, the module determines the shape and scale parameters of the Weibull distribution, along with the probability of wind inflow for each sector. The Weibull parameters are considered uniform within each sector, and the wind conditions are assumed constant over the area.

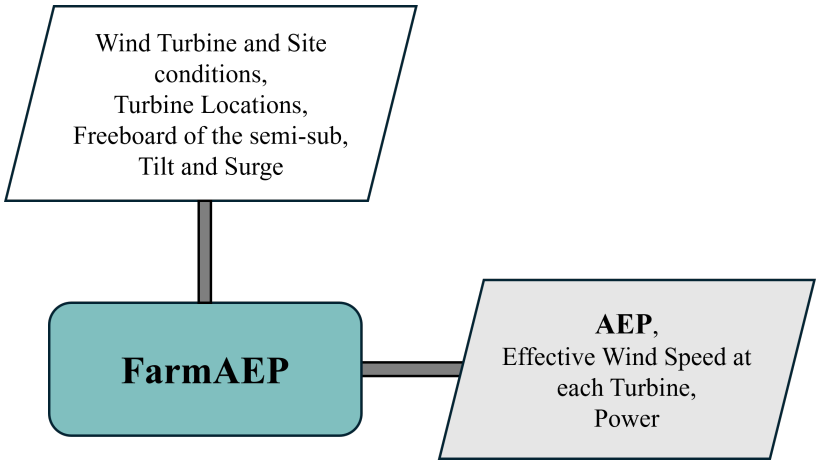

Figure 4.4: Analysis Block with inputs (white parallelogram) and generated outputs (grey parallelogram) to compute the AEP of the Wind Farm, `FarmAEP` in the MDAO Framework

A detailed visualization of the `FarmAEP` module, including its required inputs and generated outputs, is presented in Figure 4.4. The module receives the wind farm layout and wind conditions as inputs from the super-problem driver, along with the height of the semi-submersible floater above the water level (freeboard), which is passed from the sub-problem driver. The outputs include power as a function of wind speed and direction, and the Annual Energy Production (AEP) of the wind farm, accounting for wake losses.

Two additional inputs from the `FloaterDOFs` block—`ws_surge` and `ws_tilt`—are required by this module. These inputs are transformed into lookup tables and fed into the `AEP_float` function under this block. This function contains the modification employed for the AEP computation of FOWFs while incorporating the floating platform motions using the approach described in Section 2.3. This function has been included into the `FarmAEP` module via an `if` condition. When the input file specifies the farm type as `'Floating'`, this condition is triggered, enabling the calculation of AEP incorporating the effect of floater displacements.

4.3. Components of the Optimization Problem

This section outlines the key components of the optimization problem, including the design variables, constraints, and the objective function. Additionally, the selected optimization settings and algorithms have been discussed to provide a comprehensive understanding of the framework used for solving the problem.

4.3.1. The Design Variables

The super-problem focuses on minimizing the Levelised Cost of Energy (LCoE) of the wind farm, for which it has to find the optimal values of six design variables: two related to the wind farm layout, two for the mooring lines, and two for the substructure. In the sub-problem, four design variables have been considered: two for the mooring lines and two for the semi-submersible. These variables have been selected to design an optimal semi-submersible sub-structure assembly that minimizes its yearly production cost, $C_{prd,y}$. The parameterized design variables of the sub-structure and mooring lines along with the wind farm layout has been illustrated in Figure 4.5 and Figure 4.6, respectively.

The variables for the design of the semi-submersible and mooring lines are the radius of the outer column, R_{out}, the freeboard, Fr, the radial position of the outer columns, R_{off}, draft Dr, the diameter and length of the mooring lines, D_{mr} and L_{mr}, the distance between the anchor and the fairlead of the cable, R_{mr} and the relative fairlead height over the draft, $H_{mr,rel}$. The initial length of the mooring lines, L_{mr}, used to initiate the optimization has been computed as a function of the fairlead-anchor distance and the height of the fairlead using Equation 4.3. The fairlead height, denoted by H_{mr}, depends on the water depth and the draft.

$$L_{mr} = \sqrt{R_{mr}^2 + H_{mr}^2} + \frac{H_{mr}}{12} \tag{4.3}$$

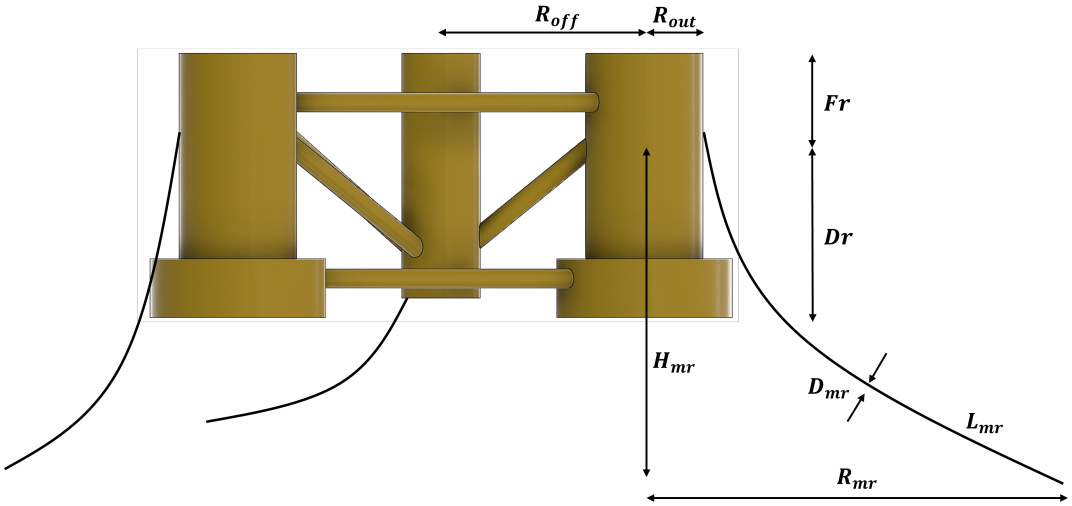

Figure 4.5: Design Variables of the Semi-submersible Substructure and the Mooring Cables

Furthermore, two design variables have been chosen for the wind farm layout: layout spacing, Sp and the layout rotation or orientation, α. The layout spacing is the distance between two wind turbines, which has been defined as a function of the anchor-fairlead distance, the outer column radius of the semi-submersible and its radial position. For simplicity, this ensures that the two turbines do not overlap on each other's mooring systems. The constraint used for this

purpose has been discussed in the next section. The layout orientation defines the alignment of the layout as a whole with respect to the substation.

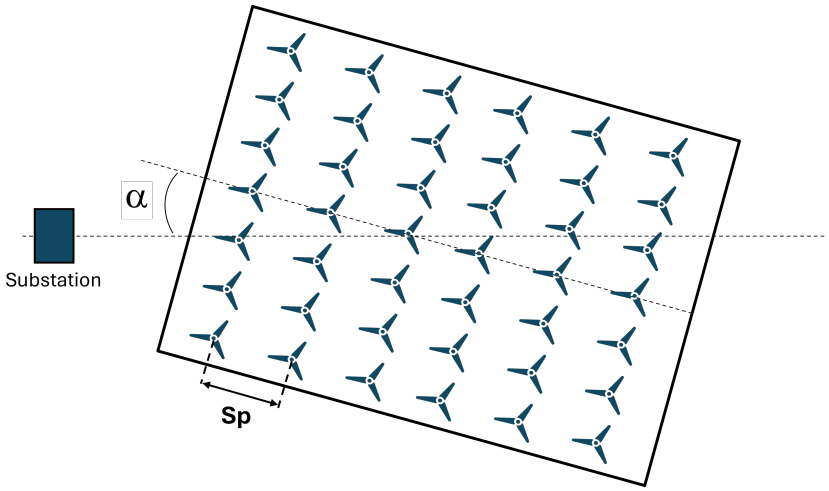

Figure 4.6: Design Variables of the Wind Farm Layout

The chosen design variables, along with their bounds have been tabulated in Table 4.1.

Symbol	Design Variables Description	Lower Bound	Upper Bound
R_{out}	Outer column radius of the Semi-Submersible [m]	3	10
Fr	Freeboard of the Semi-submersible [m]	6	50
D_{mr}	Diameter of the Mooring cable [m]	3.00E-02	2.25E-01
L_{mr}	Length of the Mooring cable [m]	481.3	633.8
R_{mr}	Distance between the Anchor and Fairlead [m]	3D	8D
$H_{mr,rel}$	Relative Fairlead height over the Draft [-]	—	—
Dr	Draft [m]	12	45
R_{off}	Radial position of the Semi-submersible outer columns [m]	40	65
Sp	Layout Spacing [m]	8.88D	13.88D
α	Layout Rotation [°]	0	360

Table 4.1: The Design Variables for the Optimization Problem

4.3.2. The Constraints

The constraints of the super-problem have been defined as follows:

1. *Minimum Draft*: This constraint, imposed at the super-problem level, ensures that the draft of the semi-submersible is greater than or equal to the minimum required draft. For the design to be feasible, the difference between the obtained and minimum draft must be greater than or equal to 0, as expressed in Equation 4.4.

$$Dr - Dr_{min} \geq 0 \tag{4.4}$$

2. *Minimum Offset Radius*: The minimum offset radius constraint ensures the outer column of the semi-submersible does not overlap with the central column. The offset radius must exceed the minimum value, defined as $1.1 \cdot (R_{cent} + R_{out})$, as shown in Equation 4.5.

$$R_{offs} \geq R_{offs,min} \tag{4.5}$$

3. *Minimum Footprint*: The minimum footprint constraint, defined in Equation 4.6, ensures the distance between two turbines is at least twice the distance between the center of the

semi-submersible and the anchor point, preventing overlap of the mooring systems.

$$d_{max} \geq d \tag{4.6}$$

Six geometric, stability, and structural constraints have been imposed for the sub-problem to ensure a feasible design for the semi-submersible substructure.

1. *Minimum Freeboard*: This constraint ensures that the freeboard of the semi-submersible is maintained at a value equal to or greater than the sum of two times the significant wave height plus the increase in draft at the displaced equilibrium position. The mathematical formulation for this constraint is shown in Equation 4.7.

$$Fr \geq Fr_{min} \tag{4.7}$$

2. *Minimum Mooring Characteristic Strength*: This constraint ensures that the difference between the mooring line characteristic strength (Mr_{str}) and the maximum tension at the fairlead (T_{Fr}) in both the initial and displaced positions is greater than zero. It can be mathematically expressed as shown in Equation 4.8.

$$Mr_{str} - T_{Fr} \geq 0 \tag{4.8}$$

3. *Maximum Vertical Force at Fairlead*: This constraint ensures that the vertical component of tension at the fairlead remains below the tension that could lift the chain off the seabed. If the vertical tension exceeds this limit, it would cause the load to act on the anchor, leading to potential failure. The constraint is defined by Equation 4.9.

$$T_{v_{max}} \geq T_v \tag{4.9}$$

4. *Maximum Surge Displacement*: This constraint ensures that the surge displacement of the floater remains within the specified maximum allowable limit, restricting the extent of the horizontal distance the turbine can drift to. The constraint has been displayed in Equation 4.10.

$$x_{max} \geq x \tag{4.10}$$

5. *Maximum Pitch Displacement*: This constraint limits the achieved heel angle in pitch to ensure it remains below the maximum permissible heel angle. The constraint has been represented by Equation 4.11.

$$\theta_{max} \geq \theta \tag{4.11}$$

6. *Failure Constraint*: This constraint ensures the feasibility and convergence of the solution. It is defined as the sum of all constraints, and its value must be less than or equal to zero. If this value exceeds zero, it indicates that either the design is infeasible or the solution has not converged. This constraint has been expressed in Equation 4.12.

$$Fail \leq 0 \tag{4.12}$$

4.3.3. The Objective Function

The primary objective of the optimization problem is to minimize the Levelized Cost of Energy (LCoE) of a Floating Offshore Wind Farm (FOWF). The LCoE has been computed using Equation 4.13, where C_{CapEx} represents the life-cycle, discounted capital expenditure, which includes the yearly production cost $C_{prd,y}$ and installation costs C_{ins}, and C_{OpEx} accounts for

the life-cycle, discounted operational and maintenance expenditure, $C_{O\&M}$ associated with the wind turbines and their substructure. The denominator represents life-cycle discounted energy production, where r represents the discount rate.

$$LCoE = \frac{C_{CapEx} + C_{OpEx}}{AEP/(1+r)^{yr}} \tag{4.13}$$

The installation costs, C_{ins}, are obtained from the `Installation Analysis` block, while the operational and maintenance costs $C_{O\&M}$ are derived from the `O&M Analysis` block. The sub-problem focuses on minimizing the yearly production cost $C_{prd,y}$, which indirectly impacts the overall LCoE of the wind farm and has been taken as an output from the `Substructure Analysis` block. This cost includes the cost of the structure of the semi-submersible, the ballast, and the mooring assembly including the cables.

Additionally, the Annual Energy Production (AEP), another key factor in LCoE calculation, has been computed in the `FarmAEP` block, as defined in Section subsection 4.2.2.

4.3.4. Problem Formulation

The final optimization problem has been formulated as follows:

Minimize

$$LCoE \tag{4.14}$$

With respect to

$$v_i = [R_{out}, Fr, D_{mr}, L_{mr}, R_{mr}, H_{mr,rel}, Dr, R_{off}, Sp, \theta] \tag{4.15}$$

Subject to

$$\begin{aligned} D_r - D_{r_{min}} &\geq 0 \\ R_{off} - R_{off_{min}} &\geq 0 \\ d_{max} - d &\geq 0 \\ Fr - Fr_{min} &\geq 0 \\ Mr_{str} - T_{Fr} &\geq 0 \\ T_{v_{max}} - T_v &\geq 0 \\ x_{max} - x &\geq 0 \\ \theta_{max} - \theta &\geq 0 \\ Fail &\leq 0 \end{aligned} \tag{4.16}$$

The drivers for the optimization problem have been defined using Python's ScipyOptimizer package. The optimizer options have been as specified in Table 4.2.

S.No.	Option	Value
1.	Optimizer	COBYLA
2.	Step Size	0.25
3.	Tolerance	1e-2
4.	Maximum number of iterations	150

Table 4.2: Optimizer options for the Super Problem

Choice of the Optimization Algorithm
Gradient-based algorithms are known to work well for continuous and smooth objective functions, while gradient-free algorithms are often selected for discontinuous functions that have multiple local optima [51]. The LCoE as a function of design variables, such as layout spacing and orientation, can exhibit a multi-modal behavior. Additionally, due to the presence of inequality constraints, gradient-free methods are a more suitable choice for optimizing the LCoE. As a result, the COBYLA (Constrained Optimization BY Linear Approximation) algorithm, a gradient-free optimization technique, has been selected as the driver for both the main and sub-problems in this optimization process.

4.4. Case Study: 42-turbine Floating Offshore Wind Farm

This section provides a summary of the case study for the wind farm optimized for Levelized Cost of Energy (LCoE) minimization in this thesis. The case study considers a wind farm consisting of 42 5 MW NREL wind turbines, each mounted on semi-submersible substructures. The site's wind conditions are derived from the ERA5 reanalysis database [53], which provides hourly time series of wind speed and wind direction at a reference height of 100 meters.

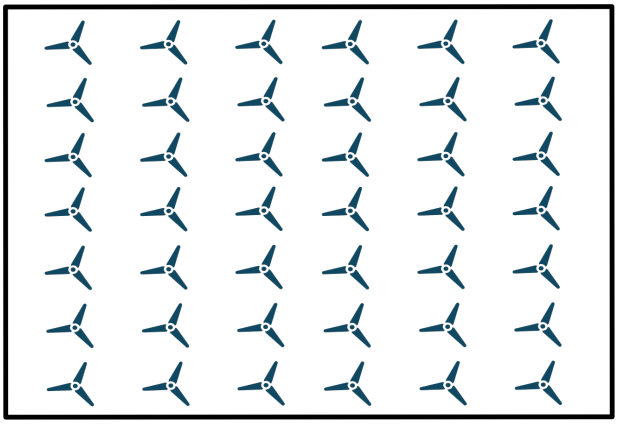

Figure 4.7: Layout of the 42 turbine Floating Offshore Wind Farm

The wind farm layout, displayed in Figure 4.7, follows a gridded rectangular design, with 42 turbines arranged in seven rows and six columns. The layout has initially been oriented at 90°, pointing towards the north and the turbines have been initially spaced at 12.88 times the wind turbine rotor diameter. The relevant turbine and site-specific parameters have been detailed in Table 4.3 for reference.

	Parameter	Value
Wind Turbine	Rated Power	5 MW
	Rotor Diameter	126 m
	Hub Height	90 m
	Cut-in Wind Speed	3 m/s
	Rated Wind Speed	11.4 m/s
	Cut-out Wind Speed	25 m/s
	Blade Chord	4.652 m
	Blade Length	61.5 m
Site	Turbulence Intensity	0.1%
	Water Depth	200 m
	Sector Width	30°
	Wake Sampling Bin Size	5°
Layout	No. of turbines	42
	Spacing between the turbines	$12.88D$
	Orientation of the Farm	90°
	Distance from substation	$6D$

Table 4.3: Wind turbine, Site, and Layout parameters for the Sample Wind Farm

These parameters, along with the properties of the semi-submersible platforms, mooring lines, cables, and design variables and their bounds, have been defined in a separate input file formatted as a dictionary. This input file is called into the main file for the optimization process.

The wind rose for the selected wind farm site, as shown in Figure 4.8, provides a comprehensive visualization of the wind distribution across various directions. A sector width of 30° has been chosen, dividing the wind rose into 12 equal sectors. Each sector represents the frequency and intensity of winds coming from that direction.

From the wind rose, it is evident that the dominant wind direction is from the southwest, specifically around 210°. This dominance in wind direction is critical for wind farm performance, as it will influence the power generation of the turbines, especially those located in the windward sectors. The figure also shows wind speeds categorized into different ranges, with higher wind speeds indicated by the outer rings. Winds in the 5.2 to 15.6 m/s range are most prevalent, though higher speeds are also seen in smaller occurrences.

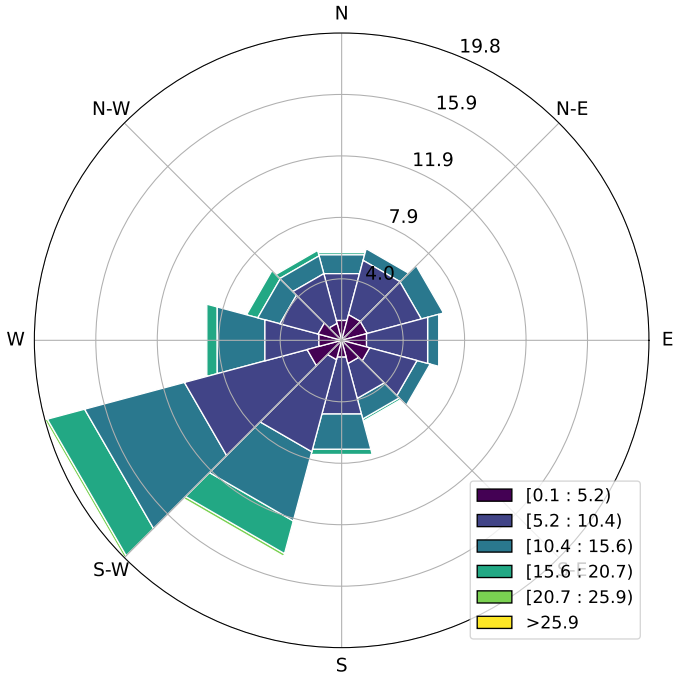

Figure 4.8: Wind Rose for the Wind Farm Site. Colors in the legend represent corresponding wind speed bins.

5

Results and Discussions

This chapter presents and discusses the results of the optimization of the Floating Offshore Wind Farm (FOWF), for two cases,

`Case A: Neglecting floater displacements`
`Case B: Accounting for floater displacements`

Initially, the outcomes of each case have been analyzed individually, followed by a comprehensive comparison to evaluate the impact of incorporating static floater displacements for AEP analysis on the optimization process and the resulting optimal values. Additionally, a post-optimization analysis has been conducted on two critical design variables to assess whether the identified optima represents the global minima within the solution space.

5.1. Floater Displacement Look-Up Tables

The tilt and surge static floater displacements for the FOWTs have been calculated based on the approach outlined in Section 2.3. The reference values of the tilt and surge as a function of wind speed were computed within the `FloaterDOFs` component of the optimization framework, as described in Section 4.2.1. These values get updated with each iteration of the sub-problem until the optimal sub-structure design is achieved which effectively minimizes the production cost, $C_{prd,y}$. They are then passed to the `FarmAEP` block, where look-up tables are generated which are used to compute the AEP of the FOWF accounting for floater displacements, as discussed in Section 4.2.2. This constitutes one iteration of the super-problem, and the process continues until the minimum LCoE is achieved. The tilt and surge look-up tables, displaying tilt and surge as wind speed functions from the final iteration of the super-problem have been displayed in Figure 5.1.

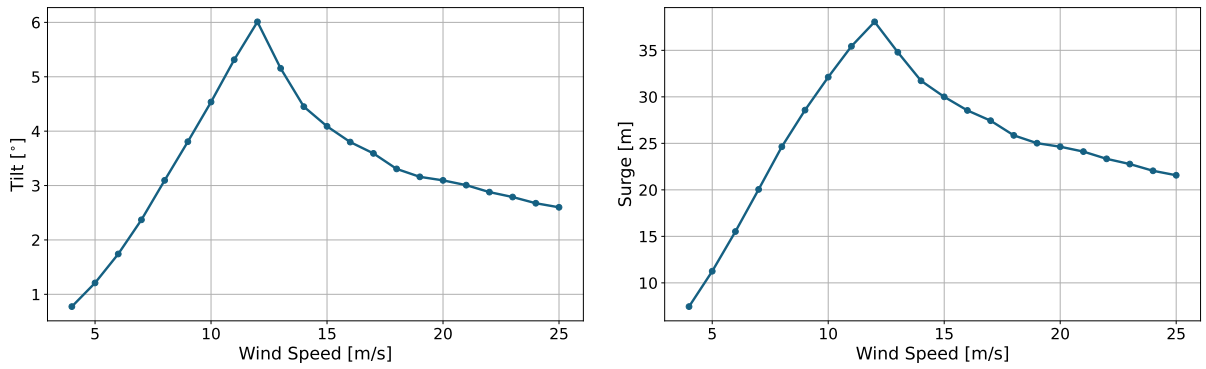

(a) Tilt in degrees

(b) Surge in meters

Figure 5.1: Look-up Tables for a) Tilt and b) Surge at varying wind speeds.

5.2. Optimization Results

The optimization process was initiated through a primary file that defines the site conditions and initializes the design variables along with their respective bounds. Following this, the optimization problem and driver—both OpenMDAO components—were configured to set up the optimization framework.

To ensure the objective function reaches the global minimum and avoids convergence to the local minima, a multi-start approach was implemented. This method involved exploring the design space using multiple starting points, with six distinct initial values assigned to each design variable. Throughout this process, certain combinations of variables failed to converge to optimal values, while others resulted in sub-optimal solutions. After careful evaluation, the set of design variables that consistently produced the best objective function value was selected for further analysis. This approach helped to increase the robustness of the optimization and minimize the likelihood of sub-optimal results.

5.2.1. Case A: Neglecting Floater Displacements

The optimization process was initially executed for the fixed platform configuration, that is for a FOWF with no degrees of freedom, to evaluate its performance under predefined conditions. The objective was to minimize the Levelized Cost of Energy (LCoE) while satisfying design constraints. The optimization process converged after 81 iterations, requiring approximately 47 minutes and 28 seconds to complete on a system equipped with an Intel Core i7-13620H CPU processor, 16 GB of RAM, and a 1 TB SSD storage. The resulting performance metrics of the optimization have been displayed in Table 5.1.

During the optimization, five constraints were identified as active—two in the super-problem and three in the sub-problem. For the super-problem, the active constraints were the footprint constraint, which ensures a minimum distance between turbines, and the draft constraint, which mandates that the draft of the semi-submersible exceed a certain minimum value. In the sub-problem, the active constraints were the freeboard constraint, which dictates the height of the semi-submersible above the waterline, and the maximum allowable pitch and surge displacements. These constraints therefore contribute to limiting the objective function to the optimal value it achieves. While increasing the limits of these constraints could potentially improve the objective function, it would render the design unfeasible.

Metric	Value
Time for convergence	47 min 28 sec
No. of Iterations	81
Total active constraints	5
No. of function evaluations for the super-problem	81
No. of function evaluations for the sub-problem (approx.)	3645
Average time per function evaluation of the super-problem	35 sec

Table 5.1: Optimization performance metrics for Case A

The initial and optimized values of the design variables for the fixed platform case have been displayed in Table 5.2. All optimized values were found to fall within the prescribed bounds.

Design Variables	Initial Value	Optimal Value
R_{out} [m]	6	3.29
Fr [m]	20	12.912
D_{mr} [m]	0.08	0.072
L_{mr} [m]	796.26	711.41
R_{mr} [m]	6D	5.12D
H_{mr}, rel [-]	0.3	0
Dr [m]	24	16.14
R_{off} [m]	50	51.38
Sp [m]	12.88D	11.12D
α [°]	90	179.81

Table 5.2: Optimal values of the Design Variables for the Case A

The optimal LCoE achieved for the fixed platform configuration is 86.89 €/MWh. The AEP was calculated at 898.96 GWh, down from the initial 909.92 GWh, as determined by the `FarmAEP` block. Additionally, the annual production cost of the substructure assembly, as computed by the `Substructure Analysis` block, amounted to 6.25 M€. The optimized layout, reveals a reduction in the turbine spacing from 12.88D to 11.12D, along with a rotation of the overall layout by 179.81°.

5.2.2. Case B: Accounting for Floater Displacements

The optimization of the FOWF, accounting for the floating turbine displacements, was executed with the same initial values for the design variables as used in Case A. The optimization process took about 4.5 hours to complete, with 77 function evaluations on a system equipped with an Intel Core i7-13620H CPU processor, 16 GB of RAM, and a 1 TB SSD storage. The performance metrics for this case have been tabulated in Table 5.3. For this case as well, the same five constraints were active, while the other four remained inactive throughout the optimization process.

Metric	Value
Time for convergence	4 hrs 8 mins
No. of Iterations	77
Total active constraints	5
No. of function evaluations for the super-problem	77
No. of function evaluations for the sub-problem (approx.)	3465
Average time per function evaluation of the super-problem	3 mins

Table 5.3: Optimization performance metrics for Case B

The optimal design variables obtained remained well within their defined bounds. The optimal values for the design variables in the floating platform case have been presented in Table 5.4. It can be observed that the optimal design variables for this case are largely similar to the fixed platform case, with the exception of the layout orientation (θ). This distinction will be further discussed in Section section 5.3.

Design Variables	Initial Value	Final Value
R_{out} [m]	6	3.28
Fr [m]	20	12.91
D_{mr} [m]	0.08	0.07
L_{mr} [m]	796.26	701.66
R_{mr} [m]	6D	5.04D
$H_{mr,rel}$ [-]	0.3	0
Dr [m]	24	16.14
R_{off} [m]	50	51.45
Sp [m]	12.88D	10.95D
α [°]	90	88.34

Table 5.4: Optimal values of the Design Variables for Case B

The Levelized Cost of Energy was optimized to 87.03 €/MWh for the floating platform case. Achieving this minimum LCoE resulted from an AEP of 896.8 GWh. Additionally, the yearly production cost of the substructure assembly was found to be 6.26 M€. This substructure cost was found to be identical in both the cases, suggesting that the optimal semi-submersible size remained the same.

5.3. Impact of Floater Displacements on the Optimization

The tilt and surge displacements of the substructure lead to a vertically upward deflection as well as a downward shift in the wake profile, directly affecting the power production and, consequently, the AEP of the floating offshore wind farm. Since the LCoE is dependent on the AEP, changes in AEP will also have an influence on the LCoE. This section analyzes the impact of incorporating floater motions on both the AEP and LCoE, in conjunction with the optimization of the substructure and wind farm layout.

The analysis begins by examining the effects of static floater displacements on the design variables, and the objective function. This is followed by a post-optimization analysis, which evaluates how the objective function responds to varying individual design variables while keeping others fixed at their optimal values. The findings have been contrasted between Case

A and Case B to highlight the differences.

5.3.1. Design Variables

The convergence history of the design variables related to the layout optimization, namely layout orientation (Figure 5.2a) and layout spacing (Figure 5.2b) have been displayed in Figure 5.2. The convergence histories of the key substructure and mooring lines-related design variables have been reported in Appendix A.

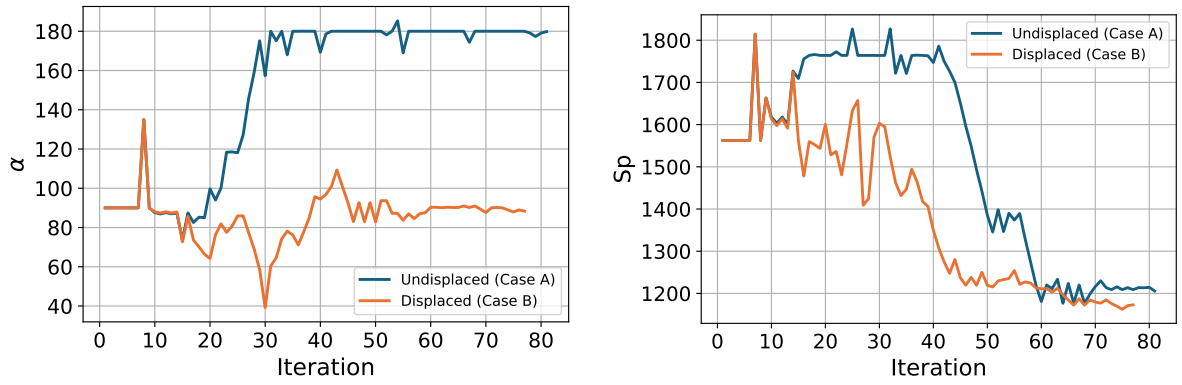

(a) Layout Orientation, α

(b) Layout Spacing, Sp

Figure 5.2: Convergence History of Wind farm layout Design Variables (DV) per iteration.

Notably, the layout orientation converges to significantly different values between the two cases, with a difference of nearly 90°. This variation has been attributed to the multi-modal nature of the objective function, as will be discussed in Section 5.4. In contrast, the layout spacing converges to similar optimal values for both cases.

In addition to converging to distinct values, the evolution of the design variables throughout the optimization process varies notably between the two configurations, as depicted in the figures. This divergence begins around the 15_{th} iteration, and is driven due to the changes in the objective function due to the tilt and surge displacements, that affects the steps taken by the optimization algorithm, to obtain the minimum from that point. While this effect is less pronounced for the other design variables, it has a significant impact on the layout spacing and orientation, leading to changes in the AEP compared to the fixed platform case. Consequently, this variation influences the objective function over the course of the optimization.

5.3.2. Annual Energy Production (AEP)

This section examines the impact of incorporating floater displacements into the optimization framework on the AEP of the 42-turbine wind farm. The optimal AEP values for the wind farm which will lead to the minimization of the LCoE, for both Case A and Case B configurations, corresponding to the respective layout spacing, have been presented in Figure 5.3.

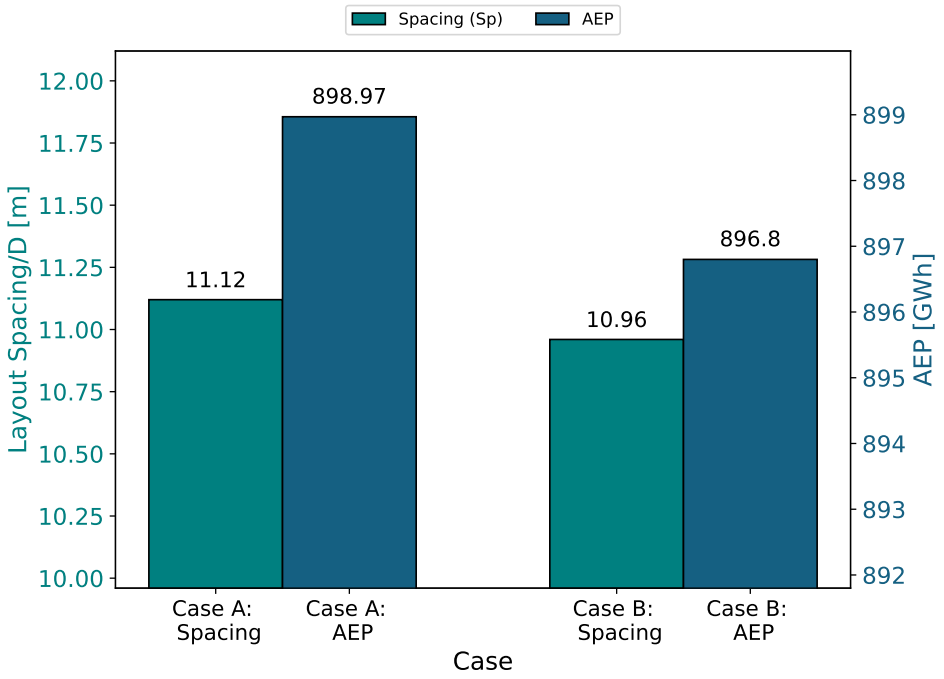

Figure 5.3: Comparison of optimal AEP at the optimal layout spacings for the floating and fixed platform cases.

As anticipated, the difference between the AEP values for the two cases is relatively minor, around 0.25%. This is largely due to the static nature of the substructure motions considered in this analysis. The AEP values reported here are based on an inter-turbine spacing of 11.12D for Case A, where the floater displacements are neglected and 10.96D for Case B, where the floater displacements are accounted for. The causes and implications of these differences have been discussed in the following subsections.

Effect of the Layout Design Variables on the AEP

This section presents a pre-optimization analysis to examine the sensitivity of the AEP to the layout-specific design variables: layout spacing and layout orientation. The analysis compares the impact of these variables on the AEP for both Case A and Case B configurations.

In Figure 5.4, the relation between the AEP and the distance between turbines can be observed for both the cases considering wind from the westward direction (270°), which is also close to the dominant wind direction for this site, and a freestream wind speed of 11 m/s, which is close to the turbines' rated wind speed. In the plot, the layout spacing is specified on the x-axis in terms of the rotor diameter of the wind turbine.

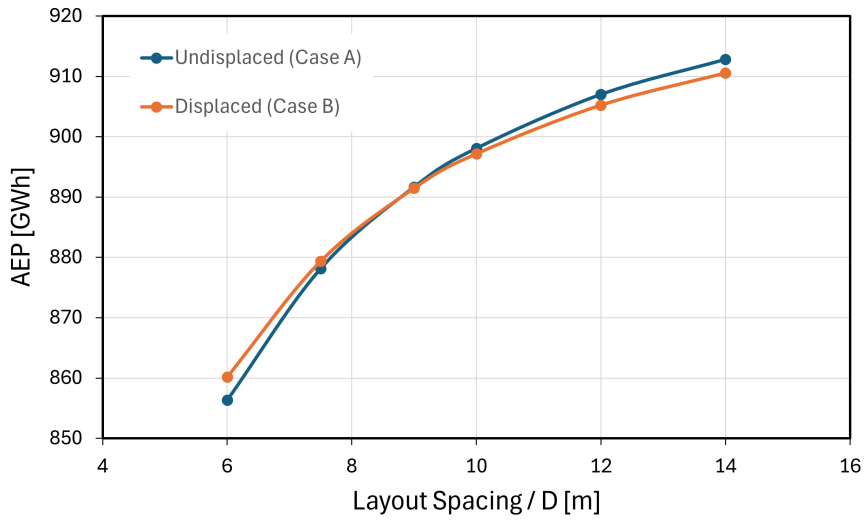

Figure 5.4: Comparison of AEP at different Layout Spacings for the Floating platform case vs the Fixed platform case.

It can be observed that as the distance between the turbines increases, the AEP also increases for both the cases at this wind speed and direction. Initially, the AEP of the FOWF for Case A is lower than that for Case B up to a spacing of approximately 9D. Beyond this point, however, the Case A AEP surpasses Case B AEP. This shift can be attributed to the fact that the tilt and surge displacements are primarily dependent on the magnitude of thrust experienced by a turbine rotor. In other words, the power generated by a turbine in the Case B configuration is directly influenced by the local effective wind speed, WS_{eff} at the turbine.

In a fixed-bottom wind farm (Case A), the wake from an upstream turbine remains directly aligned with the downstream turbine (at a wind direction of 270°), as the turbine is not allowed to move in any degrees of freedom. This results in a reduction in wind speed for the downstream turbine due to being placed in the wake deficit, directly affecting its power output. As the spacing between turbines increases, the downstream turbine experiences less wake interference, allowing it to operate close to the freestream conditions. Since the wind speeds without wake interference will be higher, the power produced will be higher, below rated conditions. Above rated wind speeds, the power production remains constant with increase in wind speed.

In contrast, for a floating wind farm (Case B), the wind turbines will tilt and surge under the action of thrust. These displacements, specifically tilt, cause the wake to deflect vertically, reducing its influence on the downstream turbine. Therefore, for smaller turbine spacing (up to 9D in this case), the Case B wind turbines benefit from this wake deflection and produce higher AEP than Case A wind turbines. However, as the spacing increases further, the turbine moves out of the wake, and the Case A turbines surpass the advantage Case B turbines had from the deflected wake.

The relationship between tilt angles and WS_{eff} as a function of freestream wind speed for both an upstream turbine (in the first column) and a downstream turbine (in the second column) has been depicted in Figure 5.5. The effective wind speed for the upstream turbine exhibits a nearly linear correlation with the freestream wind speed. Conversely, for the downstream turbine, the effective wind speed experiences a slight reduction near the rated wind speed. This outcome aligns with expectations, as the downstream turbine is affected by the wake generated by the upstream turbine, resulting in a diminished wind speed due to the wake deficit. The

corresponding impact of this phenomenon is also reflected in the tilt angles of both turbines.

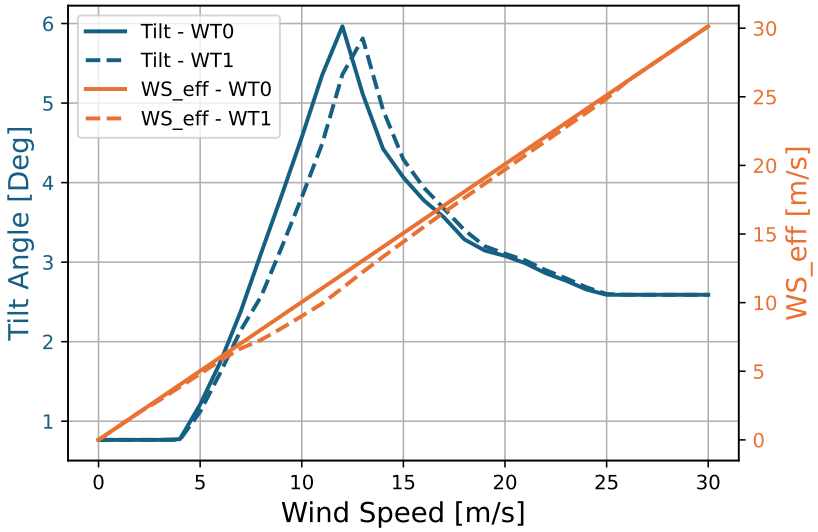

Figure 5.5: Tilt and Effective Wind Speed (WS_{eff}) variation with the Freestream Wind Speed.

A similar explanation applies to the sensitivity analysis of the AEP with respect to changes in layout orientation at a constant spacing of 7.5D, as presented in Figure 5.6. Only wind farm orientations from 0° to 90° have been displayed here, as the AEP values for the remaining orientations will have mirrored (90° to 180° quadrant) or symmetrical (180° to 270° quadrant) values. At this layout spacing, the Case B wind farm consistently achieves higher AEP than the Case A configuration, independent of the layout orientation. However, the AEP values vary depending on the specific layout orientation of the wind farm.

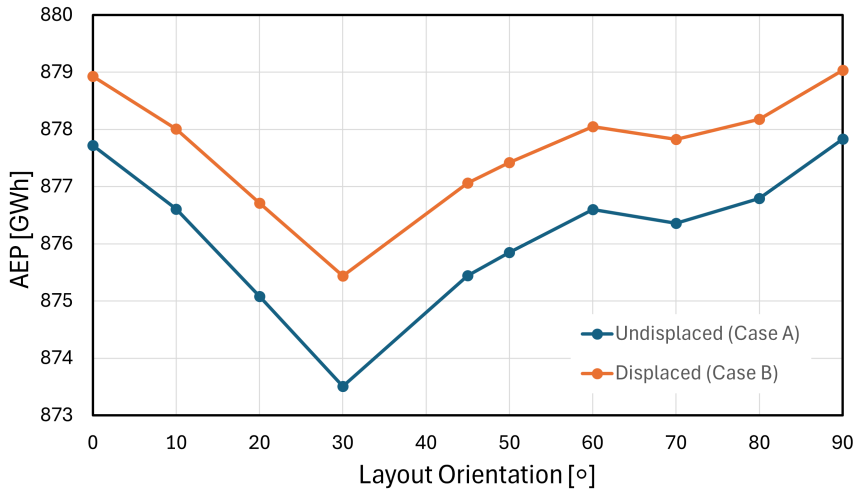

Figure 5.6: Comparison of AEP at different Layout Orientations for Case A vs Case B.

The lowest AEP has been observed when the farm is oriented at 30°, while the highest AEP occurs at 90°. This is because, at 30°, the downstream turbines are consistently positioned in the wake of the upstream turbines, regardless of the wind direction. Conversely, in the 90° orientation, there are wind directions where all downstream turbines experience freestream conditions, leading to higher AEP.

The effect of different wind directions on power gain for Case B relative to Case A at a specific wind farm orientation, 90° in this case, has been illustrated in Figure 5.7. In this figure, the y-axis represents normalized power, which has been defined as the ratio of the power generated by Case B to that produced by Case A. The normalized power has been plotted against the wind direction at a wind speed of 11 m/s, close to the rated wind speed for the turbine. A normalized power value greater than 1 indicates that the Case B configuration generates more power than the Case A configuration under the given wind conditions.

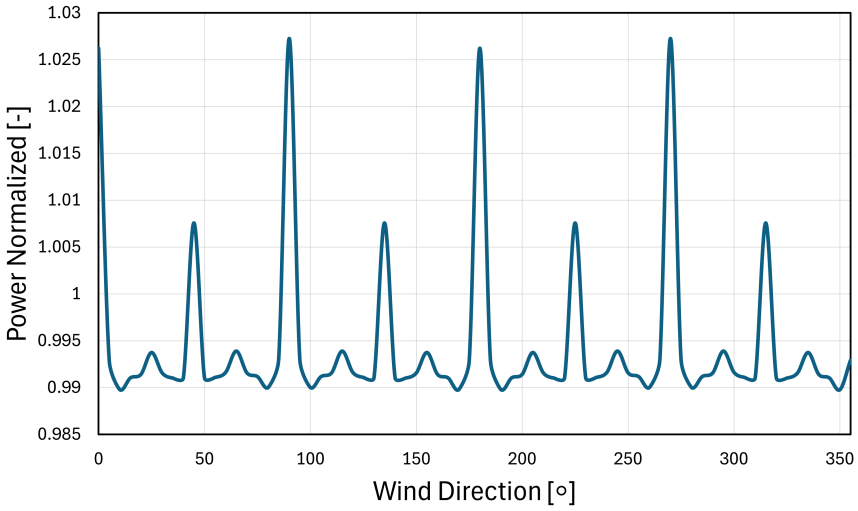

Figure 5.7: Normalized Power (Ratio of overall Wind Farm powers from Case B by Case A) vs Wind Direction.

The power gain for the floating platform configuration is most pronounced at wind directions of 0°, 90°, 180°, and 270°. This is because, at these angles, the downstream turbines are directly aligned with the wake of the upstream turbines. This can be visualized in Figure 5.8d, for the 270° wind direction, where the wind farm is aligned directly with the wind direction (the wake alignment is similar for 0°, 90° and 180° as shown in Appendix B). In the Case B configuration, floater displacements enable wake deflection, which mitigates the wake effect on downstream turbines, resulting in higher power generation compared to the Case A configuration. Consequently, Case B demonstrates a clear advantage in power output at these specific wind directions.

A similar benefit can be observed at wind directions of 45°, 135°, 225°, and 315°, although the power output for the Case B wind farm tends to decrease at other wind directions, the power gin being the lowest at 10°, 30° and 60°, and directions symmetrical to these. To better understand the wake profile at these wind directions, flow maps have been provided for the top view, in Figure 5.8a, Figure 5.8b and Figure 5.8c, respectively.

The lowest power generation from Figure 5.7 has been observed for the wind coming from 10°. For this wind direction (Figure 5.8a), none of the turbine rotors come in contact with the wake of the upstream turbines. Since all the turbines are facing the freestream wind speed, which is close to the rated wind speed here, the farm in the Case A configuration will produce close to the rated power, while at the same time, the farm in the Case B configuration will be at their maximum tilt, thus producing very low power. The power output at other wind directions can be similarly explained by the extent to which the rotor is submerged in the wake.

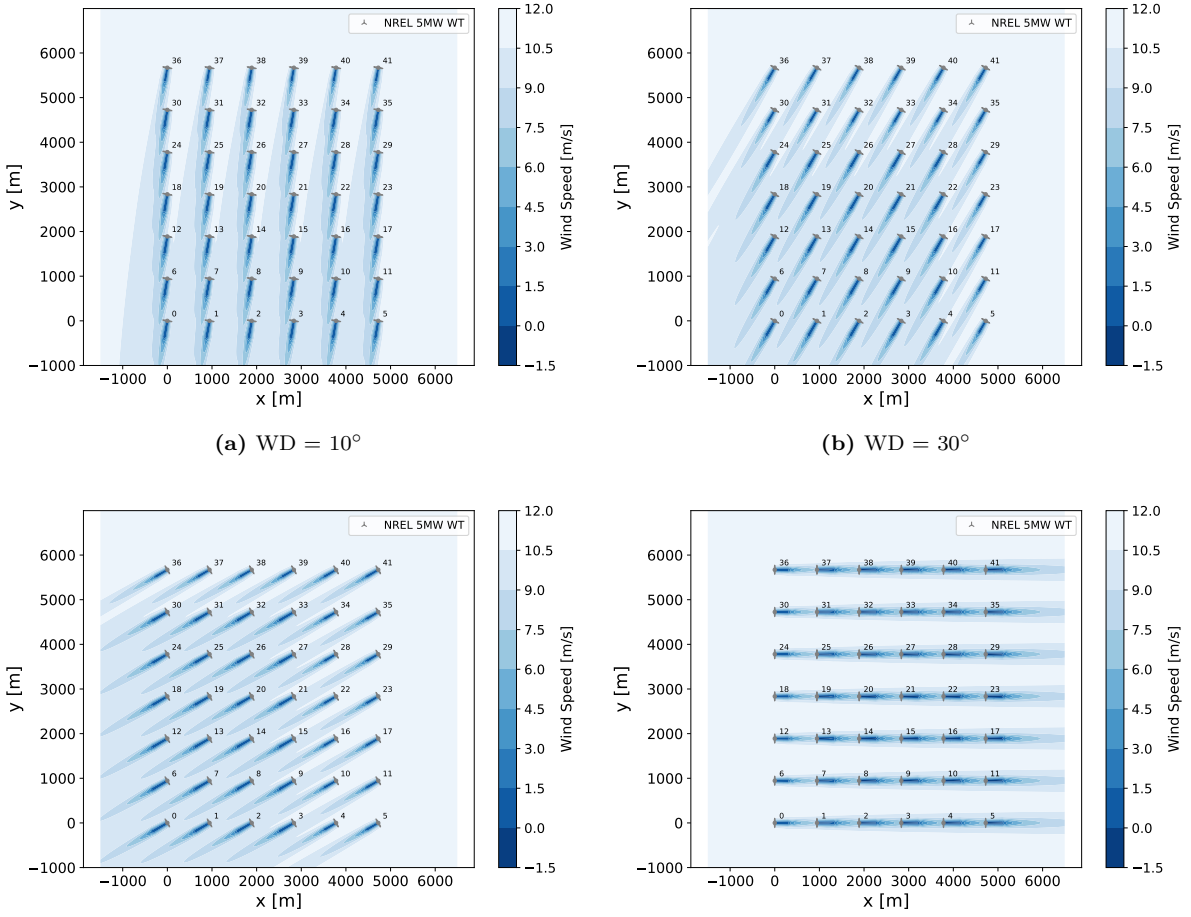

(a) WD = 10° **(b)** WD = 30°

(c) WD = 60° **(d)** WD = 270°

Figure 5.8: Top view of the wind farm layout displaying the wake profile at four different wind directions.

5.3.3. Levelized Cost of Energy (LCoE)

The convergence history of the objective function has been depicted in Figure 5.9a, with Case A (neglecting floater displacements) represented in blue and Case B (considering floater displacements) represented in orange. The plot reveals that convergence occurs in the final iterations, though the solution does not fully stabilize. To determine whether further iterations improve the solution, the tolerance limit of the fixed platform case was reduced to 1e-4. Although this adjustment resulted in the stabilization of the solution, as shown in Figure 5.9b, the Levelized Cost of Energy (LCoE) obtained remained almost identical to the previous value, differing by only 0.001 €/MWh, approximately. However, the computational time required increased by around four times compared to the convergence time with a tolerance of 1e-2. As the accuracy of the results remained nearly unchanged, a tolerance of 1e-2 was deemed sufficient for this analysis.

The Levelized Cost of Energy (LCoE) converges to nearly identical values for both cases, although differences in how the LCoE evolves throughout the optimization process can be observed. Notably, around the 25^{th} iteration, the LCoE temporarily falls below the final optimal value. However, these lower values have not been considered optimal as the model violates certain constraints in this region, particularly the minimum draft constraint, as shown in the constraint convergence history plots in Figure A.2b in Appendix A.

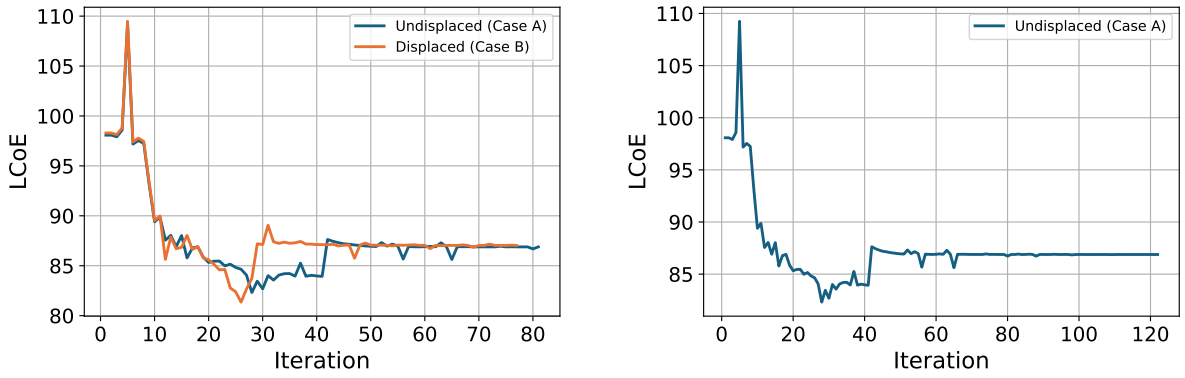

(a) tol = 1e-2 **(b)** tol = 1e-4

Figure 5.9: Convergence history of the Objective Function for different Tolerance Values.

The final optimized LCoE values have been presented in Figure 5.10, along with the percentage contributions from the production cost ($C_{prd,y}$), the installation cost (C_{ins}), and operation and maintenance costs ($C_{O\&M}$). Given that both the capital expenditure (CapEX) and operational expenditure (OpEX) remain almost unchanged across the two configurations, the observed differences in LCoE primarily stem from variations in AEP, which are influenced by the floater motions.

The analysis suggests that the optimizer slightly underestimates the minimized LCoE when floater displacements are not taken into account, with a difference of approximately 0.162 €/MWh between the two scenarios.

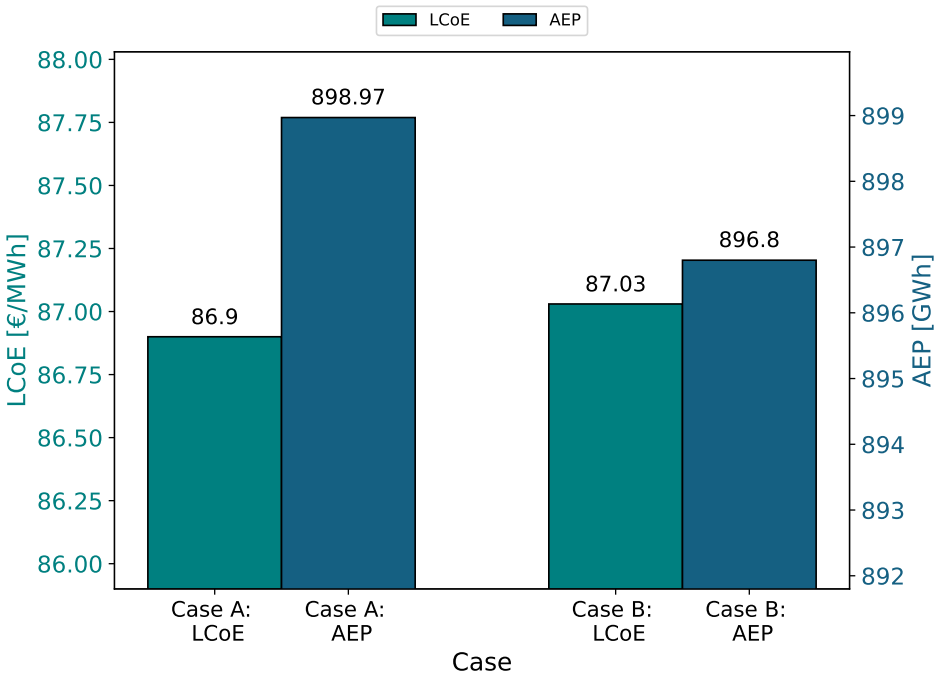

Figure 5.10: Comparison of the LCoE, corresponding to the AEP between the two Cases.

5.4. Post Optimization Analysis

This section provides an analysis of the optimal LCoE values obtained through optimization, with a focus on understanding their relationship to layout spacing and orientation. As established earlier, the difference in LCoE between the two cases is primarily driven by variations in AEP, which is largely influenced by the layout design rather than the size and design of the semi-submersible platform. Therefore, it is important to assess the impact of these two design variables in isolation.

Two setups were considered for this analysis. In the first, the layout spacing was varied within its bounds while keeping all other design variables fixed at their optimal values. In the second setup, the layout orientation was varied from 0° to 180°, with the other variables again held constant at their optimal values. The resulting LCoE and corresponding AEP for both scenarios have been presented in Figure 5.11 and Figure 5.12, respectively.

Layout Spacing

Figure 5.11 illustrates the variation in LCoE with respect to layout spacing while keeping the other design variables constant at their optimal values. The identified minimum LCoE and its corresponding layout spacing have been highlighted in red. It is noticeable that these points do not coincide with the global minimum of the objective function, which occurs at approximately 10.2D for Case A and 9.2D for Case B. This is because if the optimizer converges to these values of layout spacings, it will be violating the constraint of minimum distance between the turbines which has been defined as twice the sum of the anchor-fairlead distance, the offset, and the outer column radius of the semi-submersible. This region, termed as the infeasible region has been demarcated by the dashed lines in the plot, blue corresponding to the undisplaced floater case and orange corresponding to the displaced floater case. The zone extends up to about 11.10D for Case A and 10.95D for Case B.

The actual optimal layout spacings have been found at 11.12D and 10.96D for the undisplaced floater case (Case A) and the displaced floater case (Case B), respectively. Therefore, since the feasible region itself begins right before these points, the obtained LCoE values can be considered the global minima for both the cases.

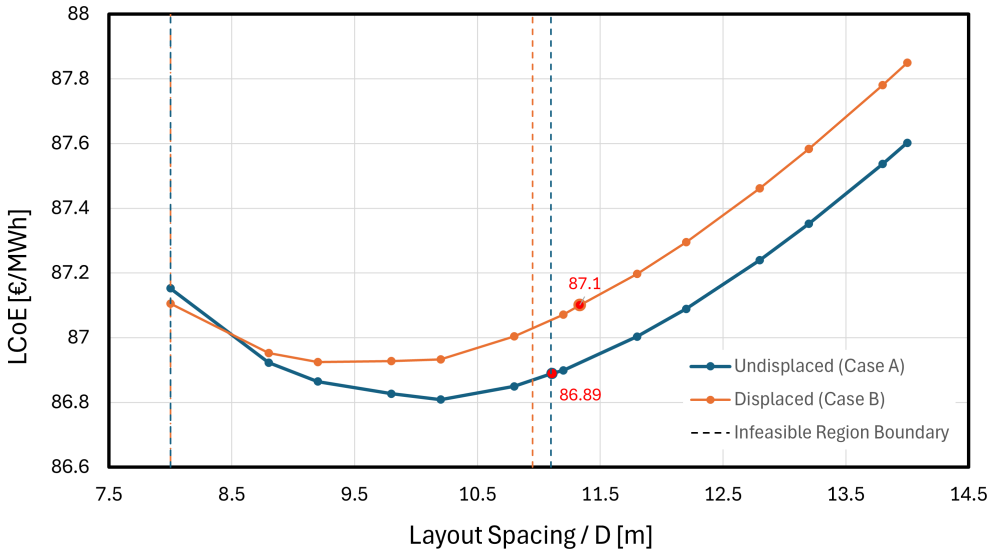

Figure 5.11: LCoE at varying Layout Spacings, with other design variables at their optimal. The blue dashed line demarcates the boundary between the feasible and infeasible regions for the Undisplaced floater case (Case A), while the orange dashed line demarcates the boundary for the Displaced floater case (Case B).

Layout Orientation

This section presents a similar analysis of LCoE with respect to layout orientation. Unlike the case of layout spacing, no constraints are violated in the analysis of LCoE versus layout orientation, and thus the obtained minima appear to be optimal. The plot shown in Figure 5.12 highlights the minima, marked in red, which were derived from the optimization process. A notable difference can be observed between the optimal layout orientations for the Case A and Case B wind farm configurations. This is due to the multi-modal nature of LCoE with respect to layout orientation. While the optimization successfully reaches the global minimum for Case B, it converges to a local minimum for Case A. However, since the difference between the global minimum and the obtained local minimum is minimal, extending to two decimal places, the local minimum is considered acceptable for the purpose of comparing the results obtained by neglecting the displacement of the wind turbine during the optimization of the wind farm.

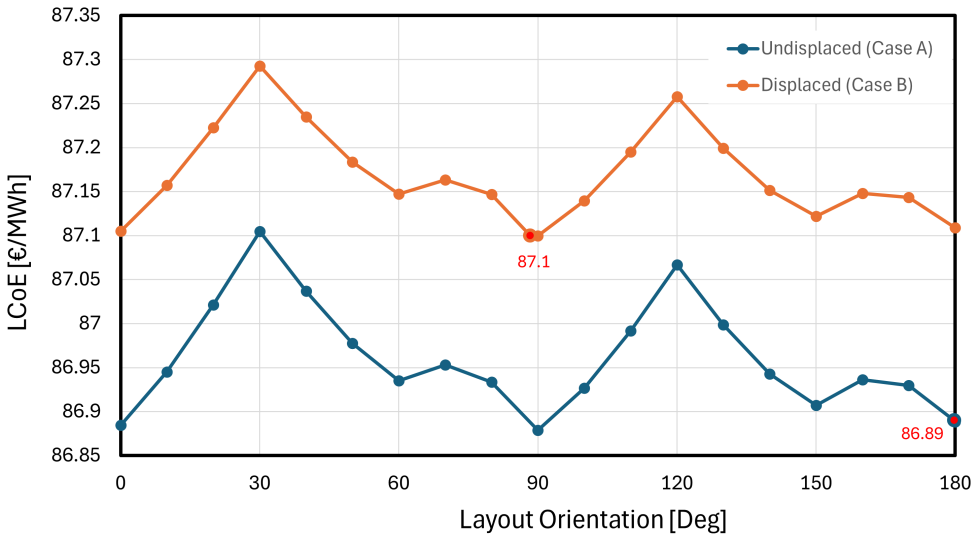

Figure 5.12: LCoE for the Undisplaced (Case A) and the Displaced (Case B) floater cases at varying Layout Orientations, with the other deign variables at their optimal.

5.5. Water Depth Analysis

The results presented thus far have been computed at a water depth of 200 meters. However, water depth can influence the optimization outcomes, as well as the differences observed between cases that account for or neglect floater displacements. This is primarily due to the dependency of the mooring line tether length on water depth, with greater depths requiring longer tethers, which in turn increases mooring costs [54]. The tether length also contributes to the surge, heave, pitch, and yaw responses of the floating substructure, which directly affect wake dynamics and consequently the power production of the turbine. Additionally, changes in water depth impact the allowable displacement of the floater. Shallower waters often necessitate shorter but heavier mooring chains due to stricter displacement limits, while in deeper waters, the mass of the catenary mooring lines increases with the longer chains required to accommodate greater depths.

This section provides an analysis of the observed variations in the water depth in the obtained results, for both Case A (neglecting displacement) and Case B (accounting for displacement), at two different water depths. A water depth of 100m has been selected for this purpose and compared with the originally chosen 200m water depth cases. The optimal values of the LCoE and the AEP for both water depths and the AEP computation cases (Case A and Case B) have been displayed in Figure 5.13a and Figure 5.13b, respectively.

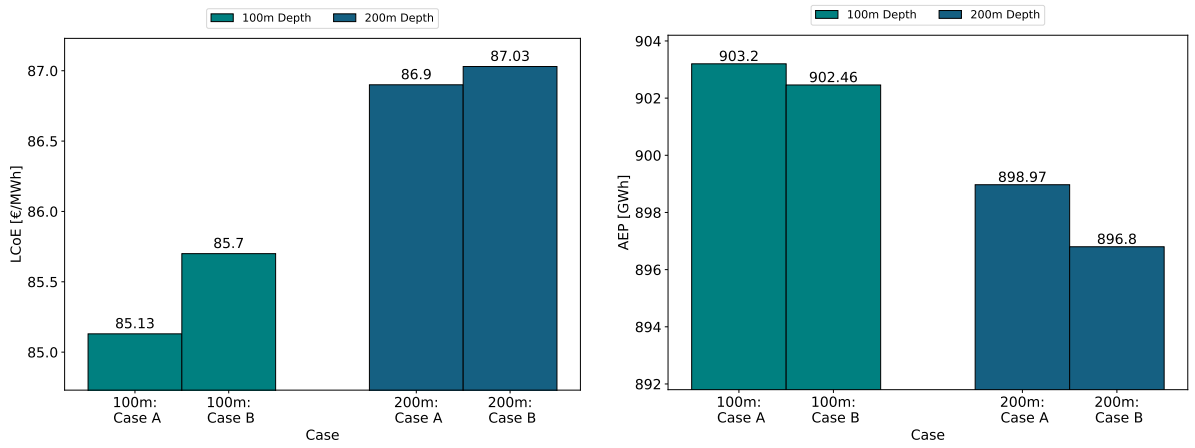

(a) Levelized Cost of Energy (LCoE)

(b) Annual Energy Production (AEP)

Figure 5.13: LCoE and AEP comparisons for floater cases the Case A (Neglecting floater displacement) and Case B (Accounting for floater displacement) at Water Depths 100m (shown in teal) and 200m (shown in blue).

The Levelized Cost of Energy (LCoE) for the 100m water depth case is significantly lower than for the 200m water depth case, both when floater displacements are considered and when they are neglected, as depicted in Figure 5.13a. Specifically, a reduction of approximately 2% is observed in Case A and about 1.5% in Case B, relative to the 200m case. On the other hand, the AEP exhibits an opposite trend, since it is inversely related to LCoE, as shown in Figure 5.13b. The AEP for the 100m case shows an increase of around 0.47% in Case A and 0.63% in Case B. However, the percentage increase in LCoE is less than the percentage decrease in AEP. This is because the mooring line lengths and types are also affected due to change in water depths, which leads to a change in the capital expenditure costs(CapEX), ultimately leading to an additional increase in the LCoE.

6

Conclusions and Recommendations

6.1. Conclusion

Floating offshore wind energy represents a rapidly evolving and innovative sector within the renewable energy industry. It offers the capability to exploit stronger and more stable wind resources found in deep-water regions, where conventional bottom-fixed turbines are not feasible. By expanding into these deeper ocean areas, floating wind technology unlocks access to vast, previously untapped wind resources, potentially making a substantial contribution to global renewable energy goals. However, despite its promise, the development of floating offshore wind farms faces several challenges, particularly due to the high Levelized Cost of Energy (LCoE). The emergence of multidisciplinary optimization frameworks represents a step forward in reducing LCoE, by allowing trade-offs between various subsystems of Floating Offshore Wind Turbines (FOWTs), in an attempt to make the technology more economically competitive with other renewable sources.

One of the major barriers in this process is the limited understanding of the impact of the displacements of the floating platform on energy yield and, ultimately, on the LCoE of the wind farm. This knowledge gap hampers efforts to identify the optimal wind farm design that minimizes LCoE while accounting for the flexibility of floating substructures to displace in six DOFs.

This thesis addressed this gap by exploring the effects of incorporating the static equilibrium displacements of the floater in two key degrees of freedom—tilt and surge—into the optimization framework, WINDOW. The study compares two scenarios: `Case A`, where floater displacements are neglected, and `Case B`, where floater displacements are accounted for. A method was developed to incorporate these two degrees of freedom into the wake modeling of FOWFs using the PyWake framework. This enhanced wake model was then integrated into the WINDOW FOWF optimization framework.

The results of this thesis show that the observed differences in AEP, LCoE and the layout design between the two cases were relatively minor. Moreover, the time required for the solver to converge to the optimal values varied significantly between the two cases, with Case A converging in approximately 50 minutes, whereas Case B requiring about 4 hours to reach the minimum. This can be attributed to the additional computational effort needed to account for the floater displacements, which necessitated repeatedly calling the PyWake solver for every wind direction and wind speed until the tilt and surge values converged for each turbine. Each AEP evaluation took about 3 minutes, significantly extending the overall computational time

taken for approximately 80 iterations. Given this, it can be inferred that the inclusion of static equilibrium displacements of the substructure could be omitted when optimizing larger wind farms, as it adds substantial computational costs without significantly affecting the results.

The key findings corresponding to the research questions posed have been summarized as follows:

- *RQ 1: What strategy can be employed to adapt PyWake for modeling static equilibrium displacements of the floating wind turbine, specifically in the tilt and surge DOFs?*

  In this thesis, the static tilt displacement of the substructure has been defined as the rotation of the wind turbine rotor in the positive or negative pitch direction along the transverse axis. The surge motion, conversely, refers to the displacement of the wind turbine structure along the x-axis, in the downwind direction. An iterative methodology was developed to account for the steady-state impact of these displacements on the wake profile and, consequently, the AEP of FOWFs, using the PyWake framework.

  The process began by providing an initial estimate of the floater displacements to PyWake, according to the freestream wind speed, which then calculates the effective wind speed based on these estimates. This effective wind speed was subsequently used to compute the corresponding floater displacements using reference tables, where tilt and surge were expressed as functions of wind speed. This iterative loop continues until convergence, i.e., when the tilt and surge values from successive iterations matched. Once convergence was achieved, the final power output and AEP of the wind farm were computed.

  Therefore, while the floater displacements were not directly integrated into PyWake, the framework was effectively adapted to model the wake of FOWTs with two degrees of freedom, using the iterative approach outlined above. The accuracy and functionality of this approach were verified against results from published research, where they were found to be generally in agreement with previous findings.

- *RQ2: What are the observable variances in the computed AEP for FOWTs when accounting for or neglecting floating turbine displacements, and what are the primary causes of these deviations?*

  The wake of FOWTs with floater displacements exhibits vertical upward deflection, induced by the turbine heeling backward in the wind direction and horizontal downwind displacement, due to the turbine surging in the downstream direction. Flow maps reveal that deflection due to tilt causes the downstream turbine to encounter a different wind speed profile depending on where the wake interacts with the rotor, as opposed to the wind speed it would experience due to the undeflected wake profile in the absence of tilt. In contrast, the surge motion of the floater did not significantly alter the wake profile. However, subtle changes in turbine spacing were observed, where the downstream turbine could be positioned either closer to or further from the upstream turbine depending on the direction of the surge, thereby experiencing varying wind speeds from the wake.

  For the verification case studies, an overall energy gain of approximately 2.85% was observed for a wind farm consisting of three turbines aligned in a row, while a reduction in AEP of around 0.5% was found for a farm with four turbines positioned at the corners of a rectangle. Furthermore, for the case study with 42 wind turbines, positioned in 7 rows and 6 columns, the AEP of Case A (neglecting floater displacements) was found to be about 2.2 GWh higher than that of Case B (accounting for floater displacements), which corresponds to about 0.25% decrease in the AEP for Case B.

The discrepancies in the AEP observed arise from the effect the wake of an upstream turbine has on the downstream turbine when neglecting or considering floater displacements. For Case A, the wake remains undeflected, which leads to the upstream turbine producing higher power as compared to the upstream turbine of Case B. However, the wake for Case B is deflected which leads to the downstream turbine producing higher power as compared to the downstream turbine of Case A. The increase or decrease of the AEP is also dependent on the spacing between two turbines in the layout as shown in Figure 5.4. For lower layout spacings (upto about 9D), as shown in the figure, Case B wind farm produces higher AEP than Case A wind farm, which surpasses as the distance between the turbines increases further. This is because the downstream turbines of Case B experience the advantage of the deflected wake which diminishes as the distance between the turbines increases. Since a tilted rotor produces lower power than a non-tilted rotor, Case B FOWF produces lower AEP as compared to Case A FOWF.

- *RQ3: What are the differences in the optimal wind farm configuration obtained when accounting for static tilt and surge vs not accounting for it?*

  Since floating turbine displacements were already integrated into the other components of the optimization framework, except for the AEP analysis block, the most significant changes in the optimization results emerged from the impact on AEP due to the inclusion of these floater displacements. The layout design variables were primarily affected, as the AEP now provided values that led to an optimal Levelized Cost of Energy (LCoE) at different turbine spacing compared to the results obtained without considering floater displacements.

  For the Case A Floating Offshore Wind Farm (FOWF), the optimal layout was oriented at approximately 179.81° in the Cartesian plane, with a turbine spacing of about 11.12 times the rotor diameter. In contrast, for the Case B FOWF, accounting for two DOFs (tilt and surge), the optimal layout shifted to an orientation of 88.34°, with a turbine spacing of 10.95 times the rotor diameter, which is a 1.5% reduction from Case A. Other than that, the majority of the other design variables and the constraints were found to only minutely shift from their original values. The evolution of the parameters during the optimization process through the iterations was also found to be different for both cases.

- *RQ4: How does the incorporation of static floater displacements in the optimization framework impact the LCoE of the wind farm?*

  The higher-level goal of this thesis was to understand the effects of integrating floater displacements within the optimization framework aimed at minimizing the Levelized Cost of Energy (LCoE). This was achieved by modifying the AEP analysis module and adding a block in the framework to compute reference floater displacement values, corresponding to the freestream wind speed.

  The LCoE for a FOWF with a floater having two DOFs (Case B) was calculated to be 87.03 €/MWh, which was approximately 0.162 €/MWh lower than that for a FOWF with a zero DOF floater (Case A). The difference is modest because it is primarily a consequence of the minor variation observed in the AEP, while other LCoE components—such as annual production, installation, and operation and maintenance costs—undergo very minute changes.

6.2. Future Recommendations

During the course of this thesis, several potential research directions have been identified that could extend and build upon the work presented here. Some of these areas could have been explored further if more time had been available. These recommendations are outlined as follows:

Validation

While the proposed FOWF wake model has been verified against existing research, a more comprehensive validation should be conducted using established computational wake modeling solvers such as FAST.Farm, DWM, and SOWFA. This would determine whether the low-fidelity PyWake-based solver can produce results comparable to other medium- and high-fidelity solvers. Additionally, experimental validation should be pursued to align the model with real-world data, further strengthening its applicability.

Time taken for the simulation

As discussed, the computation time for a single round of AEP calculations for a floating offshore wind farm is relatively long, even for a low-fidelity solver. Reducing the simulation time would significantly enhance the computational efficiency of this solver, leading to lower computational costs and making the approach more practical for larger-scale optimizations.

Wind Farm Layout Design

In this thesis, a rectangular grid-based wind farm layout with 6 turbines per row and 7 per column has been simulated. The analysis revealed that accounting for floater displacements resulted in higher power production when a multi-column wind farm layout, with more number of columns than rows in the prevailing wind direction, was considered. If this observation holds true in high-fidelity simulations and real-world applications, it could present a strong upside for of floating offshore wind farms (FOWFs). This approach has the potential to enhance power output compared to fixed-bottom farms. Future research should investigate this hypothesis by testing various layout configurations, as this could provide significant advantages to the FOWF industry.

Additionally, the current optimization framework is constrained to gridded layouts. Expanding this capability to support non-uniform layouts would allow for the optimization of real-world wind farm layouts, offering a more flexible and practical tool for the industry. This would provide an alternative representation of wind farm configurations and enable more precise optimization, potentially leading to further gains in energy efficiency and cost-effectiveness for practical wind farm layouts.

Incorporation of Dynamic Motions

This thesis focused on the static equilibrium displacement of floating wind turbines. Future work should focus on incorporating dynamic motions into low-fidelity wake models, as real-world turbines do not remain in displaced positions but move back and forth in the six degrees of freedom. This introduces enhanced wake meandering and interaction of the turbine with its own wake, which can lead to additional losses. Accurately estimating these losses could result in better micro-siting of wind turbines in the wind farm. While high-fidelity solvers account for such dynamics, integrating dynamic motions into low-fidelity solvers would allow for faster optimizations and the ability to simulate a wider range of scenarios. Additionally, this thesis only considered two degrees of freedom, tilt, and surge, which were found to have the most significant impact on wake behavior. Future research should explore the inclusion of other degrees of freedom, such as heave and yaw, as they may introduce further wake deflections and impact energy production estimates.

References

[1] Oliver Summerfield-Ryan and Susan Park. "The power of wind: The global wind energy industry's successes and failures". In: *Ecological Economics* 210 (Aug. 2023), p. 107841. ISSN: 0921-8009. DOI: 10.1016/J.ECOLECON.2023.107841.

[2] International Energy Agency. *Net Zero by 2050 - A Roadmap for the Global Energy Sector*. Tech. rep. 2050. URL: www.iea.org/t&c/.

[3] *GWEC, 2021. Global Wind Market Development: Supply Side Data 2020.* Tech. rep. URL: https://gwec.net/wp-content/uploads/2021/11/GWEC-Supply-Side-Data-2020_Final.pdf.

[4] Mehmet Bilgili and Hakan Alphan. "Global growth in offshore wind turbine technology". In: *Clean Technologies and Environmental Policy* 24.7 (Sept. 2022), pp. 2215–2227. ISSN: 16189558. DOI: 10.1007/s10098-022-02314-0.

[5] International Energy Agency. *Offshore Wind Outlook 2019: World Energy Outlook Special Report*. Tech. rep. URL: www.iea.org/t&c/.

[6] Joao Cruz and Mairead Atcheson. *Green Energy and Technology Floating Offshore Wind Energy The Next Generation of Wind Energy*. Tech. rep. URL: http://www.springer.com/series/8059.

[7] M. Baudino Bessone et al. "Including installation logistics costs in the optimal sizing of semi-submersibles for floating wind farms". In: *Journal of Physics: Conference Series*. Vol. 2265. 4. Institute of Physics, June 2022. DOI: 10.1088/1742-6596/2265/4/042018.

[8] *GWEC.NET Associate Sponsors Supporting Sponsor Leading Sponsor*. Tech. rep. URL: www.gwec.net.

[9] Antonio Pegalajar-Jurado et al. "State-of-the-art model for the LIFES50+ OO-Star Wind Floater Semi 10MW floating wind turbine". In: *Journal of Physics: Conference Series*. Vol. 1104. 1. Institute of Physics Publishing, Nov. 2018. DOI: 10.1088/1742-6596/1104/1/012024.

[10] Emma C. Edwards et al. "Evolution of floating offshore wind platforms: A review of at-sea devices". In: *Renewable and Sustainable Energy Reviews* 183 (Sept. 2023), p. 113416. ISSN: 1364-0321. DOI: 10.1016/J.RSER.2023.113416.

[11] Andrew R Henderson and David Witcher. *Floating Offshore Wind Energy-A Review of the Current Status and an Assessment of the Prospects*. Tech. rep. 1. 2010, pp. 1–16.

[12] *SBM Offshore announces the successful installation of the 3 floating wind units for the Provence Grand Large pilot project*. Aug. 2023. URL: https://www.sbmoffshore.com/newsroom/news-events/sbm-offshore-announces-successful-installation-3-floating-wind-units.

[13] Syed Azeem Uddin and Mohd Tousif. "Dynamic Analysis of a Symmetrically Moored Semisubmersible Under Various Possible Mooring Combinations". In: *Journal of Marine Science and Application* 23.1 (Mar. 2024), pp. 160–181. ISSN: 19935048. DOI: 10.1007/s11804-024-00390-w.

[14] F. González-Longatt, P. P. Wall, and V. Terzija. "Wake effect in wind farm performance: Steady-state and dynamic behavior". In: *Renewable Energy* 39.1 (Mar. 2012), pp. 329–338. ISSN: 0960-1481. DOI: 10.1016/J.RENENE.2011.08.053.

[15] B. Roscher et al. "Comparison of wind turbine loads inside a wake between engineering model and CFD calculation". In: *Journal of Physics: Conference Series*. Vol. 1037. 7. Institute of Physics Publishing, June 2018. DOI: 10.1088/1742-6596/1037/7/072039.

[16] Daniel R. Houck. "Review of wake management techniques for wind turbines". In: *Wind Energy* 25.2 (Feb. 2022), pp. 195–220. ISSN: 10991824. DOI: 10.1002/we.2668.

[17] C. T. Kiranoudis and Z. B. Maroulis. "Effective short-cut modelling of wind park efficiency". In: *Renewable Energy* 11.4 (Aug. 1997), pp. 439–457. ISSN: 0960-1481. DOI: 10.1016/S0960-1481(97)00011-6.

[18] J. K. Lundquist et al. "Costs and consequences of wind turbine wake effects arising from uncoordinated wind energy development". In: *Nature Energy* 4.1 (Jan. 2019), pp. 26–34. ISSN: 20587546. DOI: 10.1038/s41560-018-0281-2.

[19] Johan Meyers et al. *Wind farm flow control: Prospects and challenges*. Nov. 2022. DOI: 10.5194/wes-7-2271-2022.

[20] Xu Ning et al. *Numerical Study of Wake Interaction and its Effect on Wind Turbine Aerodynamics Based on Actuator Line Model*. 2019. ISBN: 9781880653852. URL: www.isope.org.

[21] Chih Hua Keni Wu and Vinh Tan Nguyen. "Aerodynamic simulations of offshore floating wind turbine in platform-induced pitching motion". In: *Wind Energy* 20.5 (May 2017), pp. 835–858. ISSN: 10991824. DOI: 10.1002/we.2066.

[22] Hyunkee Kim et al. "Windfarm layout optimization with a newly-modified multi-wake model based on aerodynamic characteristics of floating wind-turbines". In: *Journal of Mechanical Science and Technology* 37.9 (Sept. 2023), pp. 4661–4670. ISSN: 19763824. DOI: 10.1007/s12206-023-0821-y.

[23] Rabia Shakoor et al. "Wake effect modeling: A review of wind farm layout optimization using Jensen s model". In: *Renewable and Sustainable Energy Reviews* 58 (May 2016), pp. 1048–1059. ISSN: 1364-0321. DOI: 10.1016/J.RSER.2015.12.229.

[24] Shifeng Fu et al. "Wake and power fluctuations of a model wind turbine subjected to pitch and roll oscillations". In: *Applied Energy* 253 (Nov. 2019), p. 113605. ISSN: 0306-2619. DOI: 10.1016/J.APENERGY.2019.113605.

[25] Federico Taruffi et al. "An experimental study on the aerodynamic loads of a floating offshore wind turbine under imposed motions". In: (). DOI: 10.5194/wes-2023-86. URL: https://doi.org/10.5194/wes-2023-86.

[26] Danmei Hu et al. "Aerodynamic wake characteristics analysis of floating offshore wind turbine under platform pitching and yawing motions". In: *Journal of Renewable and Sustainable Energy* 15.3 (May 2023). ISSN: 19417012. DOI: 10.1063/5.0148352.

[27] J. G. Schepers and S. P. Van Der Pijl. "Improved modelling of wake aerodynamics and assessment of new farm control strategies". In: *Journal of Physics: Conference Series*. Vol. 75. 1. Institute of Physics Publishing, June 2007. DOI: 10.1088/1742-6596/75/1/012039.

[28] Giorgio Crasto and Arne Reidar Gravdahl. *CFD wake modeling using a porous disc Summary of the work*. Tech. rep.

[29] J. F. Ainslie. "Calculating the flowfield in the wake of wind turbines". In: *Journal of Wind Engineering and Industrial Aerodynamics* 27.1-3 (Jan. 1988), pp. 213–224. ISSN: 0167-6105. DOI: 10.1016/0167-6105(88)90037-2.

[30] Jens Nørkær Sørensen and Wen Zhong Shen. "Numerical modeling of wind turbine wakes". In: *Journal of Fluids Engineering, Transactions of the ASME* 124.2 (2002), pp. 393–399. ISSN: 00982202. DOI: 10.1115/1.1471361.

[31] Shudong Leng et al. "Study on the near Wake Aerodynamic Characteristics of Floating Offshore Wind Turbine under Combined Surge and Pitch Motion". In: *Energies* 17.3 (Feb. 2024). ISSN: 19961073. DOI: 10.3390/en17030744.

[32] Ping Cheng, Yang Huang, and Decheng Wan. "A numerical model for fully coupled aero-hydrodynamic analysis of floating offshore wind turbine". In: *Ocean Engineering* 173 (Feb. 2019), pp. 183–196. ISSN: 0029-8018. DOI: 10.1016/J.OCEANENG.2018.12.021.

[33] Adam S. Wise and Erin E. Bachynski. "Wake meandering effects on floating wind turbines". In: *Wind Energy* 23.5 (May 2020), pp. 1266–1285. ISSN: 10991824. DOI: 10.1002/we.2485.

[34] Jason Jonkman et al. *Development of FAST.Farm: A New Multiphysics Engineering Tool for Wind Farm Design and Analysis: Preprint*. Tech. rep. 2017. URL: www.nrel.gov/publications..

[35] Alireza Arabgolarcheh, Sahar Jannesarahmadi, and Ernesto Benini. "Modeling of near wake characteristics in floating offshore wind turbines using an actuator line method". In: *Renewable Energy* 185 (Feb. 2022), pp. 871–887. ISSN: 18790682. DOI: 10.1016/j.renene.2021.12.099.

[36] N O Jensen. *General rights A note on wind generator interaction*. Tech. rep. 1983.

[37] I ; Katic, J ; Højstrup, and N O Jensen. *A Simple Model for Cluster Efficiency*. Tech. rep. 1987, pp. 407–410.

[38] P. B.S. Lissaman. "ENERGY EFFECTIVENESS OF ARBITRARY ARRAYS OF WIND TURBINES." In: *Journal of energy* 3.6 (1979), pp. 323–328. ISSN: 01460412. DOI: 10.2514/3.62441.

[39] Takeshi Ishihara, Atsushi Yamaguchi, and Yozo Fujino. *Development of a new wake model based on a wind tunnel experiment Development of a New Wake Model Based on a Wind Tunnel Experiment Analytical Model Wind Tunnel Experiment Conclusion Verification*. Tech. rep. URL: https://www.researchgate.net/publication/229014372.

[40] Camilla Leikvoll et al. *Effect of Rotor Tilt on the Performance of Floating Offshore Wind Turbines An analysis using engineering wake models*. Tech. rep.

[41] E. Faraggiana et al. "Optimal floating offshore wind farms for Mediterranean islands". In: *Renewable Energy* 221 (Feb. 2024). ISSN: 18790682. DOI: 10.1016/j.renene.2023.119785.

[42] *PyWake, DTU Wind Energy*. URL: https://topfarm.pages.windenergy.dtu.dk/PyWake/.

[43] Yangwei Wang, Jiahuan Lin, and Jun Zhang. "Investigation of a new analytical wake prediction method for offshore floating wind turbines considering an accurate incoming wind flow". In: *Renewable Energy* 185 (Feb. 2022), pp. 827–849. ISSN: 18790682. DOI: 10.1016/j.renene.2021.12.060.

[44] Majid Bastankhah and Fernando Porté-Agel. "A new analytical model for wind-turbine wakes". In: *Renewable Energy* 70 (Oct. 2014), pp. 116–123. ISSN: 0960-1481. DOI: 10.1016/J.RENENE.2014.01.002.

[45] Morteza Khosravi, Partha Sarkar, and Hui Hu. "An experimental investigation on the aeromechanic performance and wake characteristics of a wind turbine model subjected to pitch motions". In: *34th Wind Energy Symposium*. American Institute of Aeronautics and Astronautics Inc, AIAA, 2016. ISBN: 9781624103957. DOI: 10.2514/6.2016-1997.

[46] Riccardo Riva et al. "Incorporation of floater rotation and displacement in a static wind farm simulator". In: *Journal of Physics: Conference Series* 2767.6 (June 2024), p. 062019. ISSN: 1742-6588. DOI: 10.1088/1742-6596/2767/6/062019. URL: https://iopscience.iop.org/article/10.1088/1742-6596/2767/6/062019.

[47] Christos Galinos et al. "Mapping Wind Farm Loads and Power Production - A Case Study on Horns Rev 1". In: *Journal of Physics: Conference Series*. Vol. 753. 3. Institute of Physics Publishing, Oct. 2016. DOI: 10.1088/1742-6596/753/3/032010.

[48] Ju Feng and Wen Zhong Shen. "Modelling wind for wind farm layout optimization using joint distribution of wind speed and wind direction". In: *Energies* 8.4 (2015), pp. 3075–3092. ISSN: 19961073. DOI: 10.3390/en8043075.

[49] Sanchez Perez Moreno. "A guideline for selecting MDAO workflows with an application in offshore wind energy". In: (). DOI: 10.4233/uuid:ea1b4101-0e55-4abe-9539-ae5d81cf9f65. URL: https://doi.org/10.4233/uuid:ea1b4101-0e55-4abe-9539-ae5d81cf9f65.

[50] Matteo Baudino Bessone et al. *Highlights: Relevance of life-cycle trade-offs in substructure concepts selection for floating wind farms*. Tech. rep.

[51] Sebastian Sanchez Perez-Moreno and Michiel B. Zaaijery. "How To Select MDAO Workflows". In: *AIAA/ASCE/AHS/ASC Structures, Structural Dynamics, and Materials Conference, 2018*. American Institute of Aeronautics and Astronautics Inc, AIAA, 2018. ISBN: 9781624105326. DOI: 10.2514/6.2018-0654.

[52] Mohammed Khair Al-Solihat and Meyer Nahon. "Stiffness of slack and taut moorings". In: *Ships and Offshore Structures* 11.8 (Nov. 2016), pp. 890–904. ISSN: 17445302. DOI: 10.1080/17445302.2015.1089052.

[53] *ECMWF Reanalysis v5 (ERA5)*. URL: https://www.ecmwf.int/en/forecasts/dataset/ecmwf-reanalysis-v5.

[54] Zi Lin, Xiaolei Liu, and Saeid Lotfian. "Impacts of water depth increase on offshore floating wind turbine dynamics". In: *Ocean Engineering* 224 (Mar. 2021). ISSN: 00298018. DOI: 10.1016/j.oceaneng.2021.108697.

A

Appendix A: Convergence History of the Design Variables and Constraints

Design Variables

The convergence history of some other design variables related to mooring lines and the substructure have been displayed in Figure A.1 for the two cases, Case A (neglecting floater displacements), and Case B (accounting for floater displacements).

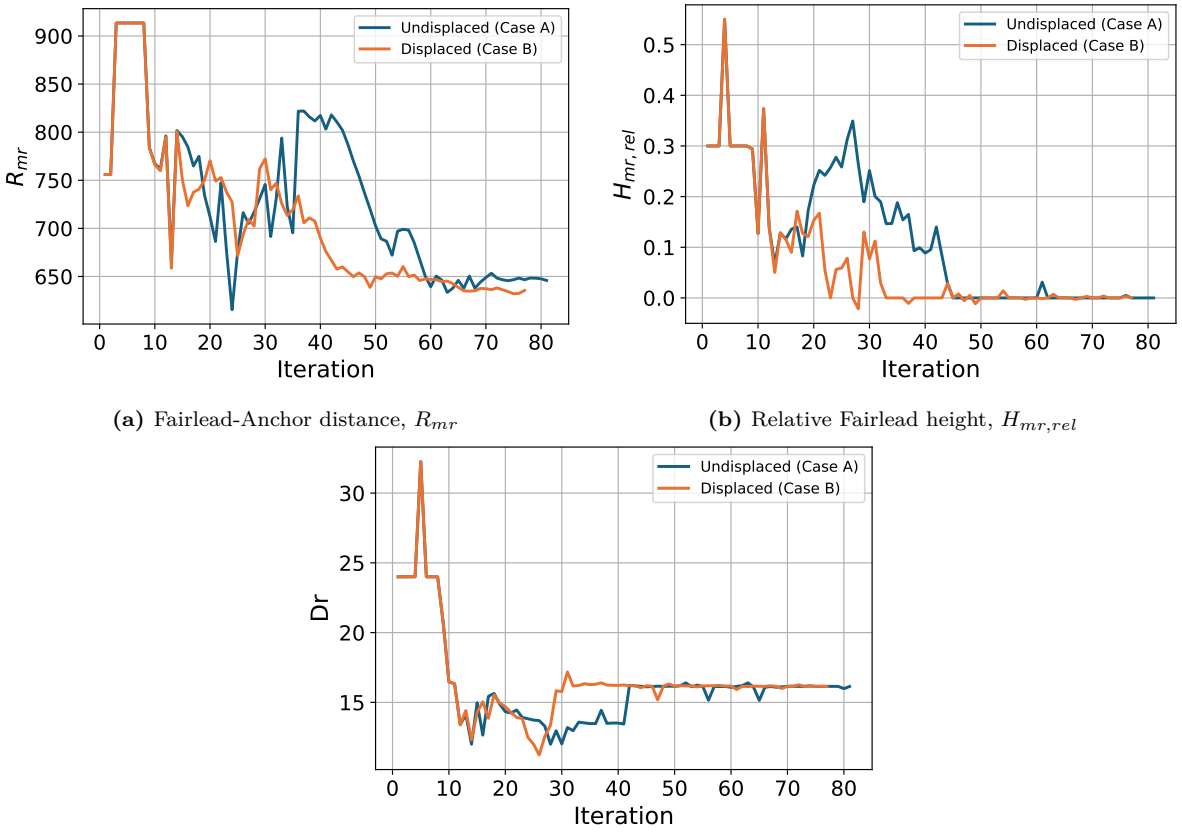

(a) Fairlead-Anchor distance, R_{mr}

(b) Relative Fairlead height, $H_{mr,rel}$

(c) Semi-submersible Draft, Dr

Figure A.1: Convergence history of Substructure and Mooring Design Variables (DV) per iteration

Constraints

The constraints handled by the super-problem: the minimum offset radius constraint, the minimum draft constraint, and the minimum distance between the turbines (footprint constraint), have been discussed in this section. The covergence history of the three constraints have been displayed in Figure A.2. These constraints were satisfied at very similar values for both Case A and Case B. The minimum draft and minimum turbine distance were found to be active, meaning that the optimal condition was found when these values were at there minimum. Meanwhile, the offset radius constraint which has been imposed to make sure the design of the substructure of the turbine is practical seems to converge at a much higher value for both the cases, thus remaining inactive throughout the optimization process.

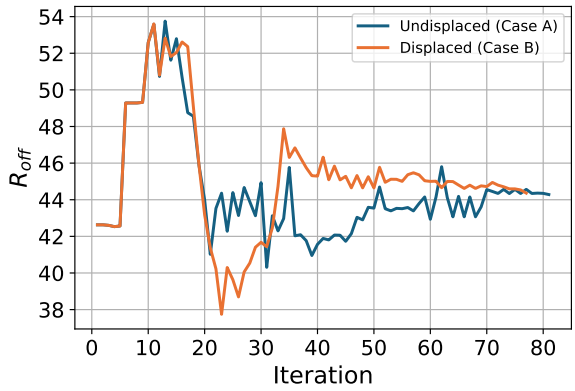

(a) Offset Radius Constraint

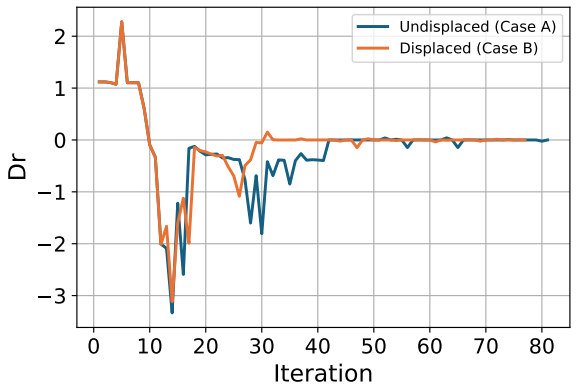

(b) Draft Constraint

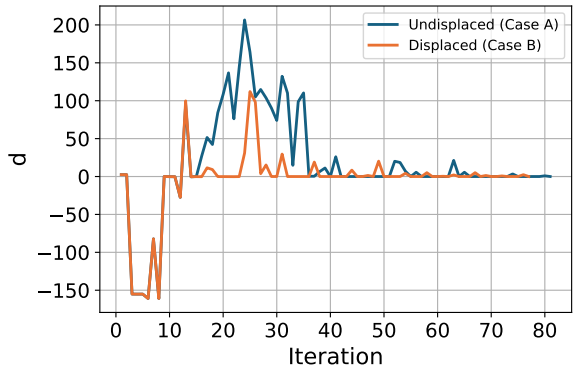

(c) Footprint Constraint

Figure A.2: Convergence history of the Super-Problem Constraints per iteration.

B

Appendix B: Flow Maps

The visualization of the flow field at other key wind directions has been displayed in this section. The flow maps shown in Figure B.1 pertain to a wind farm oriented at 270°, at four different wind directions: 0°, 45°, 90°, 180°.

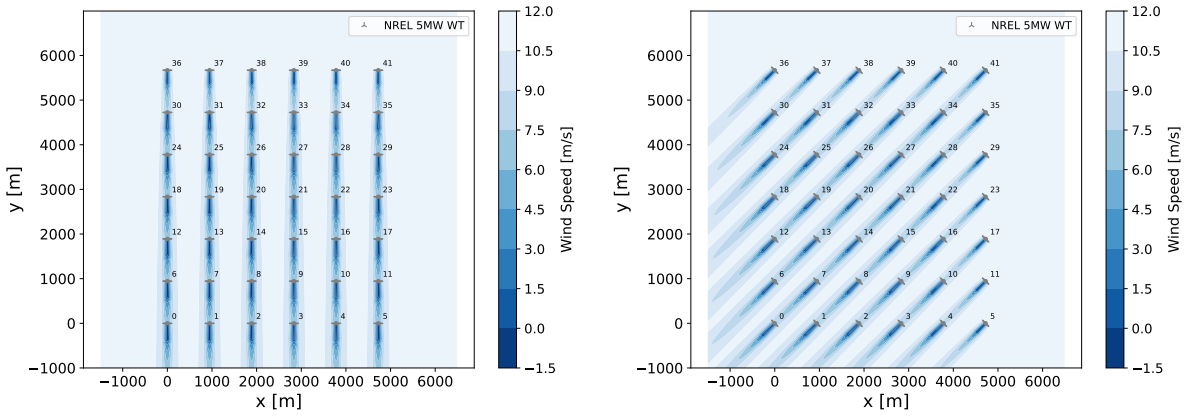

(a) WD = 0°

(b) WD = 45°

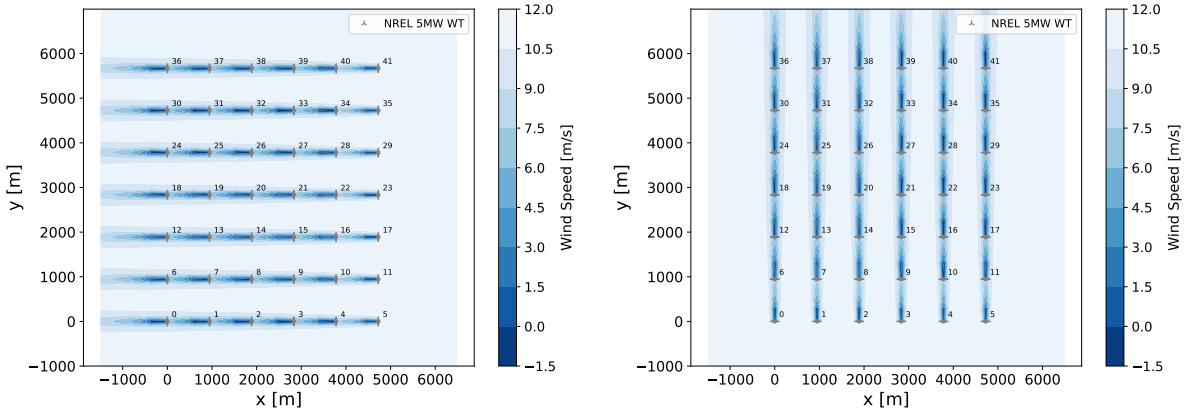

(c) WD = 90°

(d) WD = 180°

Figure B.1: Top view of the wind farm layout displaying the wake profile at four wind directions

At 90°, depicted in Figure B.1c, the freestream conditions are being faced by seven turbines. As a result, for Case B, these seven turbines will undergo high tilt (uptil rated wind conditions) and produce lower power as compared to Case A. Consequently, Case A power for these seven upstream turbines will be higher than Case B power for these turbines. However, for the downstream turbines, which are directly aligned with the wake of the upstream turbines, the wake deflection in Case B allows these turbines to generate more power than in Case A, where they are fully immersed in the wake.

In contrast, at 0° and 180° wind directions, depicted in Figure B.1a and Figure B.1d, respectively, six turbines are exposed to freestream conditions. These turbines produce more power than at 90°, but still less than in Case A, where floater displacements are neglected. Overall, for these wind directions, Case A generates less power than Case B for the entire wind farm.

However, Figure 5.7 shows that the relative power gained by the FOWTs when accounting for floater displacements (Case B) at 0° as well as 180° is slightly lower than that generated at 90°. Therefore, the difference between Case A and Case B power of 90° wind direction is slightly higher than this difference for both 0° and 180° cases. At 45°, this difference is even lower, but the Case B turbines still produce slightly higher power than Case A turbines. This is because, despite more turbines facing freestream conditions, the alignment of the downstream turbines with the wake still benefits the Case B farm due to the wake deflection.